Kinetically Trapping Co-continuous Morphologies in Polymer Blends and Composites

KINETICALLY TRAPPING CO-CONTINUOUS MORPHOLOGIES IN POLYMER BLENDS AND COMPOSITES

A Dissertation Presented

by

LE LI

Submitted to the Graduate School of the
University of Massachusetts Amherst in partial fulfillment
of the requirements for the degree of

DOCTOR OF PHILOSOPHY

February 2012

Polymer Science and Engineering

KINETICALLY TRAPPING CO-CONTINUOUS MORPHOLOGIES IN POLYMER BLENDS AND COMPOSITES

A Dissertation Presented

by

LE LI

Approved as to style and content by:

____
Thomas P. Russell, co-Chair

____
Ryan C. Hayward, co-Chair

____
Todd Emrick, Member

____
Anthony D. Dinsmore, Member

____
David Hoagland, Department Head
Department of Polymer Science and Engineering

To my parents
Mr. Jian Li and Ms. Juping Deng

ACKNOWLEDGMENTS

Foremost, I would like to express my sincere gratitude to my advisors Prof. Thomas P. Russell and Prof. Ryan C. Hayward, for their constant support, encouragement and invaluable guidance throughout my PhD life. Their patience, motivation, enthusiasm, and immense knowledge have enabled me to learn scientific skills and do research in a free and rich environment. I am thankful for all the opportunities they initiated such as presenting at conferences, international travel, research collaborations, and journal publishing. I am also grateful to Prof. Todd Emrick and Prof. Anthony D. Dinsmore for serving on my committee and providing insightful comments on my research.

I am grateful to my collaborators, P. K. Sudeep, Caroline Miesch, Jimmy Lawrence and Sirinya Chantarak, for providing nanoparticles. I also thank my colleagues, the former and current members from Russell group and Hayward group, whose expertise and help I benefited a lot from. I would like to thank other friends in and out of PSE, especially Xiangdong, Yiming, Wenjie, Jin, Peiwen, Yan, Yongping, Jun, Lang, Tsung-Han, Henry, Li Yao, Yipeng and Matsunaga-san for their friendship that made my graduate life more enjoyable and memorable. Special thanks go to our staff members, Lou, Alex, Sekar, Jack, Lisa, Laurie, Sophia, Sandi, Linda, Greg, Maria and Vivien, for helping me in many ways with research and graduate studies.

Finally, I would like to thank my family (parents, grandparents and parents-in-law). Without their love and support, it would be impossible for me to complete the task. I also want to thank my beloved son, whose growth fostered my development and achievements. Thanks to my husband for his company throughout the shadow and light.

ABSTRACT

KINETICALLY TRAPPING CO-CONTINUOUS MORPHOLOGIES IN POLYMER BLENDS AND COMPOSITES

FEBRUARY 2012

LE LI, B.Sc., FUDAN UNIVERSITY

M.S., UNIVERSITY OF MASSACHUSETTS AMHERST

Ph.D., UNIVERSITY OF MASSACHUSETTS AMHERST

Directed by: Professor Ryan C. Hayward and Professor Thomas P. Russell

Co-continuous structures generated from the phase separation of polymer blends present many opportunities for practical application. Due to the large interfacial area in such structures and the incompatibility between the components, such non-equilibrium structures tend to coarsen spontaneously into larger sizes and eventually form dispersed morphologies. Here, we utilize various strategies to kinetically stabilize the co-continuous structures in polymer blend systems at nano- to micro- size scales.

In the partially miscible blend of polystyrene and poly(vinyl methyl ether), we took advantage of the spinodal decomposition (SD) process upon thermal quenching, and arrested the co-continuous micro-structures by the addition of nanoparticles. In this approach, the critical factor for structural stabilization is that the nanoparticles are preferentially segregated into one phase of a polymer mixture undergoing SD and form a percolated network (colloidal gel) beyond a critical loading of nanoparticles. Once formed, this network prevents further structural coarsening and thus arrests the co-continuous structure with a characteristic length scale of several microns. Our findings indicate that a key to arresting the co-continuous blend morphology at modest volume

fractions of preferentially-wetted particles is to have attractive, rather than repulsive, interactions between particles.

For the immiscible blend of polystyrene and poly(2-vinyl pyridine) (PS/P2VP), we presented a strategy to compatibilize the blend by using random copolymers of styrene and 2-vinylpyridine, controlling the degree of immiscibility between PS and P2VP. Based on such compatibilization, co-continuous structured membranes, having characteristic size down to tens of nanometers, were fabricated in a facile way, via the solvent-induced macrophase separation of polymer blend thin films. The feature size was controlled by controlling the film thickness and varying the molecular weight of the PS homopolymer and the random copolymers. As the processing method (solution casting) is simple and the structures are insensitive to the solvent or substrate choices, this approach shows great potential in the large scale fabrication of co-continuous nanoscopic templates on flexible substrates via roll-to-roll processes.

Moreover, we proposed a quasi-binary blend system based on the PS/P2VP pair with the addition of a common solvent. An experimentally accessible phase mixing temperature was achieved, and the co-continuous morphologies were generated via thermally induced spinodal decomposition. The addition of solid particles significantly slowed down the coarsening kinetics and, in some cases, arrested the co-continuous structures at ~6 μm for a short period of time. This study suggests an alternative means to achieve co-continuous structures in polymer solutions and also provides better understanding of the thermodynamics and kinetics of polymer blend phase separation.

Our research demonstrates several means of kinetically trapping the non-equilibrium interconnected structures at sub-micron to tens-of-nanometer size scales that are germane to several functions including active layers of photovoltaic cells and polymer-based membranes.

TABLE OF CONTENTS

Page

ACKNOWLEDGMENTS v

ABSTRACT vi

LIST OF TABLES xi

LIST OF FIGURES xii

CHAPTER

1. INTRODUCTION 1

1.1 Motivation 1
1.2 General background of polymer blend phase separation 2
1.3 Co-continuous morphologies via spinodal decomposition 5
1.4 Co-continuous morphologies in solvent induced phase separation 7
1.5 Co-continuous morphologies in solvent mediated polymer blends 10
Reference 13

2. KINETICALLY TRAPPED CO-CONTINUOUS POLYMER MORPHOLOGIES THROUGH INTRA-PHASE GELATION OF NANOPARTICLES 15

2.1 Introduction 15
2.2 Experimental 18
2.2.1 Materials and sample preparation 18
2.2.2 Characterization methods 19
2.3 Results and discussion 20
2.3.1 Phase separated morphologies of PS/PVME pure blend 20
2.3.2 Morphologies with the addition of CdSe-TOPO nanoparticles 21
2.3.3 Aggregation behavior of CdSe-TOPO nanorod 25
2.3.4 Morphologies with the addition of CdSe-PS nanoparticles 28
2.3.5 Kinetically arrested co-continuous morphologies 29
2.4 Conclusions 31
Reference 32

3. FABRICATION OF CO-CONTINUOUS NANO-STRUCTURED AND POROUS POLYMER MEMBRANES THROUGH SPINODAL DECOMPOSITION OF HOMOPOLYMER/RANDOM COPOLYMER BLENDS 36

3.1 Introduction 36
3.2 Experimental 39

3.2.1 Materials and sample preparation 39
3.2.2 Characterization methods.....40
3.3 Results and discussion 41
3.3.1 Well-defined nanoscale co-continuous morphologies via spinodal demixing.....41
3.3.2 Controlling the size of co-continuous morphologies by molecular weight.....44
3.3.3 Effect of casting solvent and substrate.....47
3.3.4 Porous membranes based on the co-continuous morphologies.....50
3.3.5 Effect of solvent evaporation rate 52
3.3.6 Macrophase separation vs. microphase separation 54
3.4 Conclusions.....56
Reference 56

4. NANOPARTICLE EFFECTS ON THE THERMALLY INDUCED SPINODAL PHASE SEPARATION IN THE QUASI-BINARY BLEND OF POLYSTYRENE/POLY(2-VINYLPYRIDINE)/TETRAHYDROFURAN.....60

4.1 Introduction.....60
4.2 Experimental.....63
4.2.1 Materials and sample preparation 63
4.2.2 Characterization methods.....65
4.3 Results and discussion 66
4.3.1 Numerical calculations of the phase diagrams of a quasi-binary blend 66
4.3.2 Phase separation of the quasi-binary blend.....68
4.4.3 Effect of the addition of solid particles.....73
4.4 Conclusions and future work 80
Reference 80

5. CONCLUSIONS AND FUTURE WORK 84

5.1 Overview.....84
5.2 Intra-phase gelation of nanoparticles during spinodal decomposition 84
5.2.1 Nanoparticle network formation vs. spinodal decomposition 85
5.2.2 Effect of inter-particle interactions on the network formation threshold.....86
5.3 Phase separation of homopolymer/random copolymer blends 88
5.3.1 Functional membranes based on homopolymer/random copolymer phase separated templates.....89
5.3.2 UCST behavior of homopolymer/random copolymer blends.....90
5.4 Spinodal phase separation of a quasi-binary blend.....91
5.5 Summary.....91
Reference 92

BIBLIOGRAPHY.....93

LIST OF TABLES

Table Page

Table 3-1 Summary of polymers used in this study 40

Table 4-1 Estimated α values[a] (as in $q_m \sim t^{-\alpha}$) characterizing the late stage SD of PS/P2VP/THF (PS/P2VP 4/6 vol) with Au-PS NPs.......................................75

LIST OF FIGURES

Figure Page

Figure 1.1 Schematic of the droplet-dispersed-in-matrix morphology (left) and co-continuous morphology (right) 2

Figure 1.2 Phase diagrams of polymer-polymer binary blends (shaded areas represent phase separated regions). The y-axis for each diagram represents temperature and x-axis represent volume fraction. (a) miscibility over the entire composition-temperature range, (b) phase separation throughout the experimentally determined composition-temperature space, (c) LCST, (d) UCST, (e) co-existence of LCST and UCST, (f) an hour glass phase diagram of overlapped LCST and UCST behaviors, (g) double LCST, (h) double UCST and (i) a closed loop phase diagram. (Figure reprinted from Ref. [5]) 3

Figure 1.3 The binodal, spinodal curve and critical point in the phase diagram of polymer binary. (Figure reprinted from Ref. [5]) 5

Figure 1.4 Schematic of a three-component equilateral triangle phase diagram 9

Figure 1.5 Schematic of the temperature-composition prism for a polymer-1/polymer-2/solvent phase diagram. (Figure reprinted from Ref. [18]) 11

Figure 1.6 Schematic of the two-dimensional temperature-composition section from a polymer-1/polymer-2/solvent three-dimensional phase diagram. (Figure reprinted from Ref. [18]) 12

Figure 2.1 Phase separation of PS/PVME blends. (a) An optical image of a coarsened, phase separated PS/PVME blend (50 vol% PS) after annealing at 180 ℃ for 24 h (inset: cloud points for the PS/PVME blend; the dotted line is a guide to the eye). TEM images of phase separated off-critical blends containing (b) 35 vol% PS and (c) 70 vol% PS after annealing at 180 ℃ for 24 h, show brighter PVME-rich domains and darker PS-rich domains without staining. 21

Figure 2.2 Phase separation of PS/PVME blends containing CdSe-TOPO nanorods. a) TEM image of CdSe-TOPO nanorods (core diameter ~ 8 nm and length ~30 nm). Optical micrographs of near-critical blends with (b) 1 vol% CdSe-TOPO nanorods reveal droplet structures after annealing at 170 ℃ for 24 h, while (c) 2 vol% nanorods leads to co-continuous structures (inset: the FFT pattern of the optical image); (d) a cross sectional TEM image of the sample in (c) confirms the co-continuity of the structure, and reveals formation of a percolated network of nanorods within the PVME phase. (e) A schematic of the process of nanorod network formation leading to kinetic arrest of a co-continuous structure. 22

Figure 2.3 Phase separation of PS/PVME blends containing CdSe-TOPO nanospheres. (a) A TEM image of CdSe-TOPO nanospheres (core diameter ~ 4 nm). Optical micrographs of near-critical blends with (b) 1 vol% and (c) 2 vol% CdSe-TOPO spheres showed droplet structures after annealing at 170 ℃ for 24 h. However, at 3 vol% nanospheres, (d) optical micrographs and (e) TEM images revealed a co-continuous structure after annealing at 180 ℃ for 24 h.............................23

Figure 2.4 Phase separation of a near-critical PS/PVME blend with 5 vol% CdSe-TOPO nanospheres. The optical micrograph revealed a co-continuous structure after annealing at 205 ℃ for 24 hours...........................25

Figure 2.5 The influence of nanorod aggregation state on kinetic arrest of co-continuous structures. TEM images of a near-critical PS/PVME blend containing 1 vol% CdSe-TOPO nanorods (a) following solution casting reveal only slight aggregation, while (b) annealing at 110 ℃ for 12 h leads to extensive aggregation. (c) An optical micrograph of a near critical blend containing 2 vol% CdSe-TOPO nanorods pre-annealed at 110 °C for 12 h and then at 170 ℃ for 24 h shows large droplet structures, in sharp contrast to the co-continuous structure obtained without the pre-annealing step at 110 ℃. The lines running through lighter domains correspond to cracks through the polymer film introduced during cooling 28

Figure 2.6 Phase separation of PS/PVME blends containing CdSe-PS nanospheres. (a) A TEM image of CdSe-PS nanospheres (core diameter ~ 4 nm). Optical micrographs of near-critical PS/PVME blends with (b) 2 vol% and (c) 5 vol% CdSe-PS nanospheres both show droplet structures after annealing for 24 h (at 180 ℃ and 190 ℃, respectively). (d) A TEM image of the sample in (b) confirms the droplet structure. 29

Figure 2.7 Stability of co-continuous structures upon thermal annealing. Optical micrographs of near-critical PS/PVME blends containing 2 vol% CdSe-TOPO nanorods quenched to 170 ℃ for (a) 1 h and (b) 12 h reveal little coarsening over this time scale. For identical samples quenched to 180 ℃, the characteristic wavelength of the co-continuous structure is larger, but again little coarsening is observed between (c) 4 h and (d) 24 h of annealing. The insets in (a) and (c) show the measured length-scale as a function of annealing time. (e) A sample of the same composition annealed first at 170 ℃ for 48 h and subsequently at 180 ℃ for 24 h retains the structure formed at 170 ℃, providing further evidence for the kinetic stability of these co-continuous structures (inset: FFT pattern of the optical image). 31

Figure 3.1 Plan-view TEM images of 1:1 (wt.) blends of PS/P(S-*r*-2VP)56k with PS molecular weights of (a) 26k, (c) 34k, (d) 55k showing co-continuous nanostructures with molecular-weight dependent sizes. (b) A cross-sectional TEM image of the same sample as in (a) confirms that the co-continuous structure spans the film thickness. In all images, P(S-*r*-2VP) rich phases appear darker due to staining with I_2 vapor. 43

Figure 3.2 TEM images of 1:1 (wt.) blends of PS/P(S-*r*-2VP)39k with PS molecular weights of (a) 34k, (b) 136k, and (c) 570k, showing co-continuous structures with sub-100 nm sizes. The P(S-*r*-2VP) rich domains appear darker due to staining with I_2 vapor. 45

Figure 3.3 (a) TEM image of a 1:1 (wt.) blend of PS26k/P2VP38k homopolymers spin coated from chloroform showing droplets of P2VP-rich domains (dark circles) in a PS matrix. The white circles correspond to P2VP-rich domains that were extracted during floating of the film sample off of the substrate. (b-c) TEM images of 1:1 (wt.) blends of PS26k/P(S-*r*-2VP)56k spin coated from toluene (b) and chloroform (c), shown at the same magnification to highlight the dramatic difference in morphology obtained using the random copolymer blend. The P2VP-rich phases appear darker due to staining with I_2 vapor (scale bars: 500 nm). 47

Figure 3.4 TEM images of 1:1 (wt.) blends of PS/P(S-*r*-2VP) with molecular weights of (a) 26k/56k, (b) 55k/56k, (c) 26k/39k, and (d) 55k/39k, spin-coated from chloroform. In all cases, co-continuous structures are found, though with smaller length scales and more diffuse interfaces compared to equivalent blends cast from toluene, likely due to the higher volatility of chloroform. The P(S-*r*-2VP) rich phases appear darker due to staining with I_2 vapor. Insets of (a) and (c) are samples after selective solvent extraction (scale bars: 100 nm). 48

Figure 3.5 Blend films of 1:1 (wt.) PS26k/P(S-*r*-2VP)56k prepared on (a-c) a silicon wafer, (d-f) a gold-coated silicon wafer, (g-i) a mica substrate, and (j-k) a polyimide substrate, with the cross-sectional TEM image (a, d, g and j) and top-view (b, e, h and k) and cross-sectional (c, f and i) SEM images after selective solvent extraction of P(S-*r*-2VP) rich domains. Similar co-continuous structures are observed, regardless of the substrate type (scale bars: 1 μm). 49

Figure 3.6 Thin membranes of blends of PS55k/P(S-*r*-2VP)56k following selective solvent extraction of the P(S-*r*-2VP) rich phases. (a-c) For a 1:1 (wt.) blend, the high degree of contrast from TEM on an unstained sample (a), coupled with SEM top-view images (b) showing pores at the free surface and cross-sectional images (c) showing pores percolating through the film thickness indicate successful extraction of material from the co-continuous film. (d-f) By contrast, for a 2:1 (wt.) blend, TEM (d) reveals only isolated domains of random copolymer rich phases, while top-view (e) and cross-sectional (f) SEM images show that material has only been extracted from domains at the free surface. (g) Cross-sectional SEM of the same sample in (d)-(f), with exposure of the cross section and selective extraction, showing discrete pores in the thin membrane (scale bars: 500 nm). 51

Figure 3.7 Films of 1:1 (wt.) PS26k/P(S-*r*-2VP)56k blends with different film thicknesses, are found to have co-continuous structures with length scales that increase with film thickness (the dotted line is a guide to the eye). Insets: Cross-sectional TEM micrographs of corresponding thin films, with the P(S-*r*-2VP) rich phases appearing darker due to I_2 vapor staining (scale bars: 500 nm). 53

Figure 3.8 Cross-sectional TEM micrographs of thick membranes of 1:1 (wt.) blends of PS32k/P(S-*r*-2VP)56k. (a) The co-continuous structures formed upon drop-casting show a gradient in the length-scale of the co-continuous structure through the film thickness. (b) After annealing with the substrate held at 120 ℃ for 10 min while the free surface was cooled, the gradient is enhanced (scale bars: 1 μm). P(S-*r*-2VP) phases appear darker due to staining with I_2 vapor; the dark lines (indicated by red arrows) represent gold films deposited to mark the polymer/air interface. 54

Figure 3.9 SAXS profiles for polymer thin films of (a) P(S-*r*-2VP)39k, (b) P(S-*r*-2VP)56k and (c) the Debye-Buche fittings. TEM micrographs of thin films of (d) P(S-*r*-2VP)39k, (e) P(S-*r*-2VP)56k, and (f) PS26k, that show only features of a few nanometers which are artifacts due to staining by I_2 vapor (scale bars: 100 nm). 55

Figure 4.1 The estimated phase diagrams of the quasi-binary blend of PS/P2VP/THF: (a) binodal (solid lines) and spinodal (dotted lines) curves for the case of $\phi_S = 0.9$, $\phi_{PS} = \phi$, $\phi_{P2VP} = 0.1-\phi$, with various N values; and (b) critical temperatures as a function of ϕ_S 67

Figure 4.2 Cloud point curve of PS26k/P2VP38k with 88 vol % THF 69

Figure 4.3 Small angle light scattering patterns of the PS/P2VP blend with volume ratio 4/6 containing 88 vol % THF quenched to -30 ℃ at cooling rate of 100 ℃/min, with increasing time: 0s (a), 5s (b), 7s (c), 9s (d), 11s (e), 13s (f), 19s (g), 29s (h), 38s (i), 68s (j), 99s (k) and 162s (l). The onset of phase separation is set as time zero (Red arrow is to guide the eye, indicating ring pattern formation; the bright lines across each image arise from the geometry of the capillary sample cell). 70

Figure 4.4 Optical micrographs of the PS/P2VP blend with volume ratio 4/6 containing 88 vol % THF quenched to -30 ℃ at cooling rate of 100 ℃, with increasing time: 0s (a), 6s (b), 8s (c), 12s (d), 14s (e), 18s (f), 30s (g), 40s (h), 45s (i), 100s (j), 128s (k) and 170s (l). The onset of phase separation is set as time zero (scale bar: 100 μm). 71

Figure 4.5 Small angle light scattering of the PS/P2VP blend with volume ratio 4/6 containing 86 wt% THF quenched to -30 ℃ at cooling rate of 100 ℃/min: scattering intensity I as a function of wavenumber q (a) and (b) with phase separation time; q_m (c) and I_m (d) as a function of time. 72

Figure 4.6 Phase separation of PS/P2VP/THF (PS/P2VP 4/6 vol) with 7.6 v% Au-PS NPs quenched to -30 ℃ with cooling rate of 100 ℃/min: I vs. q profiles with increasing phase separation time. The onset of phase separation was set as time zero. 74

Figure 4.7 Phase-separated PS/P2VP/THF (PS/P2VP 4/6 vol) with Au-PS NPs: q_m vs. t for the blend containing 1.8 v%, 5.0 v% and 7.6 v% nanoparticles quenched to either -10 ℃ or -30 ℃ with cooling rate of 100 ℃/min. The onset of phase separation was set as time zero. 75

Figure 4.8 Phase-separated PS/P2VP/THF (PS/P2VP 4/6 vol) with silica particles: q_m *vs.* time for the blend containing 5.2 v%, 9.8 v%, 15.3 v% and 20.2 v% SiO_2 particles quenched to either -30 ℃ or -50 ℃ with cooling rate of 100 ℃/min. The onset of phase separation was set as time zero. 77

Figure 4.9 Phase separation of PS/P2VP/THF (PS/P2VP 4/6 vol) with 15.3 v% silica particles quenched to -30 ℃ with cooling rate of 100 ℃/min: *I* vs. *q* profiles with increasing phase separation time, showing fixed q_m at early times (a) and an abrupt coarsening at late times (b). The onset of phase separation was set as time zero. 78

Figure 4.10 Phase separation of PS/P2VP/THF (PS/P2VP 4/6 vol) with 9.8 v% silica particles quenched to -50 ℃ with cooling rate of 100 ℃/min: *I* vs. *q* profiles with increasing phase separation time, showing fixed q_m throughout the experiment. The onset of phase separation was set as time zero. 79

Figure 5.1 The aggregation behaviors of CdSe nanospheres in the PS/PVME (1:1 vol) blends after solution casting. TEM images of the blends containing (a) 2 vol% and (b) 4 vol% CdSe-TOPO nanospheres, reveal a network like structure of the nanoparticles; while the blends containing (c) 2 vol% and (b) 4 vol% CdSe-PS nanospheres, indicate good dispersion with little aggregation (inset: higher magnification TEM images). 86

Figure 5.2 Phase separated morphologies of PS/PVME blends (1:1 vol) containing 1 vol % Fe_3O_4 nanoparticles stabilized with oleic acid and oleic amine (core diameter of 3 – 10 nm). Optical micrographs show the morphologies for the blend (a) after annealing at 170 ℃ for 24 h, (b) after pre-annealing at120 ℃ for 12 h and then quenched to 170 ℃ for 24 h and (c) after annealing at 180 ℃ for 24 h; (d) a TEM image taken from the sample in (c) confirms the co-continuous morphology with a percolated network of nanoparticles preferentially located in one phase..87

Figure 5.3 The aggregation behaviors of Fe_3O_4 nanoparticles in the PS/PVME (1:1 vol) blends. TEM images of the blend containing 1 vol% Fe_3O_4 nanoparticles (a) following solution casting and (b) annealing at 120 ℃ for 12 h, both reveal slight aggregation. 88

Figure 5.4 The estimated critical temperatures for the PS/P(S-*r*-2VP) blends..................90

CHAPTER 1

INTRODUCTION

1.1 Motivation

The properties and subsequent uses of polymer blends depend critically on the nature of phase morphology. Two major classes of morphologies can be distinguished in a binary two-phase blend: isolated droplets dispersed in a matrix and a co-continuous morphology, illustrated in Figure 1.1. In the former, the physical properties of the blends are mainly controlled by the matrix properties. The co-continuous morphology consists of continuous and interconnected phases percolated throughout the blend volume, in which each phase contributes in parallel to the properties of the blend in all directions. Such morphology is of practical interest due to the synergistic combination of mechanical, electrical, optical, and transport properties of each phase.[1, 2] An important technical challenge is to kinetically trap such non-equilibrium interconnected structure at sub-micron to tens-of-nanometer size, which may offer promise in the contexts including the active layers of bulk heterojunction organic photovoltaic devices [3] and polymer-based membranes.[4]In the following chapters of this thesis, we will describe various methods to fabricate or stabilize co-continuous structures in different polymer blend systems.

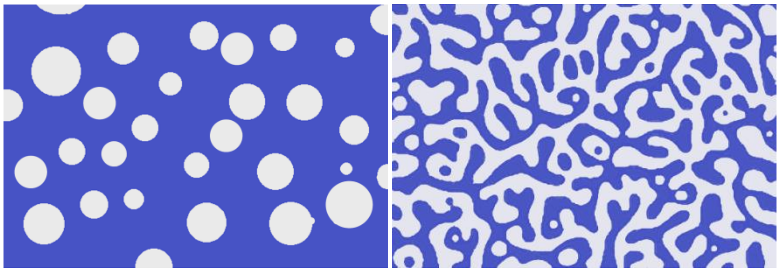

Figure 1.1 Schematic of the droplet-dispersed-in-matrix morphology (left) and co-continuous morphology (right)

1.2 General background of polymer blend phase separation

Like low molecular weight mixtures, polymer blends can exhibit various levels of ranging from being completely miscible to completely immiscible.[5] The unique factor affecting the thermodynamics of polymer blends is the high molecular weights. In low molecular weight mixtures, the most important parameter leading to miscibility is the combinatorial entropy contribution. The entropy of mixing for polymer-polymer pairs is much smaller, owing to the small number of molecules of each polymer in the blend, as a consequence of their high molecular weights.[6] For miscibility to occur, the free energy of mixing:

$$\Delta G_m = \Delta H_m - T\Delta S_m, \tag{1.1}$$

must be less than 0, where ΔH_m is the enthalpy of mixing and ΔS_m is the entropy of mixing. Although the entropy change always favors mixing, it is usually too small to result in the necessary negative ΔG_m, since ΔH_m is generally positive.

The effect of molecular weight on the phase behavior is also manifest in the temperature dependence of miscibility. For low molecular weight mixtures, increasing temperature generally leads to increased miscibility as the $T\Delta S_m$ term increases, driving

ΔG_m to more negative values. For polymer blends, the term $T\Delta S_m$ is small and other factors, such as the non-combinatorial entropy contributions and the temperature dependent ΔH_m values, can dominate and lead to decreased miscibility with increasing temperature. Therefore liquid-liquid and polymer-solvent mixtures usually exhibit upper critical solution temperature (UCST), while polymer-polymer mixtures generally exhibit lower critical solution temperatures (LCST). Figure 1.2 illustrates various phase diagrams observed in polymer-polymer binary blends.

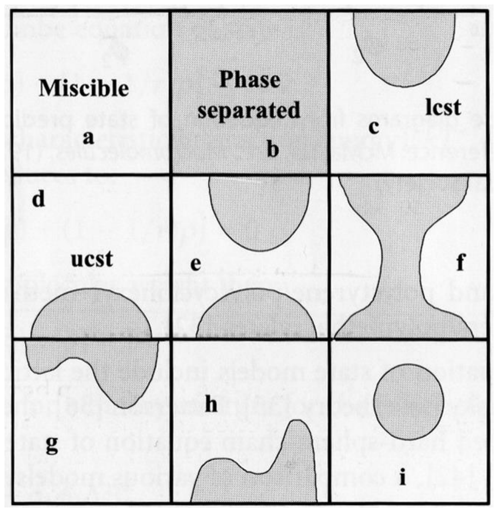

Figure 1.2 Phase diagrams of polymer-polymer binary blends (shaded areas represent phase separated regions). The y-axis for each diagram represents temperature and x-axis represent volume fraction. (a) miscibility over the entire composition-temperature range, (b) phase separation throughout the experimentally determined composition-temperature space, (c) LCST, (d) UCST, (e) co-existence of LCST and UCST, (f) an hour glass phase diagram of overlapped LCST and UCST behaviors, (g) double LCST, (h) double UCST and (i) a closed loop phase diagram. (Figure reprinted from Ref. [5])

For a mixture to be miscible, ΔG_m must be negative, however this is not a sufficient requirement. In a binary blend, the thermodynamic criterion for two phases at equilibrium is that the chemical potentials of polymer A and polymer B be equal in the two coexisting phases:

$$\Delta\mu_1^a = \Delta\mu_1^b \qquad \Delta\mu_2^a = \Delta\mu_2^b \tag{1.2}$$

where 1, 2 represent the two polymers and a, b represent the phases. The chemical potential is defined as partial derivative of the Gibbs free energy of the system with respect to the number of moles of a specific component, and is expressed as following:

$$\mu_i = (\partial G_m / \partial N_i)_{T,p,n_j \neq i} \tag{1.3}$$

The co-existence curve is also called the binodal, whose values can also be determined from the common tangent to the ΔG_m curve. In addition, the two inflection points in the ΔG_m curve define the spinodal, at which the curvature vanishes (Equation 1.4):

$$(\partial^2 \Delta G_m / \partial \phi^2)_{T,p} = 0 \tag{1.4}$$

Between these two points, the curvature is negative and a homogeneous mixture is in an unstable state, because any small fluctuation in composition will cause a decrease in the free energy and hence phase separation.

The critical point is where the binodal and spinodal intersect (Figure 1.2), determined from the following equations:

$$(\partial^2 \Delta G_m / \partial \phi^2)_{T,p} = (\partial^3 \Delta G_m / \partial \phi^3)_{T,p} = 0 \tag{1.5}$$

The above phase separation criteria are illustrated in Figure 1.2, showing the single phase region, the binodal, the spinodal as well as the critical points in the LCST/UCST binary blends.

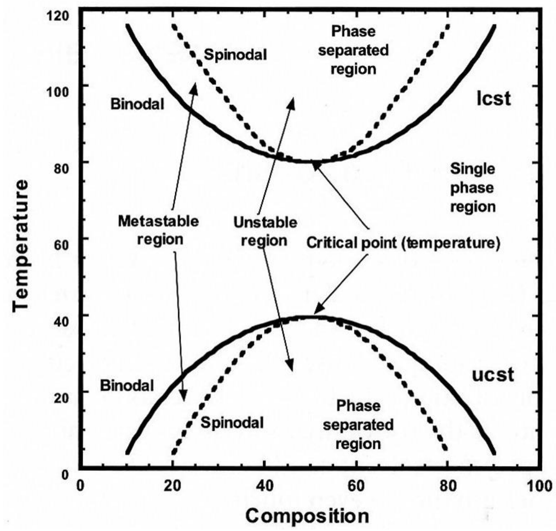

Figure 1.3 The binodal, spinodal curve and critical point in the phase diagram of polymer binary. (Figure reprinted from Ref. [5])

When a single phase mixture or solution crosses the phase boundary into either the metastable region or the unstable region, phase separation will occur. This transition can be induced by temperature change, solvent removal, non-solvent addition, by applied shear forces or by pressure change. During phase separation, the composition within each phase changes and the domains grow in size, ultimately yielding the droplets dispersed in a matrix, a state representing a minimization of the interfacial energy.

1.3 Co-continuous morphologies via spinodal decomposition

For polymer blend systems with an accessible phase separation temperature (Figure 1.3), phase separation occurs once the single phase mixture is brought into the two phase region within the binodal/coexistence curve. In particular, co-continuous morphologies may be formed if the blend is quenched into the spinodal envelope near the critical composition, where the spinodal decomposition (SD) mechanism dominates.

The early stages of SD has been described in the linear theory introduced by Cahn and Hilliard.[7, 8] In this theory, concentration fluctuations spontaneously grow into phase separated regions, increasing in amplitude while maintaining a constant size with time. The size of the initially-formed co-continuous structure is determined by the quench depth ($\chi_s - \chi$) and the dimensions of the polymer chain[9] (generally sub-micron sizes), as described by the following equation:

$$\xi_0 \sim R_g \left(\frac{\chi - \chi_s}{\chi_s} \right)^{-1/2}, \tag{1.6}$$

where χ_s is the interaction parameter at the spinodal line.

In the late stages, the structure will start to grow in a self-similar fashion, yielding co-continuous morphologies with increasing size. Several theories have been proposed to describe the coarsening process during the late stages of SD, including the coalescence model by Binder and Stauffer,[10] Ostwald ripening process by Lifshitz and Slyozov,[11] and the hydrodynamic mechanism by Siggia[12] Later, Furukawa summarized previous proposals in terms of scaling and suggested that the structure factor for a d-dimensional isotropic system should scale as:[13]

$$S(q,t) = q_m(t)^{-d}\,\tilde{S}(x), 0 < \tilde{S}(x) < 1 \tag{1.7}$$

where $\hat{S}(x)$ is a universal scaling function which is independent of time, and the quantity x is defined as $x = q/q_m(t)$. At the end of the coarsening process, the co-continuous structure ultimately equilibrates into large dispersed domains, losing the co-continuous nature.

In Chapter 2, we take advantage of the spinodal phase separation in the partially miscible blend of polystyrene and poly(vinyl methyl ether) upon thermal quenching, and arrest the co-continuous micro-structures by the addition of nanoparticles. The critical factor for structural stabilization in this approach is that the nanoparticles are preferentially segregated into one phase and form a percolated network (colloidal gel) beyond a critical loading of nanoparticles. Once formed, this network prevents the further structural coarsening, thereby arresting the phase separation, entrapping the co-continuous structure with a characteristic length scale of several microns. Our findings indicate that a key to arresting the co-continuous blend morphology at modest volume fractions of preferentially-wetted particles is to have attractive, rather than repulsive, interactions between particles.

1.4 Co-continuous morphologies in solvent induced phase separation

Most binary polymer blends are immiscible over an experimentally accessible temperature range, where the upper bound is the degradation temperature. It is thus impractical to achieve co-continuous structures via SD from the homogeneous state. To achieve finely dispersed domains in immiscible systems, usually an immiscible polymer blend is heated to the melt state and mechanically mixed, resulting in co-continuous structures at appropriate conditions.[1] Although small domain sizes can be achieved with longer melt-mixing times, the threads of the phases are prone to break with longer and stronger mechanical agitation,[1] leading to the loss of co-continuity. This makes the size of the co-continuous structure formed by the melt-mixing process limited to the micron-scale.

The use of a solvent is a common and practical method to bring the critical conditions for phase separation into an experimentally accessible range, to generate co-continuous morphologies in immiscible polymer blends. Homogeneous solutions can be achieved by dissolving the immiscible polymers in a common solvent, generating a polymer/polymer/solvent ternary solution.[14] In such three-component systems, an equilateral triangle is used to describe the three-component phase diagram at constant T and p (Figure 1.4). Each corner represents one of the pure components, each edge represents the mixtures of the two components shown on the adjacent corners, and the interior of the triangle represents mixtures of all three components. Most commonly, the mixture of polymers is incompatible in the absence of solvent and the addition of solvent mediates the interactions between the polymers and also increases the entropic contribution to the free energy. Consequently, no matter how immiscible two polymers may be, it is always possible to make a very dilute solution containing both polymers, as long as the solvent dissolves both polymers.[15] There are also polymer mixtures compatible in the absence of solvent, and each polymer is separately miscible with the solvent in all proportions, but phase separation occurs in some compositions when all three components are mixed.[16] For example, the linear polyethylene/atactic polypropylene/diphenyl ether blend exhibits a closed immiscibility loop, possibly because of the small polymer/polymer interaction parameter and the significant difference between the polymer/solvent interactions.[17]

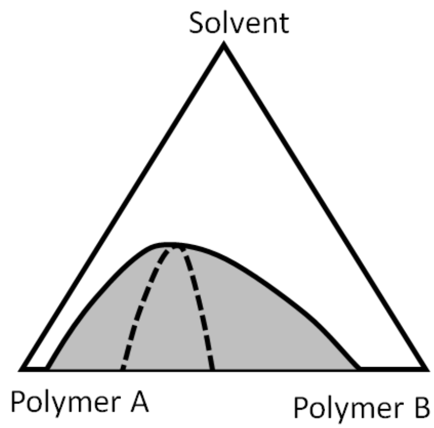

Figure 1.4 Schematic of a three-component equilateral triangle phase diagram

The removal of solvent at constant *T* and *p*, gives rise to compositional changes in the mixture, and can bring it from the homogenous state into the phase-separated region of the triangular phase diagram. This process is known as the solvent induced phase separation (SIPS). Analogous to the binary blend phase separation, co-continuous morphologies can also be generated during SIPS, provided that the composition change quenches the system into the unstable region and induces SD. Such structures may be kinetically frozen during phase separation as a result of the increasing of glass transition temperature of the mixture upon solvent removal.

In Chapter 3, we design a binary polymer blend based on the immiscible pair of polystyrene (PS) and poly(2-vinylpyridine) (P2VP) and describe a simple approach to prepare co-continuous morphologies with characteristic domains, tens of nanometers in size, via SIPS. The degree of immiscibility between PS and P2VP is tuned by incorporating styrene monomers into the backbone of P2VP to form a random copolymer, mediating the unfavorable interactions between the two components. The size scale of the co-continuous morphology was controlled by varying the molecular weight of the PS homopolymer and the random copolymers, as well as the film thickness. This strategy is shown to be robust in that: 1) the process involves a simple solution casting method; 2) co-continuity of the morphology occurs provided the solvent dissolves both components; and 3) the co-continuous morphology is insensitive to the substrate surface chemistry. Porous membranes with continuous channels and gradient co-continuous structures can also be generated from the phase separated blend films.

1.5 Co-continuous morphologies in solvent mediated polymer blends

Phase diagrams of ternary systems also vary with temperature, adding a third dimension to the triangle, generating a redundant phase diagram. The complexity of such phase diagram is illustrated in Figure 1.5, showing the temperature-composition prism, where the binodal surface as well as the spinodal surface exists. It can be seen that it is possible to have more than one immiscibility region, depending on the temperature dependence of the interaction parameters.

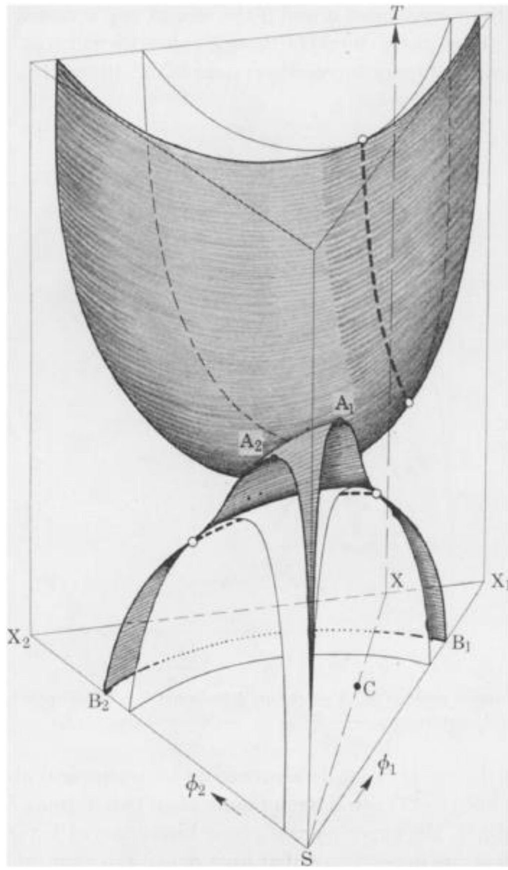

Figure 1.5 Schematic of the temperature-composition prism for a polymer-1/polymer-2/solvent phase diagram. (Figure reprinted from Ref. [18])

To simplify, we consider a given composition of the mixture, at point C in Figure 1.5. We can intercept a plane SXT, in which we have two independent variables: temperature and volume fraction of solvent, with fixed volume ratio between polymers. Figure 1.6 shows such two-dimensional phase diagram of the ternary system, revealing complicated temperature dependence due to the two separate miscibility gaps.

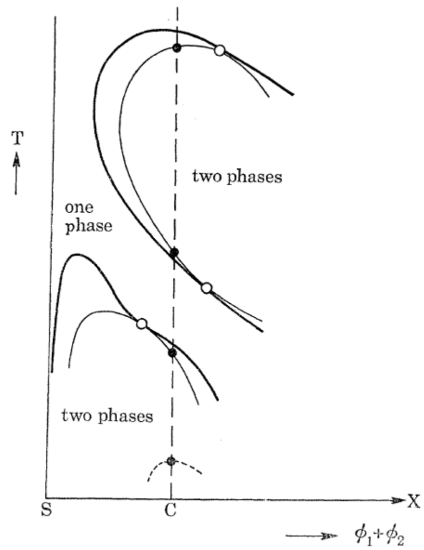

Figure 1.6 Schematic of the two-dimensional temperature-composition section from a polymer-1/polymer-2/solvent three-dimensional phase diagram. (Figure reprinted from Ref. [18])

To further simplify, we assume that the solvent only dilutes the unfavorable interactions between the incompatible pair[14] and thus treat the ternary system as a quasi-binary blend. The simplified solution for the phase separation criteria is to replace the interaction parameter χ by the effective value χ_{eff}. The theoretical predictions for the quasi-binary blend systems have agreed with experimental data[18] quantitatively. For further simplification, the criteria for phase miscibility and stability in binary polymer blend systems (Equation 1.2, 1.4 and 1.5) are thought to be applicable in the case of the symmetric quasi-binary polymer-polymer-solvent systems.

Given the right interactions among the components, quenching such homogeneous quasi-binary mixtures into the spinodal envelop will result in the formation of co-continuous structure and subsequent coarsening, similar to the case of a binary polymer blend. In Chapter 4, we design a quasi-binary blend system of

PS/P2VP/tetrahydrofuran and achieve co-continuous morphologies by temperature induced phase separation via SD. Addition of particles to the blend greatly decreases the rate of coarsening, even bringing about kinetic arrest of phase separation in certain cases. Our research suggests an alternative means to achieve co-continuous structures in polymer solutions and also provides better understanding of the thermodynamics and kinetics of polymer blend phase separation.

Reference

1. Potschke, P. and D.R. Paul, *Formation of Co-continuous structures in melt-mixed immiscible polymer blends.* Journal of Macromolecular Science-Polymer Reviews, 2003. **C43**(1): p. 87-141.
2. Mathiowitz, E., et al., *Novel desiccants based on designed polymeric blends.* Journal of Applied Polymer Science, 2001. **80**(3): p. 317-327.
3. Hoppe, H. and N.S. Sariciftci, *Morphology of polymer/fullerene bulk heterojunction solar cells.* Journal of Materials Chemistry, 2006. **16**(1): p. 45-61.
4. Kesting, R.E., *Synthetic polymeric membranes: a structural perspective*. 1985, New York: Wiley-Interscience. 368.
5. Robeson, L.M., *Polymer Blends: A Comprehensive Review*. 2007, Cicinnati, OH: Hanser Gardner Publications, Inc.
6. Paul, D.R., *Polymer blends*, ed. D.R. Paul and S. Newman. Vol. 1. 1978, New York: Academic Press, Inc. 501.
7. Cahn, J.W., *Phase separation by spinodal decomposition in isotropic systems.* Journal of Chemical Physics, 1965. **42**(1): p. 93.
8. Cahn, J.W. and J.E. Hilliard, *Free Energy of a Nonuniform System .1. Interfacial Free Energy*. Journal of Chemical Physics, 1958. **28**(2): p. 258-267.
9. Van Aartsen, J.J., *Theoretical observations on spinodal decomposition of polymer solutions.* European Polymer Journal, 1970. **6**(7): p. 919.
10. Binder, K. and D. Stauffer, *Theory for Slowing Down of Relaxation and Spinodal Decomposition of Binary-Mixtures.* Physical Review Letters, 1974. **33**(17): p. 1006-1009.
11. Lifshitz, I.M. and V.V. Slyozov, *The Kinetics of Precipitation from Supersaturated Solid Solutions.* Journal of Physics and Chemistry of Solids, 1961. **19**(1-2): p. 35-50.
12. Siggia, E.D., *Late Stages of Spinodal Decomposition in Binary-Mixtures.* Physical Review A, 1979. **20**(2): p. 595-605.
13. Furukawa, H., *Dynamics of Phase Separations of a Dissipative System and a Fluid Mixture.* Physical Review A, 1981. **23**(3): p. 1535-1545.

14. Scott, R.L., *The Thermodynamics of High Polymer Solutions .5. Phase Equilibria in the Ternary System - Polymer-1 Polymer-2 Solvent.* Journal of Chemical Physics, 1949. **17**(3): p. 279-284.
15. Berek, D., D. Lath, and V. Durdovic, *Phase Relations in Ternary System Atactic Polystyrene-Atactic Polypropylene-Toluene.* Journal of Polymer Science Part C-Polymer Symposium, 1967(16PC): p. 659.
16. Koningsveld, R., L.A. Kleintjens, and H.M. Schoffeleers, *Thermodynamic Aspects of Polymer Compatibility.* Pure and Applied Chemistry, 1974. **39**(1-2): p. 1-32.
17. Zeman, L. and Patterso.D, *Effect of Solvent on Polymer Incompatibility in Solution.* Macromolecules, 1972. **5**(4): p. 513.
18. Koningsveld, R., H.A.G. Chermin, and M. Gordon, *Liquid-Liquid Phase Separation in Multicomponent Polymer Solutions .8. Stability Limits and Consolute States in Quasi-Ternary Mixtures.* Proceedings of the Royal Society of London Series a-Mathematical and Physical Sciences, 1970. **319**(1538): p. 331.

CHAPTER 2

KINETICALLY TRAPPED CO-CONTINUOUS POLYMER MORPHOLOGIES THROUGH INTRA-PHASE GELATION OF NANOPARTICLES*

2.1 Introduction

In the previous chapter, we introduced the phase separation of polymer blends and importance of controlling the phase separated morphologies. A co-continuous structure will synergistically combine the properties of different materials in parallel. Such structures are typically not at equilibrium, and the ability to kinetically trap them on the nano- to microscale is technologically important for applications ranging from active layers in photovoltaic cells[1] to polymer-based membranes.[2]

To stabilize co-continuous morphologies in polymer blends, several types of additives have been used. Block or graft copolymers have been widely used as compatibilizers,[3-21] since they reduce interfacial energies,[4, 5, 11, 15] suppress coalescence, ,[7, 9, 13, 17, 20, 22, 23] and, in some cases, lead to kinetically-trapped[17, 19, 20] or even thermodynamically-stabilized[6, 14] co-continuous structures. In many cases however, the use of pre-made copolymer stabilizers is impractical, while the *in situ* formation of copolymers by reactive blending typically requires suitably functionalized precursor polymers.[24-27]

The addition of nanoparticles as stabilizers offers an alternative means that may be more generally applicable and provides additional opportunities to tailor the properties of the composite material. Most commonly, an immiscible polymer blend is

---

* Reprinted with permission from *Nano Letters* **2011**, 11, (5), 1997-2003. Copyright 2011 American Chemical Society.

combined with fillers by melt mixing, giving rise to co-continuous structures under appropriate conditions.[28-34] For example, Gubbels *et al.*[28, 29] have achieved kinetic stabilization of co-continuous morphologies in blends of polyethylene/polystyrene by adding carbon black, through both interfacial segregation and preferential location of the filler within one domain. However, the selectivity of particle segregation has been found to be sensitive to the processing conditions as well as the sequence of adding components. Therefore, due to the complexity of processing and the often ill-defined state of the nanoparticle dispersion, the mechanisms by which co-continuous structures are formed, and their long-term stabilities, are not well understood.[30, 35-37]

Transient co-continuous morphologies can be generated by thermally quenching a homogeneous mixture to a temperature within the spinodal envelope.[38] For near-critical compositions, the material will phase separate into a co-continuous morphology with a characteristic wavelength (generally sub-micron) that is determined by the balance between interfacial energy and diffusion. Once formed, the structure will coarsen over time in a self-similar fashion, yielding a co-continuous morphology of increasing size. An elegant route to kinetically trap this non-equilibrium structure is to add particles that adsorb to the interface formed during demixing, ultimately leading to an interfacial jamming of particles. Such a material, termed a ‘bijel’, was simultaneously predicted by Cates and co-workers for low-viscosity fluids and interfacially-active colloids,[39] and demonstrated experimentally by Composto and co-workers for a polymer blend kinetically trapped by interfacial segregation of nanoparticles.[40] An important point is that bijel formation requires that the particle additives exhibit nearly neutral wetting by the phases; even particles that irreversibly adsorb to the interface but prefer one of the two phases yield structures that ultimately coarsen and lose their co-continuous nature.[41] Especially for polymer blends, where the interfacial tension between the demixing fluids is quite low,[7, 9] a delicate control of the surface chemistry of the nanoparticles is therefore required.

Here, we demonstrate a new route to achieve co-continuous micron-scale structures that can be indefinitely kinetically trapped in phase-separating polymer blends by aggregation of rod-like or spherical nanoparticles into a percolated network *within* one of the two polymer phases, rather than at the interface. As a consequence, the requirement to precisely control the nanoparticle surface chemistry is relaxed. Indeed, we find that the nanoparticles provide effective kinetic stabilization when used simply bearing the native alkyl ligands emanating from the particle synthesis. While a similar kinetic stabilization was predicted for demixing polymer blends containing preferentially-wetted nanorods with anisotropic rod-rod repulsions,[42] prior experimental studies of demixing polymer blends containing selectively-wetted and well-dispersed particles have indicated only a slowing of the kinetics of phase separation, and no structural arrest, even at very high particle loadings.[43-46] Our findings indicate that a key to arresting a co-continuous blend morphology at modest volume fractions of preferentially-wetted particles is to have *attractive*, rather than *repulsive*, interactions between particles.

2.2 Experimental

2.2.1 Materials and sample preparation

Polystyrene (PS) was purchased from Polymer Source Inc. with a weight-average molecular weight (M_w) of 16,500 g/mol and a polydispersity index of 1.04. The poly(vinyl methyl ether) (PVME)was purchased from Polysciences Inc. with a M_w of 30,000 g/mol, in the form of 50 % aqueous solution and was dried at 120 ℃ under vacuum for three days prior to usage.

The CdSe nanospheres and nanorods coated with the native ligands trioctylphosphine oxide (TOPO), were prepared as described previously by others[47, 48] and repeatedly precipitated with a mixture of chloroform/methanol in a ratio of 3/10 for the CdSe nanospheres and toluene/methanol in a ratio 1/1 for the CdSe nanorods to remove most of the TOPO not bound to the nanoparticles. The CdSe-PS nanospheres were obtained by a ligand exchange process from CdSe-TOPO nanospheres and thiol-terminated PS (PS-SH) (MW 3,600 g/mol, PDI 1.3). The PS-SH was synthesized by atom transfer radical polymerization (ATRP) as described in the literature[49]. Typically, CdSe-TOPO nanospheres (181 mg) were refluxed with pyridine (2 mL) under inert atmosphere for 24 hours, and then precipitated into hexanes. The pyridine-covered nanospheres were heated overnight to 60 ℃ in anhydrous toluene (5 mL) containing PS-SH (300 mg). The CdSe-PS nanospheres were purified by precipitation into hexanes, centrifuged and washed several times with a mixture of chloroform/hexanes in a ratio of 3/10.

Blend films were prepared by casting from toluene solutions containing 10 wt% polymers and desired amount of nanoparticles, then vacuum dried for 3 days, resulting in homogeneous films with thicknesses of ~ 10 - 20 μm. Thermal quenching and subsequent annealing was performed by placing the blend films on glass substrates into vacuum ovens pre-heated to the desired temperature, allowing thermal equilibrium to be established rapidly.

2.2.2 Characterization methods

Cloud points were measured using a light scattering apparatus, with a He-Ne laser (632.8 nm) as the light source and the transmitted intensity of the direct beam was monitored. Above the cloud point, the transmitted intensity was found to decrease nearly linearly with temperature at constant heating rate. Thus, the cloud point was determined by extrapolating this linear portion of the curve back to its intersection with the baseline. All measurements were performed at several heating rates (1, 2, 3 and 5 ºC/min) under nitrogen atmosphere and the reported cloud point was taken as the linear extrapolation to a rate of 0 ºC/min.

Optical morphologies of the PS/PVME blend with nanoparticles were imaged using a Zeiss Axiovert 200 inverted optical microscope with 10x, 40x and 100x (oil-immersion) objectives. To obtain cross sectional structures, the blend films were embedded in an epoxy resin, and cured at room temperature for 24 h. Ultrathin transmission electron microscopy (TEM) sections with thicknesses of ~70 nm were obtained by cryo-microtomy (Leica Ultracut) using a diamond knife at -75 ºC to ensure that no alteration of the morphology took place during cutting. Bright field TEM measurements were performed with a JEOL 200CX electron microscope operated at an accelerating voltage of 200 kV.

Differential scanning calorimetry (DSC) measurements were carried out on a TA Instruments 2910 Modulated DSC. Samples were first heated from -50 to 120 ℃, cooled back to -50 ℃ and re-heated to 120 ℃ with each step at a rate of 10 ℃ /min. The glass transition temperature was determined from the second heating ramp.

2.3 Results and discussion

2.3.1 Phase separated morphologies of PS/PVME pure blend

As a model polymer system we used a blend of polystyrene/poly(vinyl methyl ether) (PS/PVME)[50] that exhibits a lower critical solution temperature (LCST). The cloud-point curve (Figure 1a, inset) for homogeneous blend films cast onto glass substrates from toluene solution[51] was determined by monitoring the transmission of light during heating. Small-angle light scattering patterns showed a diffuse isotropic ring of scattering, characteristic of a polymer blend undergoing spinodal decomposition, for a near-critical composition of PS/PVME blend (50 vol% PS), with a critical temperature of 160 ℃. After annealing for 24 h at 180 ℃, 20 ℃ above the critical temperature, the morphology coarsened into ~100-μm-sized droplets of a PVME-rich phase dispersed in a PS-rich matrix (Figure 2.1a). Smaller droplets were found dispersed within both phases, presumably resulting from a secondary phase separation within the initially formed PVME-rich and PS-rich phases (these small droplets were absent following a shallower quench to 170 ℃ for 24 h). Two off-critical compositions (35 and 70 vol% PS) were also investigated; TEM images after 24 h at 180 ℃ showed droplets of the minority phase in both cases (Figure 2.1b-c), indicating that the PS-rich phase is naturally darker in TEM micrographs obtained without staining, likely due to the degradation of PVME in the electron beam.[52]

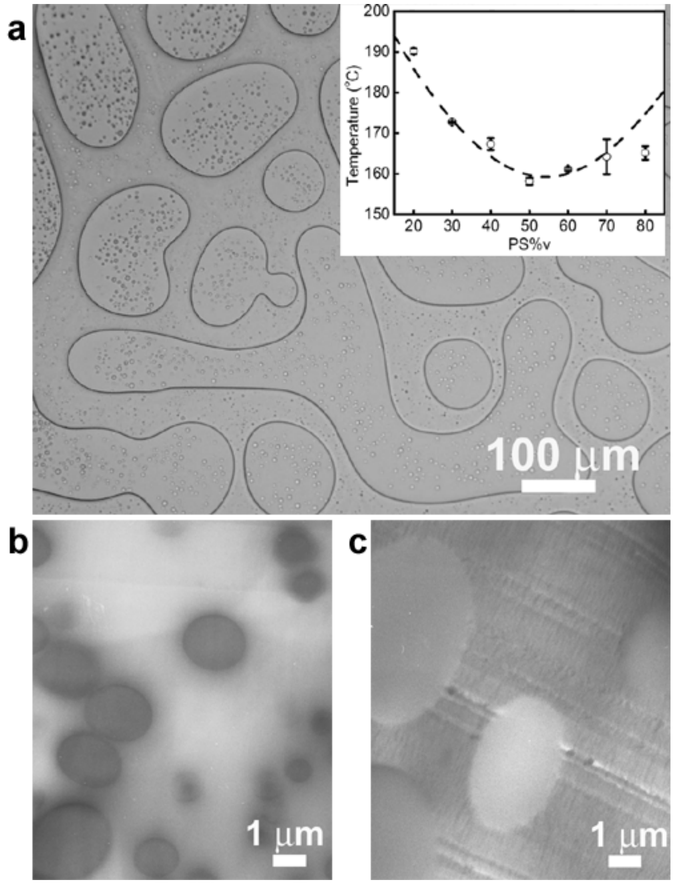

Figure 2.1 Phase separation of PS/PVME blends. (a) An optical image of a coarsened, phase separated PS/PVME blend (50 vol% PS) after annealing at 180 ℃ for 24 h (inset: cloud points for the PS/PVME blend; the dotted line is a guide to the eye). TEM images of phase separated off-critical blends containing (b) 35 vol% PS and (c) 70 vol% PS after annealing at 180 ℃ for 24 h, show brighter PVME-rich domains and darker PS-rich domains without staining.

2.3.2 Morphologies with the addition of CdSe-TOPO nanoparticles

Remarkably, adding only 2 vol% of CdSe-TOPO nanorods (Figure 2.2a; 8 nm by 30 nm), to the near-critical blend, yielded a co-continuous structure with a characteristic length of ~ 3 μm (Figure 2.2c) after annealing for 24 h at 170 ℃. In contrast, lowering the content of CdSe-TOPO nanorods to 1 vol% resulted in PVME-rich droplets dispersed in PS-rich matrix for the same quench conditions (Figure 2.2b). Co-continuity of the sample with 2 vol% nanorods was confirmed by TEM (Figure 2.2d), which showed the (darker) PS-rich continuous phase to be free of nanorods, while the lighter PVME-rich phase contained nanoparticles distributed throughout the entire domain, apparently reflecting a percolated network of rods.

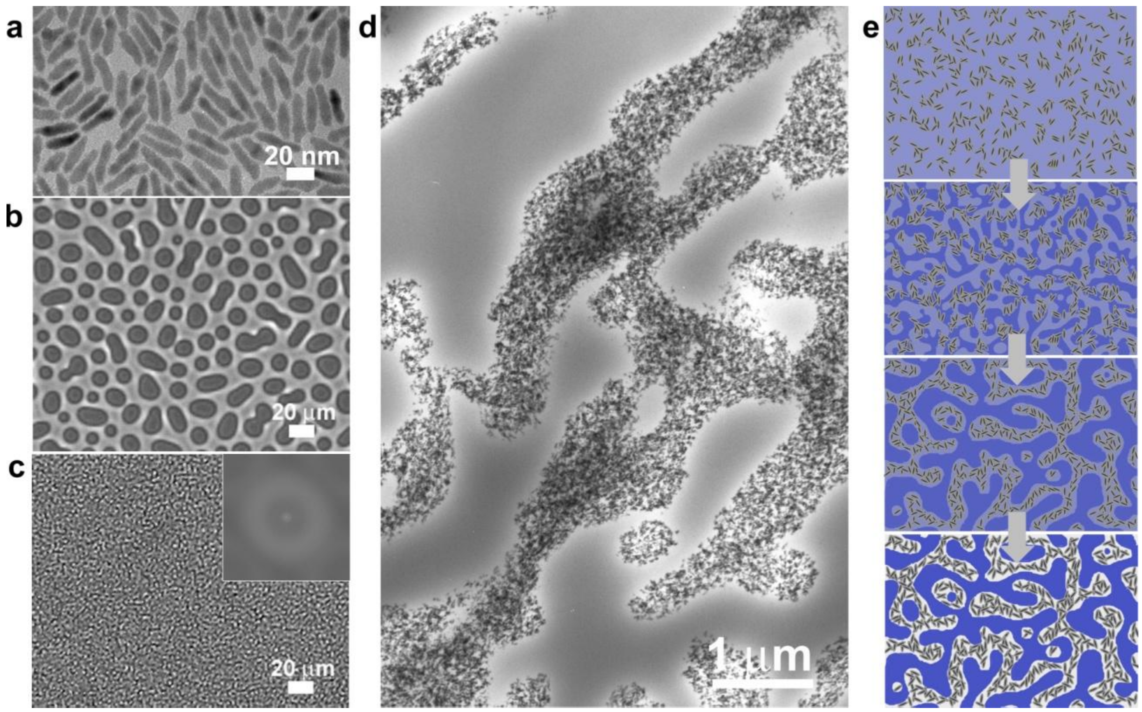

Figure 2.2 Phase separation of PS/PVME blends containing CdSe-TOPO nanorods. a) TEM image of CdSe-TOPO nanorods (core diameter ~ 8 nm and length ~30 nm). Optical micrographs of near-critical blends with (b) 1 vol% CdSe-TOPO nanorods reveal droplet structures after annealing at 170 ℃ for 24 h, while (c) 2 vol% nanorods leads to co-continuous structures (inset: the FFT pattern of the optical image); (d) a cross sectional TEM image of the sample in (c) confirms the co-continuity of the structure, and reveals formation of a percolated network of nanorods within the PVME phase. (e) A schematic of the process of nanorod network formation leading to kinetic arrest of a co-continuous structure.

The proposed mechanism of kinetic arrest is illustrated in Figure 2.2e: after heating the material above the LCST, nanorods aggregate into increasingly larger clusters, while the blend simultaneously undergoes spinodal demixing. Since the particles are preferentially wetted by the PVME-rich domains, they are selectively partitioned into this phase as it forms. Above a critical loading of nanorods (between 1 and 2 vol % for the system considered here), aggregation leads to formation of a network structure that percolates throughout the continuous PVME-rich domain. Once the nanoparticles have formed a sufficiently strong network, the polymer blend is kinetically pinned by surface energy, since further coarsening of the co-continuous blend structure would necessarily require contact between nanoparticles and the PS-rich phase.

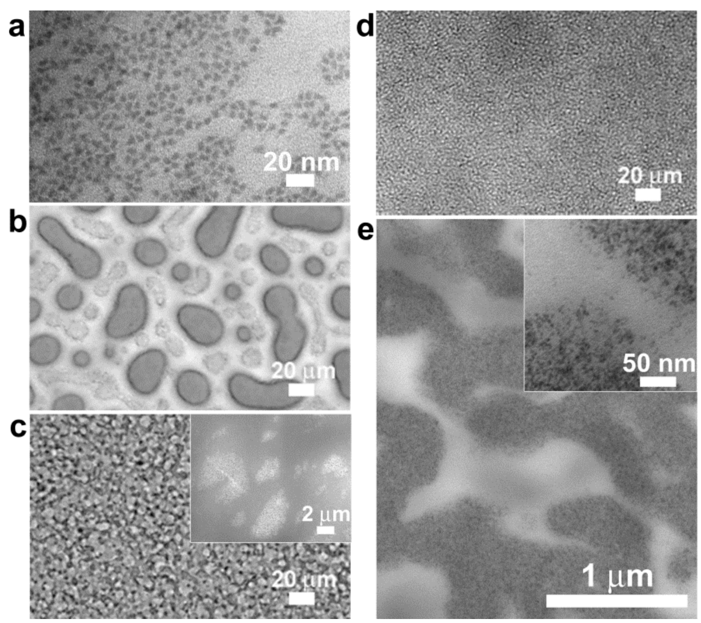

Figure 2.3 Phase separation of PS/PVME blends containing CdSe-TOPO nanospheres. (a) A TEM image of CdSe-TOPO nanospheres (core diameter ~ 4 nm). Optical micrographs of near-critical blends with (b) 1 vol% and (c) 2 vol% CdSe-TOPO spheres showed droplet structures after annealing at 170 ℃ for 24 h. However, at 3 vol% nanospheres, (d) optical micrographs and (e) TEM images revealed a co-continuous structure after annealing at 180 ℃ for 24 h.

The importance of nanoparticle shape was tested by addition of CdSe-TOPO nanospheres with 4-nm core diameters (Figure 2.3a). For both 1 and 2 vol% particles, the composite blends phase separated into droplet morphologies after 24 h at 170 °C, as shown in Figure 2.3b and 2.3c, respectively, though the domain sizes decreased from ~ 100 μm for the pure polymer blends to ~ 30 μm and ~ 5 μm for 1 and 2 vol% mixtures, respectively. TEM images of these samples (Figure 2.3c, inset) showed that the nanoparticles segregated to the PVME-rich dispersed phase. However, further increasing the nanosphere loading to 3 vol% led to a co-continuous structure, as shown in Figure 2.3d. Once again, TEM indicated that nanoparticles had apparently formed a percolating network within the PVME phase (Figure 2.3e), thus the mechanism for kinetic arrest with nanospheres is apparently equivalent to that illustrated in Figure 2.2e for nanorods. Greater concentrations of nanoparticles (e.g. 5 vol% in Figure 2.4) were also found to trap co-continuous structures, though a detailed study of the dependence of size scale on particle loading was not undertaken due to significant shifts in the cloud point at such high loadings.[46, 53-55]

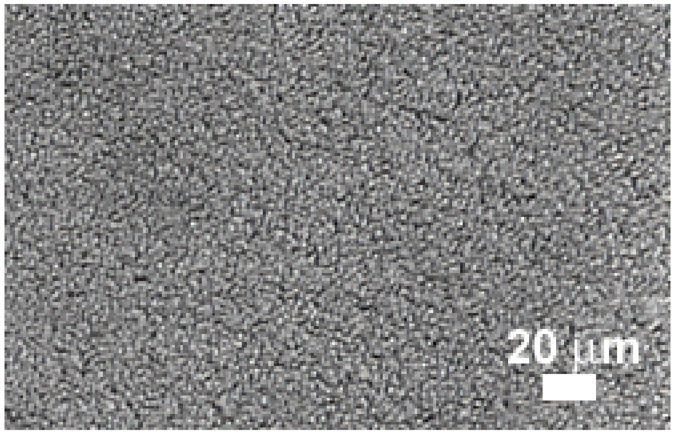

Figure 2.4 Phase separation of a near-critical PS/PVME blend with 5 vol% CdSe-TOPO nanospheres. The optical micrograph revealed a co-continuous structure after annealing at 205 ℃ for 24 hours.

2.3.3 Aggregation behavior of CdSe-TOPO nanorod

The kinetic arrest of co-continuous structures for demixing polymer blends containing preferentially-wetted nanorods with anisotropic repulsive interactions was previously predicted,[42] yielding an organization of the rods into chains, typically one rod in width, within the preferentially wetting fluid domains. Thus, while our experiments confirm the predicted intra-phase gelation behavior, both the fundamental mechanism and observed morphology differ considerably in our experiments. Simulations by Hore and Laradji using a different repulsive interparticle potentials showed only that preferentially wetted rods are more effective at slowing down the kinetics of spinodal demixing than an equal loading of spheres, with no kinetic arrest in either case.[56] Consistent with these predictions, several prior experimental studies of demixing polymer blends containing preferentially-wetted spherical colloidal particles found only a reduced rate of structural coarsening,[43-46] even when the particle loading was sufficient to form ordered colloidal structures within one phase.[43]

In our experiments, the observation that a network of nanoparticles percolates throughout the PVME domains at relatively small particle volume fractions indicates that kinetic arrest occurs due to *attractive* interactions between particles, in similar fashion to colloidal gels formed in suspensions of attractive particles.[57-61] While we anticipate that the driving force for aggregation in the present system is primarily enthalpic, due to the chemical mismatch between the alkyl ligands on the nanoparticle surfaces and both polymer phases, entropic depletion forces may also contribute.[62-64] The smaller critical loading of between 1 – 2 vol % necessary for nanorods, as compared to between 2 – 3 vol % for nanospheres, is qualitatively consistent with prior results that percolation threshold decreases inversely with particle aspect ratio,[65] though, given the larger sizes of the nanorods, we cannot rule out the possibility that particle size also plays a role. We note that aggregation-induced gelation of particles has recently been suggested to play a role in stabilizing co-continuous morphologies prepared by melt mixing of blends of polyethylene/polystyrene/carbon black[29] and of acrylonitrile-butadiene-styrene with polyamide 6 filled with carbon black.[34] the interfacial segregation of nanoparticles in a polymer blend has led to trapped structures with slightly finer size scales,[40] the key point of the current study is that careful control of the nanoparticle surface chemistry to achieve neutral wetting is unnecessary, providing an alternative approach to lock-in co-continuous morphologies.

To further elucidate the role of nanoparticle aggregation in the observed kinetic stabilization, we studied the morphology of several near critical PS/PVME blends containing nanoparticles subjected to different thermal treatments. We first studied the state of particle dispersion in blends after casting from toluene solution. As shown in Figure 2.5a, for a sample containing 1 vol % CdSe-TOPO nanorods, most of the nanorods were found to aggregate into ~ 100 nm sized anisotropic bundles within the otherwise homogeneous polymer blend. This suggests that the nanorods are thermodynamically immiscible with the PS/PVME blend, as expected given the lack of any favorable interactions between the alkyl ligands and the two polymers. However, as the solvent evaporates during casting, the rods only have time to form small aggregates before the system vitrifies. Upon annealing at 110 ℃, well above the glass transition temperature of the mixture (measured to be - 20 ℃ by DSC at a heating rate of 10 ℃/min) but below the LCST, numerous larger (μm-scale) aggregates were produced, as shown in Figure 2.5b, confirming that once mobility is restored to the system, the nanoparticles continue to aggregate. Notably, when a sample containing 2 vol% CdSe-TOPO nanorods was pre-annealed at 110 ℃ for 12 h to induce extensive pre-aggregation, a subsequent quench above the LCST (to 170 ℃) for 24 h led to ~40-μm-sized droplets (Figure 2.5c), rather than the co-continuous structure obtained for an otherwise equivalent sample heated directly from room temperature to above the LCST (Figure 2.2c). The formation of a percolated network of particles thus appears to require a fairly uniform initial dispersion of nanoparticles.

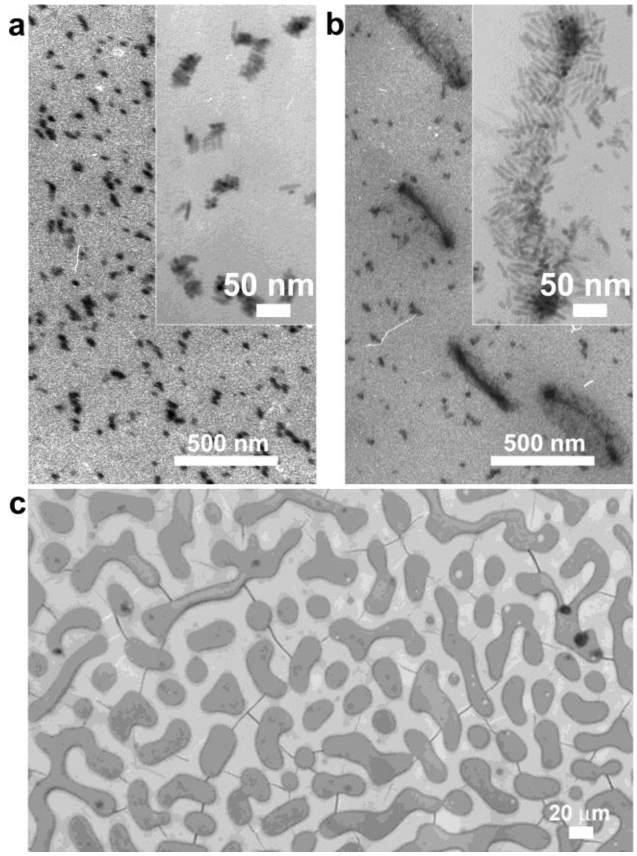

Figure 2.5 The influence of nanorod aggregation state on kinetic arrest of co-continuous structures. TEM images of a near-critical PS/PVME blend containing 1 vol% CdSe-TOPO nanorods (a) following solution casting reveal only slight aggregation, while (b) annealing at 110 ℃ for 12 h leads to extensive aggregation. (c) An optical micrograph of a near critical blend containing 2 vol% CdSe-TOPO nanorods pre-annealed at 110 ℃ for 12 h and then at 170 ℃ for 24 h shows large droplet structures, in sharp contrast to the co-continuous structure obtained without the pre-annealing step at 110 ℃. The lines running through lighter domains correspond to cracks through the polymer film introduced during cooling

2.3.4 Morphologies with the addition of CdSe-PS nanoparticles

We examined the importance of inter-particle interactions by using CdSe nanospheres coated with PS ligands having an average molecular weight of 3,600 g/mol (Figure 2.6a). The optical micrographs in Figure 2.6b-c show that even upon increasing the loading of CdSe-PS nanoparticles to 5 vol%, droplet morphologies persisted. The TEM image in Figure 2.6d shows that the CdSe-PS nanoparticles selectively segregated to the PS-rich matrix, as expected since they are coated with PS ligands. Furthermore, while some clustering of the CdSe-PS nanoparticles is observed, the aggregates formed are much smaller than in the case of CdSe-TOPO and consist of dispersed clusters rather than a percolating network (Figure 2.2d and 2.3e). These results underscore the fact that nanoparticle aggregation is the driving force for the formation of a percolated network and consequently to a kinetically-trapped co-continuous polymer blend morphology.

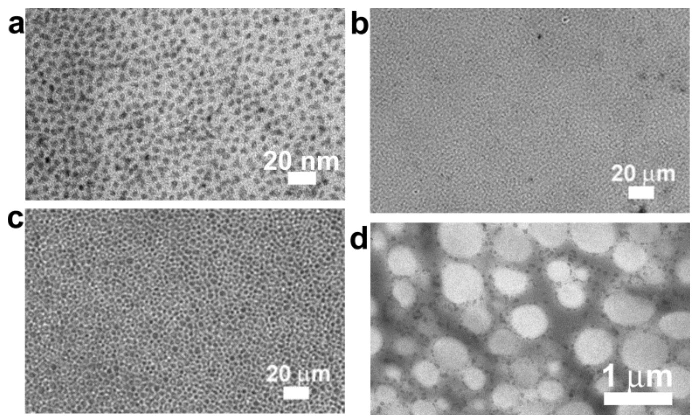

Figure 2.6 Phase separation of PS/PVME blends containing CdSe-PS nanospheres. (a) A TEM image of CdSe-PS nanospheres (core diameter ~ 4 nm). Optical micrographs of near-critical PS/PVME blends with (b) 2 vol% and (c) 5 vol% CdSe-PS nanospheres both show droplet structures after annealing for 24 h (at 180 ℃ and 190 ℃, respectively). (d) A TEM image of the sample in (b) confirms the droplet structure.

2.3.5 Kinetically arrested co-continuous morphologies

Moreover, we studied the stability of the co-continuous structures upon annealing of near-critical blends containing 2 vol% CdSe-TOPO nanorods. Following a quench to 170 ℃, a co-continuous morphology was observed after 1 h of annealing above the LCST, and only a slight coarsening (to a length-scale of ~ 4 μm) took place after 48 h of annealing (Figure 2.7a and 2.7b). For the same composition at 180 ℃, larger co-continuous domains (~ 14 μm) were obtained, but again with little coarsening over time. While the initial length-scale for spinodal phase separation should be sub-micron and should decrease with increasing quench depth[66], both the larger interfacial tension and lower viscosity at higher temperature will drive more rapid coarsening. Since some time is required for the nanoparticles to aggregate into a network, the faster coarsening at larger quench depths apparently dominates the length-scale at kinetic arrest. (We also note that secondary phase separation occurred when the system was quenched to 180 ℃ for 24 h, as seen in Figure 2.7d, consistent with the behavior of the pure blend behavior shown in Figure 2.1b.) To further verify that the co-continuous morphology was truly arrested, we also studied a sample initially quenched to 170 ℃ for 48h, followed by a further annealing at 180 ℃ for 24 h. In this case, the co-continuous morphology (Figure 2.7e) maintained a length scale of ~4 μm, characteristic of a 170 ℃ quench, rather than coarsening to the larger sizes typical of a 180 ℃ quench.

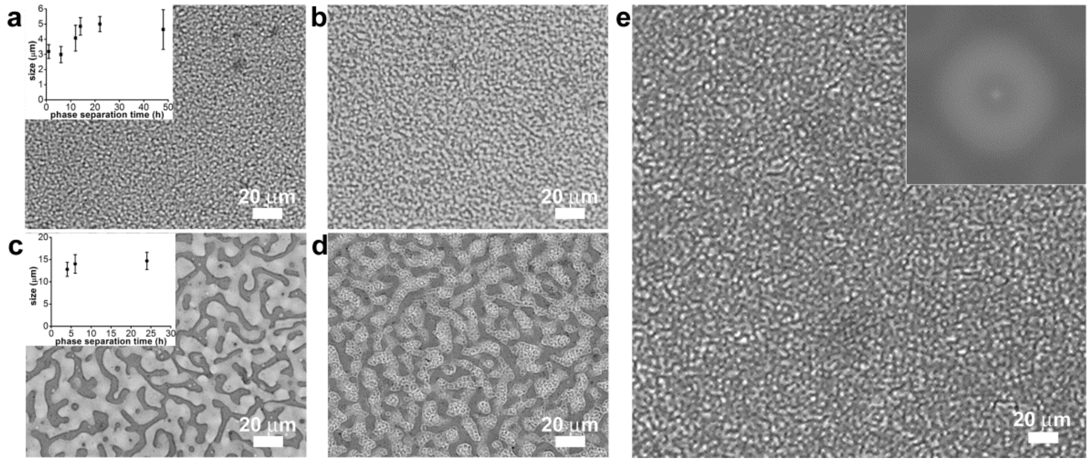

Figure 2.7 Stability of co-continuous structures upon thermal annealing. Optical micrographs of near-critical PS/PVME blends containing 2 vol% CdSe-TOPO nanorods quenched to 170 °C for (a) 1 h and (b) 12 h reveal little coarsening over this time scale. For identical samples quenched to 180 °C, the characteristic wavelength of the co-continuous structure is larger, but again little coarsening is observed between (c) 4 h and (d) 24 h of annealing. The insets in (a) and (c) show the measured length-scale as a function of annealing time. (e) A sample of the same composition annealed first at 170 °C for 48 h and subsequently at 180 °C for 24 h retains the structure formed at 170 °C, providing further evidence for the kinetic stability of these co-continuous structures (inset: FFT pattern of the optical image).

2.4 Conclusions

In summary, we have shown that nanorods and nanospheres can kinetically arrest co-continuous morphologies in demixing polymer blends due to gelation of the nanoparticles within one of the polymer phases. Network formation requires a critical concentration of nanoparticles, which is found to be lower for nanorods than for nanospheres. We suggest that this provides a more general route to the kinetic trapping of demixing fluids than interfacial jamming since the stringent requirement of obtaining neutral wetting of particles is relaxed, although a corresponding sensitivity to the initial aggregation state of the particles is introduced. Our results establish that intra-phase gelation is a viable and potentially very flexible route to prepare co-continuous micro- and possibly nanostructured blends of polymers and nanoparticles. Future work will be focused on studying the interplay between the kinetics of nanoparticle aggregation and those of spinodal decomposition.

Reference

1. Hoppe, H. and N.S. Sariciftci, *Morphology of polymer/fullerene bulk heterojunction solar cells.* Journal of Materials Chemistry, 2006. **16**(1): p. 45-61.
2. Kesting, R.E., *Synthetic polymeric membranes: a structural perspective*. 1985, New York: Wiley-Interscience. 368.
3. Ramos, A.R. and R.E. Cohen, *Influence of diblock copolymers on structure and properties of polybutadiene-polyisoprene blends.* Polymer Engineering and Science, 1977. **17**(8): p. 639-646.
4. Leibler, L., *Theory of phase-equilibria in mixtures of copolymers and homopolymers. 2. Interfaces near the consolute point.* Macromolecules, 1982. **15**(5): p. 1283-1290.
5. Noolandi, J. and K.M. Hong, *Effect of block copolymers at a demixed homopolymer interface.* Macromolecules, 1984. **17**(8): p. 1531-1537.
6. Leibler, L., *Emulsifying effects of block copolymers in incompatible polymer blends.* Makromolekulare Chemie-Macromolecular Symposia, 1988. **16**: p. 1-17.
7. Anastasiadis, S.H., I. Gancarz, and J.T. Koberstein, *Compatibilizing effect of block copolymers added to the polymer polymer interface.* Macromolecules, 1989. **22**(3): p. 1449-1453.
8. Shull, K.R., et al., *Segregation of Block Copolymers to Interfaces between Immiscible Homopolymers.* Macromolecules, 1990. **23**(22): p. 4780-4787.
9. Park, D.W. and R.J. Roe, *Effect of added block copolymer on the phase-separation kinetics of a polymer blend .2. optical microscopic observations.* Macromolecules, 1991. **24**(19): p. 5324-5329.
10. Semenov, A.N., *Theory of diblock-copolymer segregation to the interface and free-surface of a homopolymer layer.* Macromolecules, 1992. **25**(19): p. 4967-4977.
11. Shull, K.R., et al., *Vanishing interfacial-tension in an immiscible polymer blend.* Journal of Chemical Physics, 1992. **97**(3): p. 2095-2104.
12. Balsara, N.P., et al., *Thermodynamic interactions and correlations in mixtures of 2 homopolymers and a block-copolymer by small-angle neutron-scattering.* Journal of Chemical Physics, 1993. **99**(12): p. 10011-10020.
13. Macosko, C.W., et al., *Compatibilizers for melt blending: Premade block copolymers.* Macromolecules, 1996. **29**(17): p. 5590-5598.
14. Bates, F.S., et al., *Polymeric bicontinuous microemulsions.* Physical Review Letters, 1997. **79**(5): p. 849-852.

15. Mekhilef, N., B.D. Favis, and P.J. Carreau, *Morphological stability, interfacial tension, and dual-phase continuity in polystyrene-polyethylene blends.* Journal of Polymer Science Part B-Polymer Physics, 1997. **35**(2): p. 293-308.
16. Hudson, S.D. and A.M. Jamieson, *Morphology and Properties of Blends Containing Block Copolymers*. Polymer Blends, Vol. 1: Formulation, ed. D.R. Paul and C.B. Bucknall. Vol. 15. 2000, New York: John Wiley & Sons, Inc. 600.
17. Veenstra, H., J. Van Dam, and A.P. de Boer, *On the coarsening of co-continuous morphologies in polymer blends: effect of interfacial tension, viscosity and physical cross-links.* Polymer, 2000. **41**(8): p. 3037-3045.
18. Kim, J.K., et al., *Phase behavior of polystyrene and poly(n-pentyl methacrylate) blend with small amounts of symmetric polystyrene-block-poly(n-pentyl methacrylate) copolymers.* Macromolecules, 2004. **37**(23): p. 8599-8605.
19. Galloway, J.A., et al., *Block copolymer compatibilization of cocontinuous polymer blends.* Polymer, 2005. **46**(1): p. 183-191.
20. Yuan, Z.H. and B.D. Favis, *Influence of the efficacy of interfacial modification on the coarsening of cocontinuous PS/HDPE blends during quiescent annealing.* Journal of Polymer Science Part B-Polymer Physics, 2006. **44**(4): p. 711-721.
21. Bell, J.R., et al., *Annealing of cocontinuous polymer blends: effect of block copolymer molecular weight and architecture.* Macromolecules, 2010. **43**(11): p. 5024-5032.
22. Roe, R.J. and C.M. Kuo, *Effect of added block copolymer on phase-separation kinetics of a polymer blend .1. A light-scattering study.* Macromolecules, 1990. **23**(21): p. 4635-4640.
23. Lyu, S., et al., *Role of block copolymers on suppression of droplet coalescence.* Macromolecules, 2002. **35**(20): p. 7845-7855.
24. Kim, B.S., T. Chiba, and T. Inoue, *Morphology development via reaction-induced phase-separation in epoxy poly(ether sulfone) blends - morphology control using poly(ether sulfone) with functional end-groups.* Polymer, 1995. **36**(1): p. 43-47.
25. Kim, J.K. and H. Lee, *The effect of PS-GMA as an in situ compatibilizer on the morphology and rheological properties of the immiscible PBT/PS blend.* Polymer, 1996. **37**(2): p. 305-311.
26. Pernot, H., et al., *Design and properties of co-continuous nanostructured polymers by reactive blending.* Nature Materials, 2002. **1**(1): p. 54-58.
27. Ishino, S., et al., *Designing a polymer blend with phase separation tunable by visible light for computer-assisted irradiation experiments.* Macromolecular Rapid Communications, 2006. **27**(10): p. 758-762.
28. Gubbels, F., et al., *Selective Localization of Carbon-Black in Immiscible Polymer Blends - a Useful Tool to Design Electrical Conductive Composites.* Macromolecules, 1994. **27**(7): p. 1972-1974.
29. Gubbels, F., et al., *Design of electrical conductive composites - key role of the morphology on the electrical-properties of carbon-black filled polymer blends.* Macromolecules, 1995. **28**(5): p. 1559-1566.

30. Potschke, P. and D.R. Paul, *Formation of Co-continuous structures in melt-mixed immiscible polymer blends.* Journal of Macromolecular Science-Polymer Reviews, 2003. **C43**(1): p. 87-141.
31. Li, Y.J. and H. Shimizu, *Novel morphologies of poly(phenylene oxide) (PPO)/polyamide 6 (PA6) blend nanocomposites.* Polymer, 2004. **45**(22): p. 7381-7388.
32. Zou, H., et al., *Manipulating the phase morphology in PPS/PA66 blends using clay.* Journal of Applied Polymer Science, 2007. **106**(4): p. 2238-2250.
33. Filippone, G., et al., *The role of organoclay in promoting co-continuous morphology in high-density poly(ethylene)/poly(amide) 6 blends.* Polymer, 2008. **49**(5): p. 1312-1322.
34. Wu, G.Z., B.P. Li, and J.D. Jiang, *Carbon black self-networking induced co-continuity of immiscible polymer blends.* Polymer, 2010. **51**(9): p. 2077-2083.
35. Zhang, Q., H. Yang, and Q. Fu, *Kinetics-controlled compatibilization of immiscible polypropylene/polystyrene blends using nano-SiO2 particles.* Polymer, 2004. **45**(6): p. 1913-1922.
36. Wu, K.H. and S.Y. Lu, *Preferential partition of nanowires in thin films of immiscible polymer blends.* Macromolecular Rapid Communications, 2006. **27**(6): p. 424-429.
37. Robeson, L.M., *Polymer Blends: A Comprehensive Review*. 2007, Cicinnati, OH: Hanser Gardner Publications, Inc.
38. Cahn, J.W., *On spinodal decomposition.* Acta Metallurgica, 1961. **9**(9): p. 795-801.
39. Stratford, K., et al., *Colloidal jamming at interfaces: A route to fluid-bicontinuous gels.* Science, 2005. **309**(5744): p. 2198-2201.
40. Chung, H., et al., *Self-regulated structures in nanocomposites by directed nanoparticle assembly.* Nano Letters, 2005. **5**(10): p. 1878-1882.
41. Herzig, E.M., et al., *Bicontinuous emulsions stabilized solely by colloidal particles.* Nature Materials, 2007. **6**(12): p. 966-971.
42. Peng, G.W., et al., *Forming supramolecular networks from nanoscale rods in binary, phase-separating mixtures.* Science, 2000. **288**(5472): p. 1802-1804.
43. Tanaka, H., A.J. Lovinger, and D.D. Davis, *Pattern evolution caused by dynamic coupling between wetting and phase-separation in binary-liquid mixture containing glass particles.* Physical Review Letters, 1994. **72**(16): p. 2581-2584.
44. Yurekli, K., et al., *Influence of layered silicates on the phase-separated morphology of PS-PVME blends.* Macromolecules, 2003. **36**(19): p. 7256-7267.
45. Chung, H.J., et al., *Mobile nanoparticles and their effect on phase separation dynamics in thin-film polymer blends.* Europhysics Letters, 2004. **68**(2): p. 219-225.
46. Gharachorlou, A. and F. Goharpey, *Rheologically determined phase behavior of LCST blends in the presence of spherical nanoparticles.* Macromolecules, 2008. **41**(9): p. 3276-3283.
47. Peng, Z.A. and X.G. Peng, *Nearly monodisperse and shape-controlled CdSe nanocrystals via alternative routes: Nucleation and growth.* Journal of the American Chemical Society, 2002. **124**(13): p. 3343-3353.

48. Peng, Z.A. and X.G. Peng, *Formation of high-quality CdTe, CdSe, and CdS nanocrystals using CdO as precursor.* Journal of the American Chemical Society, 2001. **123**(1): p. 183-184.
49. Garamszegi, L., et al., *Synthesis of thiol end-functional polystyrene via atom transfer radical polymerization.* Reactive & Functional Polymers, 2003. **55**(2): p. 179-183.
50. Nishi, T., T.T. Wang, and T.K. Kwei, *Thermally induced phase separation behavior of compatible polymer mixtures.* Macromolecules, 1975. **8**(2): p. 227-234.
51. Bank, M., Leffingw.J, and C. Thies, *Influence of solvent upon compatibility of polystyrene and poly(vinyl methyl ether).* Macromolecules, 1971. **4**(1): p. 43.
52. Polios, I.S., et al., *Late stages of phase separation in a binary polymer blend studied by rheology, optical and electron microscopy, and solid state NMR.* Macromolecules, 1997. **30**(15): p. 4470-4480.
53. Karim, A., et al., *Modification of the phase stability of polymer blends by fillers.* Polymer, 2000. **41**(23): p. 8455-8458.
54. Lipatov, Y.S., *Polymer blends and interpenetrating polymer networks at the interface with solids.* Progress in Polymer Science, 2002. **27**(9): p. 1721-1801.
55. Ginzburg, V.V., *Influence of nanoparticles on miscibility of polymer blends. A simple theory.* Macromolecules, 2005. **38**(6): p. 2362-2367.
56. Hore, M.J.A. and M. Laradji, *Prospects of nanorods as an emulsifying agent of immiscible blends.* Journal of Chemical Physics, 2008. **128**(5): p. 054901.
57. Lin, M.Y., et al., *Universality in colloid aggregation.* Nature, 1989. **339**(6223): p. 360-362.
58. Poon, W.C.K. and M.D. Haw, *Mesoscopic structure formation in colloidal aggregation and gelation.* Advances in Colloid and Interface Science, 1997. **73**: p. 71-126.
59. Trappe, V., et al., *Jamming phase diagram for attractive particles.* Nature, 2001. **411**(6839): p. 772-775.
60. Zaccarelli, E., *Colloidal gels: equilibrium and non-equilibrium routes.* Journal of Physics-Condensed Matter, 2007. **19**(32): p. 323101.
61. Lu, P.J., et al., *Gelation of particles with short-range attraction.* Nature, 2008. **453**(7194): p. 499-U4.
62. Araki, T. and H. Tanaka, *Wetting-induced depletion interaction between particles in a phase-separating liquid mixture.* Physical Review E, 2006. **73**(6): p. 061506.
63. Frischknecht, A.L., *Forces between nanorods with end-adsorbed chains in a homopolymer melt.* Journal of Chemical Physics, 2008. **128**(22): p. 224902.
64. Hore, M.J.A. and R.J. Composto, *Nanorod Self-Assembly for Tuning Optical Absorption.* ACS Nano, 2010. **4**(11): p. 6941-6949.
65. Yi, J.Y. and G.M. Choi, *Percolation behavior of conductor-insulator composites with varying aspect ratio of conductive fiber.* Journal of Electroceramics, 1999. **3**(4): p. 361-369.
66. Van Aartsen, J.J., *Theoretical observations on spinodal decomposition of polymer solutions.* European Polymer Journal, 1970. **6**(7): p. 919.

CHAPTER 3

FABRICATION OF CO-CONTINUOUS NANO-STRUCTURED AND POROUS POLYMER MEMBRANES THROUGH SPINODAL DECOMPOSITION OF HOMOPOLYMER/RANDOM COPOLYMER BLENDS†

3.1 Introduction

Multi-phase polymeric materials with nanoscale structural co-continuity are of importance, for example, as active layers of organic photovoltaic cells wherein donor and acceptor domains must interpenetrate on a scale commensurate with the diffusion length of excitons,[1] or as membranes for separations and fuel cells where continuous pathways for mass transport are required within a supporting matrix. [2] One route to such nanostructures is the self assembly of diblock copolymers into the bicontinuous gyroid morphology; however, the requirements on the segmental interaction parameter and polymer composition to achieve this structure are restrictive and often difficult to achieve.[3] Bicontinuous microemulsions,[4] consisting of a nearly symmetric block copolymer blended with the corresponding homopolymers, also provide thermodynamically stable co-continuous structures of ~100 nm in size, but are similarly only found over narrow ranges in phase space. Reactive blending, i.e., in situ formation of block copolymers in an immiscible blend, can also yield nanoscale co-continuous structures under some conditions, but this method typically requires suitably functionalized reactive precursor polymers.[5-7]

† Reproduced with permission from *Angewandte Chemie International Edition* to be submitted for publication. Unpublished work copyright 2011, Wiley-VCH Verlag GmbH & Co. KGaA.

Spinodal phase separation of a polymer blend, triggered by quenching a homogeneous mixture of near critical composition into the spinodal envelope, ,[8] presents an alternate route to co-continuous morphologies, provided that the structure can be kinetically trapped at the desired length scale. The characteristic wavelength ξ_o of the initially formed co-continuous structure is determined by a balance between diffusion and interfacial energy. For binary polymer blends, this can be expressed in terms of the size of the polymer chain R_g and the value of the interaction parameter χ at the quench temperature as:[9]

$$\xi_o \sim R_g \left(\frac{\chi - \chi_s}{\chi_s} \right)^{-1/2} \tag{3.1}$$

where χ_s is the value of the interaction parameter at the spinodal curve. While this initial length-scale is generally sub-micron, the mixture can reduce its total energy by decreasing interfacial area, and thus the initial phase separated morphology evolves into increasingly large domains via a self-similar coarsening of the co-continuous structure. Due to the large molecular weights of polymers, thermally-induced demixing is only feasible for a limited set of partially miscible pairs with an interaction parameter that is both small and significantly temperature dependent, e.g. polystyrene/polyvinyl methyl ether (PS/PVME)[10, 11] or polymethyl methacrylate/poly(styrene-ran-acrylonitrile) (PMMA/SAN).[12, 13] Further, due to the tendency of these systems to undergo rapid structural coarsening, kinetic trapping of co-continuous morphologies has so far only been achieved on the micron size scale.[14-16]

Solvent induced phase separation (SIPS),[17, 18] i.e., demixing driven by removal of a common solvent, is a more general method for immiscible polymer blends.

Moreover, since rapid solvent evaporation may be achieved during the process, large quench depths may be achieved, which in principle according to Equation 3.1 may lead to the formation of co-continuous structures with nanometer-scale domains. However, the solvent also enhances mobility of the polymers, leading to rapid structural coarsening. As a result, SIPS has typically led to the formation of rather large-scale structures (~10 μm).[19-21] Additionally, since the solvent usually has a preference for one of the polymers,[22] nucleation and growth is the typical method of separation for most compositions and quench depths. While spin-coating of blend solutions from almost nonselective solvents has been shown to lead to spinodal decomposition, the resulting kinetically-trapped co-continuous structures are typically micron-size and therefore only two-dimensional in nature, and further are found only over a narrow range of blend compositions,[23] and with nearly balanced substrate interactions.[24-27] Furthermore, even a slight difference in the component solubilities gives rise to significant topographic features of the resulting films, since the less soluble component solidifies first and eventually forms elevated domains. .[25, 28, 29] We note that while it has been argued that SIPS can generate phase separated morphologies on the size scale of tens of nanometers,[30-32] recent work has demonstrated that such morphologies are formed as a result of crystallization, rather than spinodal demixing.[33-36]

In the current report, we demonstrate a SIPS approach for mixtures of homopolymers (A) with random copolymers (A-*r*-B) that yields smooth films with nanoscale co-continuous morphologies. The compositions of the random copolymers are chosen to tune the effective interaction parameter between the polymers χ_{eff}. This allows the quench depth into the spinodal envelope achieved during solvent casting to be modulated, and therefore enables the system to be trapped by vitrification during the initial stages of spinodal decomposition. We demonstrate that a simple spin casting process leads to co-continuous morphologies with characteristic length scales down to several tens of nanometers, and that the method is not highly sensitive to the choice of solvent or substrate chemistry.

3.2 Experimental

3.2.1 Materials and sample preparation

The polymers used in this work were polystyrene (PS), poly(2-vinylpyridine) (P2VP) and poly(styrene-ran-2-vinylpyridine) (P(S-*r*-2VP)), as listed in Table 1. All polymers were purchased from Polymer Source and used without purification, with the exception of PS32k which was synthesized by standard atom transfer radical polymerization (ATRP) method. Solvents for casting were analytic grade toluene and chloroform (Sigma Aldrich, used without purification). Films were prepared by spin-casting or drop casting from toluene, or chloroform when indicated, solutions containing a specified weight ratio of different polymers, and an overall polymer concentration of 50 - 100 mg / mL. Sample drying was carried out in a vacuum oven at room temperature for 2 h for spin-cast films or overnight for drop-cast ones. The resulting film thicknesses ranged from 300 nm to 1.2 μm depending on solution concentration, and spin-coating speed and duration, or ~ 10 μm in the case of drop-casting.

Table 3-1 Summary of polymers used in this study

	styrene % mol	M_w (kg/mol)	M_n (kg/mol)	PDI
P(S-*r*-2VP)39k	78%	39	28	1.38
P(S-*r*-2VP)56k	70%	56	40.5	1.38
PS26k	100%	26	25	1.04
PS32k	100%	32.4	30	1.08
PS34k	100%	34	33	1.04
PS55k	100%	55	54	1.02
PS136k	100%	136	120	1.13
PS570k	100%	570	520	1.10
P2VP38k	-	37.5	35	1.07

Typically, silicon wafers with a native oxide layer were used as the substrate. Organic residues on the silicon oxide surface were removed by cleaning the silicon wafer under a jet of CO_2-ice crystals ("snow-jet"). Gold surfaces were prepared by sputtering a thin gold layer onto the silicon substrate and used immediately after gold deposition to avoid contamination. Mica and Kapton (HN500, DuPont) films were also used as substrates without any additional preparation. Selective removal of random copolymer-rich phases was achieved by soaking films in a 1:1 (vol.) mixture of methanol and acetic acid, and subsequently drying in air.

3.2.2 Characterization methods

Film structures were investigated by transmission electron microscopy (TEM). To prepare the samples, the blend films on silicon wafers with a thick oxide layer were floated onto 5 wt % aqueous hydrofluoric acid solution and retrieved with a copper grid. To obtain cross sectional structures, a thin layer of gold was first coated on the samples to mark the polymer-air interface. The blend films were then embedded into an epoxy resin and cured at 60 ℃ for 24 h. Ultrathin TEM sections with thicknesses of ~70 nm were obtained by microtomy (Leica Ultracut) using a diamond knife at room temperature. The TEM samples of the blend films were exposed to I_2 vapor for 3 – 5 h, such that the 2VP-containing phase appeared darker than the PS phase. The Bright field TEM measurements were performed with a JEOL 200CX electron microscope operated at an accelerating voltage of 200 kV.

The surface topographies of the porous membranes were investigated by scanning electron microscopy (SEM). For side-view SEM measurements, the samples were cracked to expose the interior of the porous membrane and mounted vertically to reveal the cross sections. A thin layer of gold was coated on the samples after cleaving, which were imaged using a JEOL 6320 FXV SEM at an accelerating voltage of 5 kV.

Transmission small angle X-ray scattering (SAXS) experiments were conducted at beamline 7.3.3 at the Advanced Light Source (ALS), Lawrence Berkeley National Laboratory (LBNL). The wavelength of incident X-ray was 0.124 nm and the sample-to-detector distance was 4097 mm. The scattering signals were collected by a two dimensional Pilatus 1M detector with a high dynamics range of 20 bits and an active area of 169*179mm^2. The resulting two-dimensional scattering data were averaged azimuthally to obtain intensity at each value of the scattering vector $q = 4\pi/\lambda * \sin(\theta/2)$, where θ is the total scattering angle.

3.3 Results and discussion

3.3.1 Well-defined nanoscale co-continuous morphologies via spinodal demixing

We design our polymer blend system based on the immiscible pair of PS and P2VP which exhibit a value of χ of ~ 0.1.[37, 38] According to mean-field theory of phase behavior in random copolymer blends,[39-41] we expect that this interaction strength may be modulated by incorporating styrene monomers into the P2VP chains, i.e. using P(S-*r*-2VP) random copolymers. While previous studies on similar homopolymer/random copolymer blends exist, their primary focus has been testing the validity of theoretical descriptions of the phase behavior and extracting interaction parameters between the respective homopolymer pairs.[29, 37, 40, 42-47] For a binary A/A_x-*r*-B_{1-x} mixture the effective interaction parameter should depend on the co-monomer mole fraction,[37, 48] assuming equal segment volumes, according to:

$$\chi_{eff} = (1-x)^2 \chi_{AB} . \tag{3.2}$$

To achieve a modest degree of immiscibility, i.e. $\chi_{eff} N \sim 5$, where N is the average degree of polymerization, we use a random copolymer P(S-*r*-2VP) with molecular weight of 56 kg/mol (denoted as P(S-*r*-2VP)56k), and a mole fraction of styrene of x = 0.70, and blend it with PS homopolymers with molecular weights of 26, 34, and 55 kg/mol (PS26k, PS34k and PS55k). Phase separation is induced by solvent evaporation during spin-casting of a 1:1 by weight mixture of PS and P(S-*r*-2VP) in toluene. Remarkably, as shown by the TEM images in Figure 3.1, the result of this simple process is films with co-continuous structures with characteristic size-scales as small as ~ 80 nm in the case of PS26k/P(S-*r*-2VP)56k (Figure 3.1a), which is unusual for macrophase separated polymer blends. Since the size scale is considerably less than the film thickness (~ 500 nm), the co-continuous morphology is truly three-dimensional, rather than the lateral, two-dimensionally co-continuous micron-scale structures reported by others.[23, 25-28] This is verified by cross-sectional TEM (Figure 3.1b), which confirms that the co-continuous morphology penetrates throughout the thickness, and reveals that the film has a smooth surface (marked by the dark line, which corresponds to a deposited film of gold).

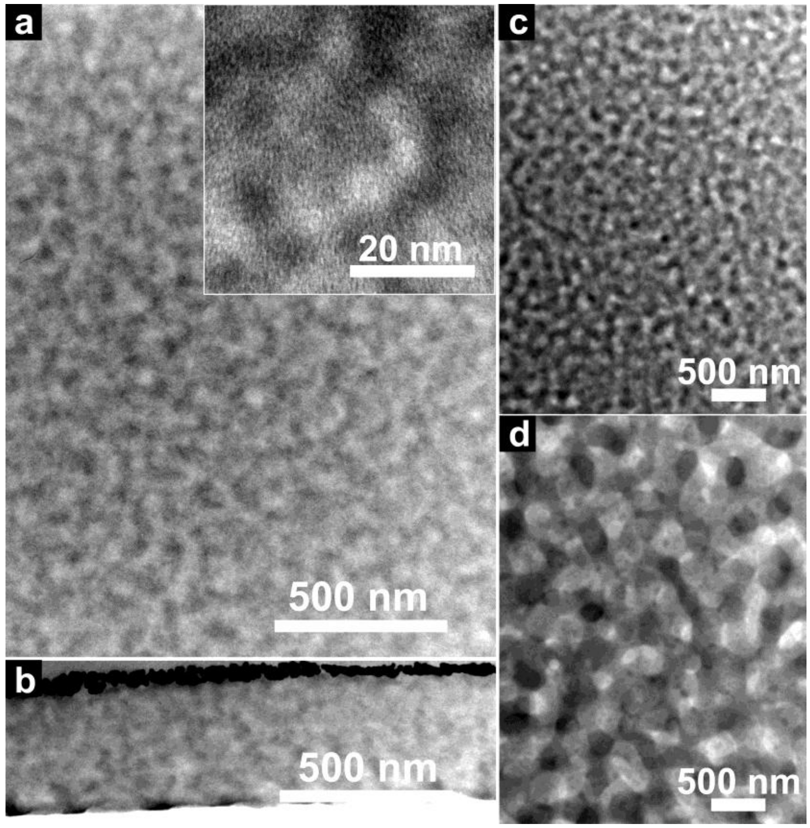

Figure 3.1 Plan-view TEM images of 1:1 (wt.) blends of PS/P(S-*r*-2VP)56k with PS molecular weights of (a) 26k, (c) 34k, (d) 55k showing co-continuous nanostructures with molecular-weight dependent sizes. (b) A cross-sectional TEM image of the same sample as in (a) confirms that the co-continuous structure spans the film thickness. In all images, P(S-*r*-2VP) rich phases appear darker due to staining with I_2 vapor.

During spin coating, solvent evaporation apparently quenches the system into the spinodal region of the phase diagram, so that demixing occurs by formation of a co-continuous morphology with a small characteristic wavelength. To reduce interfacial area, these domains will coarsen over time, however, the speed of solvent removal is sufficiently fast to kinetically trap the structure due to vitrification at an early stage of coarsening. From Flory-Huggins theory, we estimate the critical interaction parameter necessary to drive phase separation,

$$\chi_c = \frac{1}{2}\left(\frac{1}{\sqrt{N_1}} + \frac{1}{\sqrt{N_2}}\right)^2, \tag{3.3}$$

as ~ 6 x 10^{-3} for the PS26k/P(S-*r*-2VP)56k blend. Assuming that the presence of solvent at a volume fraction of ϕ_s serves only to dilute the unfavorable interactions between polymers,[49] phase separation should occur when $\chi_c = (1\text{-}\phi_s)\, \chi_{eff}$. From these considerations, we estimate that demixing takes place at $\phi_s \approx 40$ vol %. From the Fox equation and the glass transition temperatures (T_g) of the components (116 K for toluene[50] and ~ 373 K for the polymers), we estimate that T_g of the mixture will reach room temperature at $\phi_s \approx 12$ vol %. Thus, the polymer solution is already quite concentrated when demixing begins, and its viscosity will climb rapidly as solvent is further evaporated and the glassy state is approached, allowing for the kinetic trapping of nanoscale co-continuous structures.

3.3.2 Controlling the size of co-continuous morphologies by molecular weight

Examining the effects of molecular weight provides further support for this proposed mechanism. Increasing N should lead to phase separation at larger ϕ_s, allowing for more extensive coarsening of the structure prior to vitrification, and thus providing a means to tune length scale by adjusting the molecular weight of either polymer. As expected, larger co-continuous structures were obtained for PS34k and PS55k, as shown in Figure 3.1b and c. Notably, the characteristic length scales observed, ~ 150 and 500 nm, respectively, depend more strongly on N than would be expected based on Equation

3.1, consistent with the observed length scale being set by the amount of coarsening before vitrification, rather than the initial length scale of demixing.

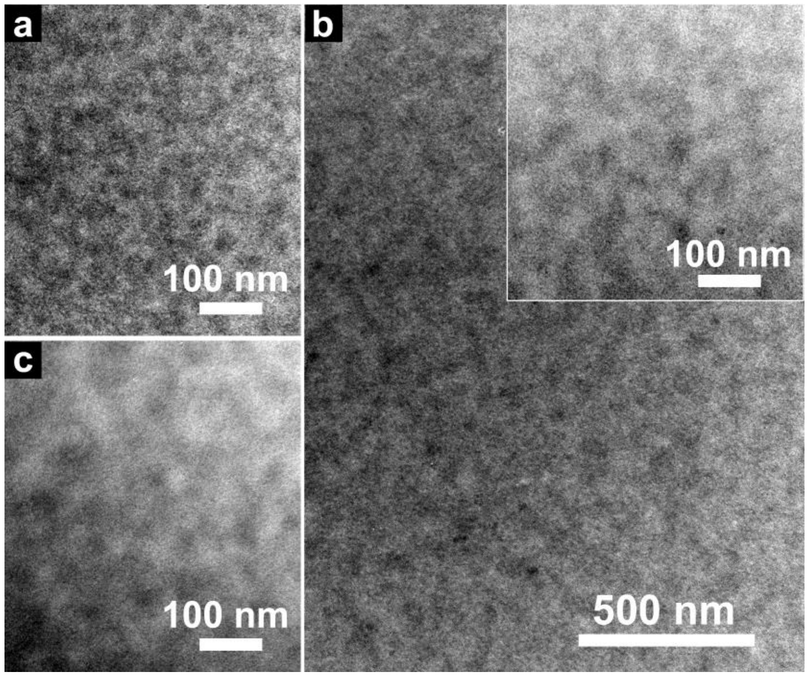

Figure 3.2 TEM images of 1:1 (wt.) blends of PS/P(S-*r*-2VP)39k with PS molecular weights of (a) 34k, (b) 136k, and (c) 570k, showing co-continuous structures with sub-100 nm sizes. The P(S-*r*-2VP) rich domains appear darker due to staining with I_2 vapor.

We also investigated the behavior of a lower molecular weight (39 kg/mol) P(S-*r*-2VP) random copolymer containing fewer 2VP monomers in the polymer chain (x = 0.78). As shown in Figure 3.2a, very small features (~ 50 nm) were observed for blends of P(S-*r*-2VP)39k with PS34k, though the contrast between domains observed by TEM was very weak. Based on mean field theory, i.e., Equations 3.1 and 3.2, this system should be just at the verge of phase separation in the neat blend, thus it appears that the material has been trapped very close to the onset of demixing. Further increases in PS molecular weight to 136 and 510 kg/mol, led to an increase in the characteristic length scale to 80 and 100 nm, respectively (Figure 3.2b and c). Since the critical composition will also shift with asymmetry in molecular weight, it is notable that co-continuous morphologies are observed for all samples indicated here, indicating that the PS/P(S-*r*-2VP) blends can quite generally be quenched to within the spinodal envelope by solvent removal.

To demonstrate the importance of using a random copolymer to reduce the effective interaction parameter, we also studied the morphology of as-spun films for 1:1 (wt.) mixtures of PS26k and P2VP38k homopolymers. Since toluene is a non-solvent for P2VP, we instead used the nearly non-selective solvent chloroform. However, in contrast to the co-continuous morphologies seen for the PS/P(S-*r*-2VP) blends, the homopolymer system gave rise to larger (~300 – 500 nm) P2VP-rich droplets within a PS-rich matrix (Figure 3.3a), suggesting that demixing has instead occurred by nucleation and growth. To ensure that the choice of solvent was not responsible for this dramatic difference in morphology compared to the homopolymer/random copolymer blends, we also spin coated a PS26k/P(S-*r*-2VP)56k blend film from chloroform (Figure 3.3c), which gave a co-continuous morphology similar to that from toluene (Figure 3.3b).

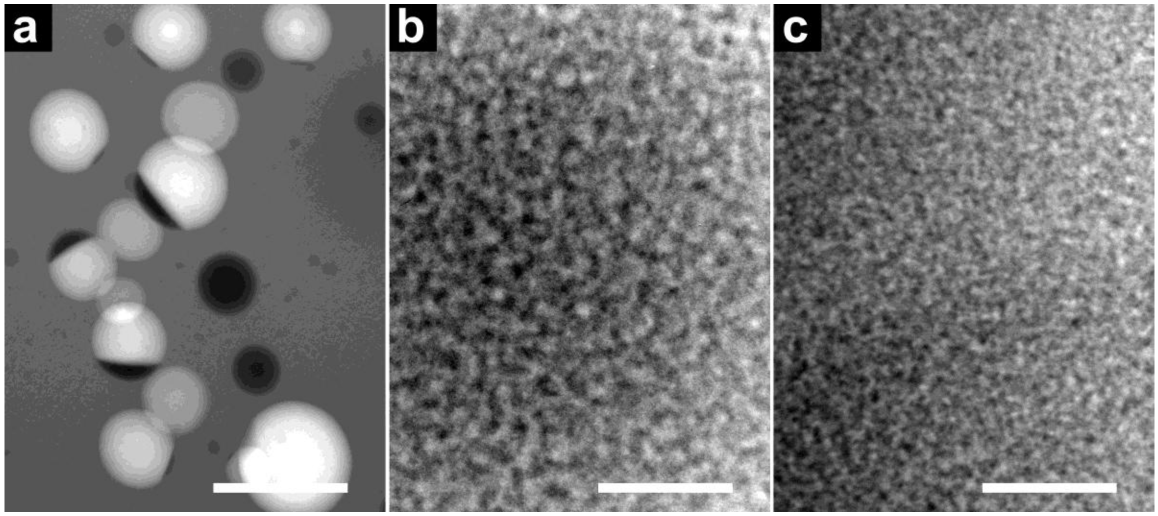

Figure 3.3 (a) TEM image of a 1:1 (wt.) blend of PS26k/P2VP38k homopolymers spin coated from chloroform showing droplets of P2VP-rich domains (dark circles) in a PS matrix. The white circles correspond to P2VP-rich domains that were extracted during floating of the film sample off of the substrate. (b-c) TEM images of 1:1 (wt.) blends of PS26k/P(S-*r*-2VP)56k spin coated from toluene (b) and chloroform (c), shown at the same magnification to highlight the dramatic difference in morphology obtained using the random copolymer blend. The P2VP-rich phases appear darker due to staining with I_2 vapor (scale bars: 500 nm).

3.3.3 Effect of casting solvent and substrate

To further investigate the effect of casting solvent, we prepared a series of PS/P(S-*r*-2VP) blend films spin-cast from chloroform (Figure 3.4). In each case, co-continuous morphologies similar to those found from toluene solutions were observed. However, the samples prepared from chloroform under otherwise identical conditions have smaller features sizes and more diffuse interfaces (Figure 3.3b vs. 3.3c and Figure 3.1d vs. 3.4b), most likely reflecting that the greater speed of evaporation of chloroform leads to kinetic arrest earlier in the coarsening process. Selective solvent extraction using a mixture of methanol and acetic acid (1:1 vol) resulted in partial removal of the P(S-*r*-2VP) phases, because the co-continuous morphologies was vitrified at an early stage of phase separation and each phase was not enriched in one component. The observation of similar morphologies in the case of chloroform, which is a good solvent for both PS and P2VP, and toluene, which is a non-solvent for P2VP, highlights another important role played by the random copolymer, namely to minimize the solubility differences between the components.

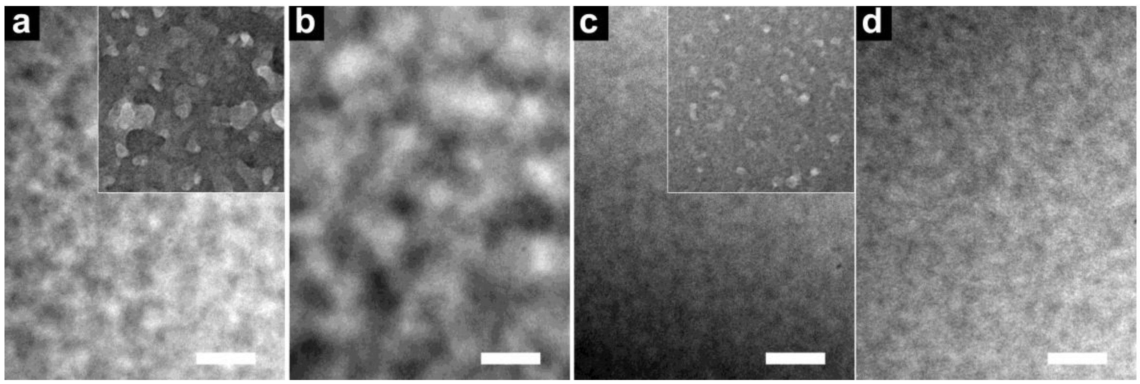

Figure 3.4 TEM images of 1:1 (wt.) blends of PS/P(S-*r*-2VP) with molecular weights of (a) 26k/56k, (b) 55k/56k, (c) 26k/39k, and (d) 55k/39k, spin-coated from chloroform. In all cases, co-continuous structures are found, though with smaller length scales and more diffuse interfaces compared to equivalent blends cast from toluene, likely due to the higher volatility of chloroform. The P(S-*r*-2VP) rich phases appear darker due to staining with I_2 vapor. Insets of (a) and (c) are samples after selective solvent extraction (scale bars: 100 nm).

Given the three-dimensional nature of the co-continuous structures found here, we also expect less dependence of the morphology on the nature of the substrate than in previous reports.[25, 27, 28] To this end, we tested four different substrates including silicon wafers with a native oxide layer, gold-coated silicon wafers, mica, and polyimide films. In all cases, similar co-continuous morphologies were observed (Figure 3.5), with a thin wetting layer of the PS-rich phase at the free surface due to the lower surface energy of PS. For the case of silicon and gold substrates, the preferential wetting by P(S-*r*-2VP) results in a random copolymer-rich layer at the polymer-substrate interface (Figure 3.5a and 3.5d), while little preference was found in the case of mica and Kapton (Figure 3.5g and 3.5i).

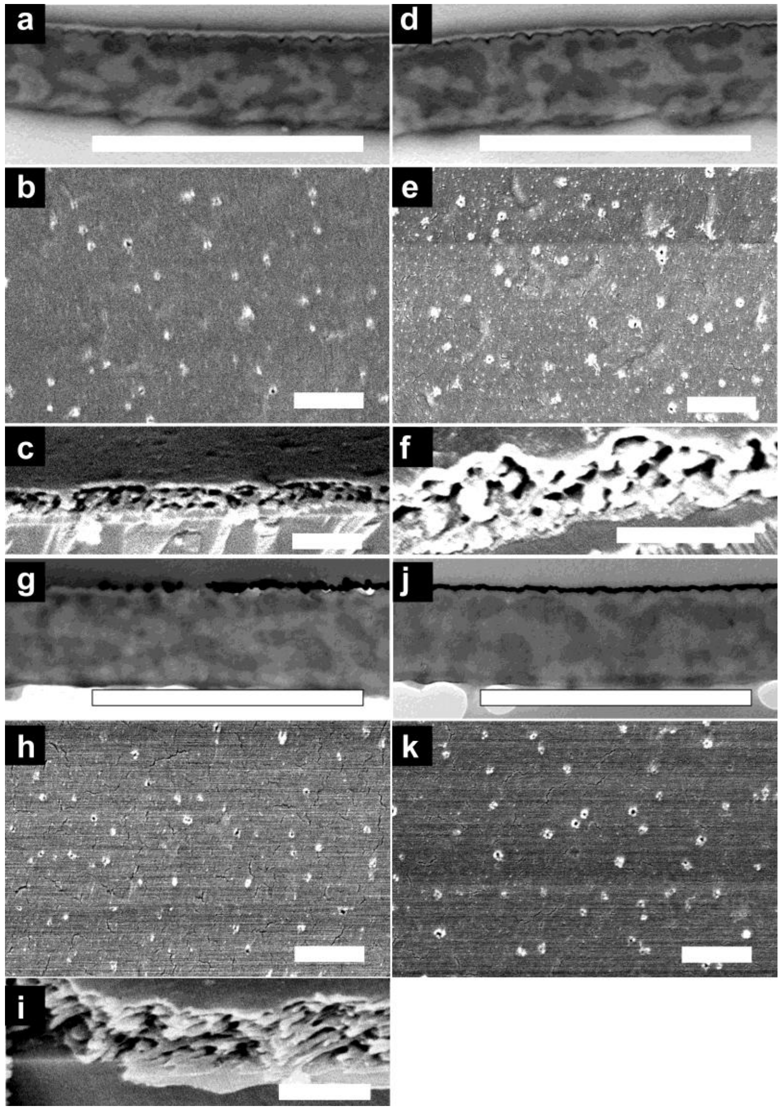

Figure 3.5 Blend films of 1:1 (wt.) PS26k/P(S-*r*-2VP)56k prepared on (a-c) a silicon wafer, (d-f) a gold-coated silicon wafer, (g-i) a mica substrate, and (j-k) a polyimide substrate, with the cross-sectional TEM image (a, d, g and j) and top-view (b, e, h and k) and cross-sectional (c, f and i) SEM images after selective solvent extraction of P(S-*r*-2VP) rich domains. Similar co-continuous structures are observed, regardless of the substrate type (scale bars: 1 μm).

3.3.4 Porous membranes based on the co-continuous morphologies

To conclusively establish the co-continuity of the observed morphologies, we selectively extracted the P(S-*r*-2VP)-rich phase from blend films by immersion in a mixture of methanol and acetic acid (1:1 vol). As shown for a 1:1 (wt.) blend of PS55k/P(S-*r*-2VP)56k, plan-view TEM images on unstained samples showed excellent contrast (Figure 3.6a), while SEM images of the film cross section (Figure 3.6c) revealed a continuous porous structure percolating through the film thickness. In contrast, for an asymmetric blend of 2:1 (wt.) PS55k/P(S-*r*-2VP)56k, P(S-*r*-2VP)-rich droplets dispersed in a PS-rich matrix were observed, characteristic of a morphology generated by a nucleation and growth. Solvent extraction following sample fracture led to pores found only on the surface of the film, while the domains were not extracted from the interior of the film (Figure 3.6d-f). By removing random copolymer-rich domains from the film cross section, discrete pores were revealed (Figure 3.6g), confirming the droplet morphology. These results indicate that only the P(S-r-2VP)-rich domains accessible to the free surface are extracted by the selective solvents, while the PS-rich matrix acts as an effective diffusion barrier.

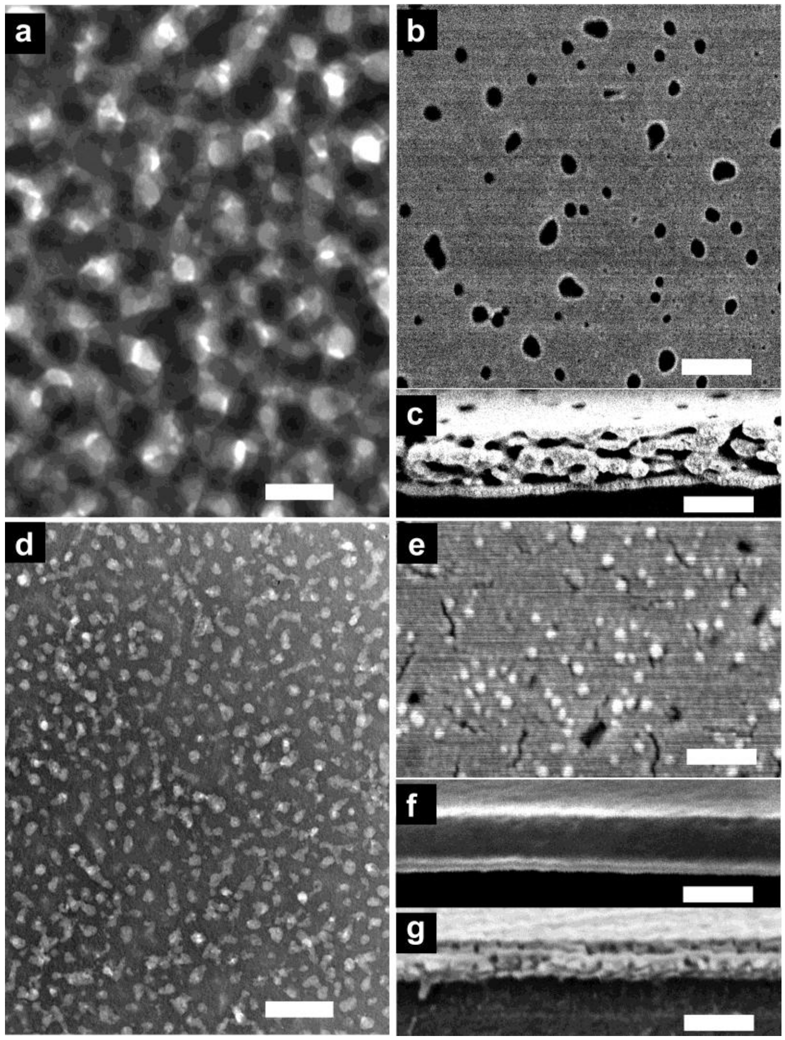

Figure 3.6 Thin membranes of blends of PS55k/P(S-*r*-2VP)56k following selective solvent extraction of the P(S-*r*-2VP) rich phases. (a-c) For a 1:1 (wt.) blend, the high degree of contrast from TEM on an unstained sample (a), coupled with SEM top-view images (b) showing pores at the free surface and cross-sectional images (c) showing pores percolating through the film thickness indicate successful extraction of material from the co-continuous film. (d-f) By contrast, for a 2:1 (wt.) blend, TEM (d) reveals only isolated domains of random copolymer rich phases, while top-view (e) and cross-sectional (f) SEM images show that material has only been extracted from domains at the free surface. (g) Cross-sectional SEM of the same sample in (d)-(f), with exposure of the cross section and selective extraction, showing discrete pores in the thin membrane (scale bars: 500 nm).

We note that similar nanoporous polymer membranes with continuous channels throughout the film have been previously produced using gyroid-forming block copolymers or bicontinuous microemulsions as templates[2, 51-54]. However, since the gyroid or bicontinuous microemulsion morphologies only exist over a narrow composition range and each molecular weight gives rise to one specific structural size, generating such morphologies requires stringently controlled polymerization conditions. Given the simplicity of the SIPS process presented here, and the access to a wide range of pore sizes from a simple set of homopolymers, it represents an attractive route to membrane fabrication.

3.3.5 Effect of solvent evaporation rate

Based on the idea that a slower rate of solvent evaporation should lead to more extensively coarsened morphologies, we also varied the conditions of film casting. We first varied the solution concentration and the speed and duration of spin-coating, each of which will influence the resulting film thickness. Remarkably, for a single blend system, 1:1 (wt.) PS26k/P(S-*r*-2VP)56k, the characteristic size of the co-continuous structures was found to vary nearly linearly with the film thickness, as shown in Figure 3.7. Presuming that the rate limiting step for solvent removal is evaporation at the film/air interface, this can be easily understood since more time will be required to remove solvent from a thicker film, hence allowing more extensive structural coarsening. While the general trend is clear, there is significant scatter in the data especially at small film thickness, presumably since there is not a perfect correspondence between evaporation rate and film thickness (determined primarily by concentration, but also by spinning speed and duration).

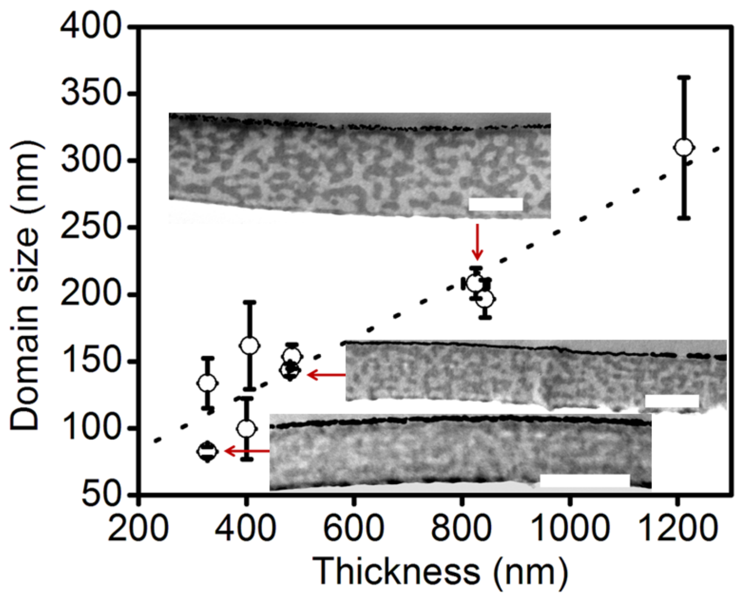

Figure 3.7 Films of 1:1 (wt.) PS26k/P(S-*r*-2VP)56k blends with different film thicknesses, are found to have co-continuous structures with length scales that increase with film thickness (the dotted line is a guide to the eye). Insets: Cross-sectional TEM micrographs of corresponding thin films, with the P(S-*r*-2VP) rich phases appearing darker due to I_2 vapor staining (scale bars: 500 nm).

We also prepared significantly thicker (~10 μm) films by drop casting of the blend solution. As shown in Figure 3.8, these films showed a co-continuous structure, but with a significant gradient in size scale through the film thickness. Near the polymer/air interface, the characteristic length scale was ~ 500 nm, while at the bottom surface, it was ~ 2 μm. In these thick films, evaporation leads to a gradient in solvent concentration, with the smallest amount of solvent at the free surface. Consequently, the surface of the film can vitrify while the remainder has sufficient residual solvent to allow the structure to coarsen. This gradient in structure can be further enhanced by annealing in a temperature gradient, i.e. by applying heat to the substrate while blowing cold nitrogen gas onto the surface of the film, as shown in Figure 4b. Such gradient structures with continuous channels are of practical interest for applications as filtration membranes.[55]

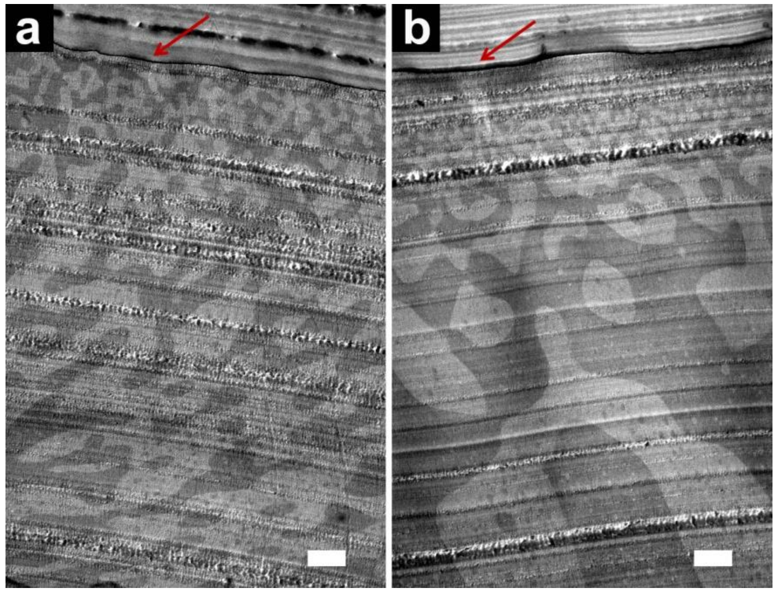

Figure 3.8 Cross-sectional TEM micrographs of thick membranes of 1:1 (wt.) blends of PS32k/P(S-*r*-2VP)56k. (a) The co-continuous structures formed upon drop-casting show a gradient in the length-scale of the co-continuous structure through the film thickness. (b) After annealing with the substrate held at 120 ℃ for 10 min while the free surface was cooled, the gradient is enhanced (scale bars: 1 μm). P(S-*r*-2VP) phases appear darker due to staining with I_2 vapor; the dark lines (indicated by red arrows) represent gold films deposited to mark the polymer/air interface.

3.3.6 Macrophase separation vs. microphase separation

Finally, we consider the potential alternative explanation that the co-continuous morphologies formed by PS/P(S-*r*-2VP) blends is due to microphase separation of a random copolymer that has a "blocky" distribution of S and 2VP units along the chain, with the PS homopolymer swelling the PS-rich microdomains.[56, 57] We performed small angle X-ray scattering on P(S-*r*-2VP) samples (Figure 3.9a and 3.9b) and found a monotonic decay in intensity. Fitting the SAXS data using the Debye-Beuche equation results in a correlation length of 3.5 nm for both P(S-*r*-2VP) samples (Figure 3.9c).[33]

TEM micrographs (Figure 3.9d and 3.9e) of I_2-stained P(S-*r*-2VP) also show no evidence of microphase separation, exhibiting similar contrast as I_2-stained PS homopolymer samples (Figure 3.9f), with feature size of several nanometers. The observed length-scales of 50 nm to 300 nm for the blend systems, as well as the ability to coarsen upon thermal annealing strongly suggest that microphase separation is not responsible for the observed behavior. Consequently, we conclude that the co-continuous morphologies formed here result from kinetically-trapped demixing of PS and P(S-*r*-2VP), rather than microphase separation.

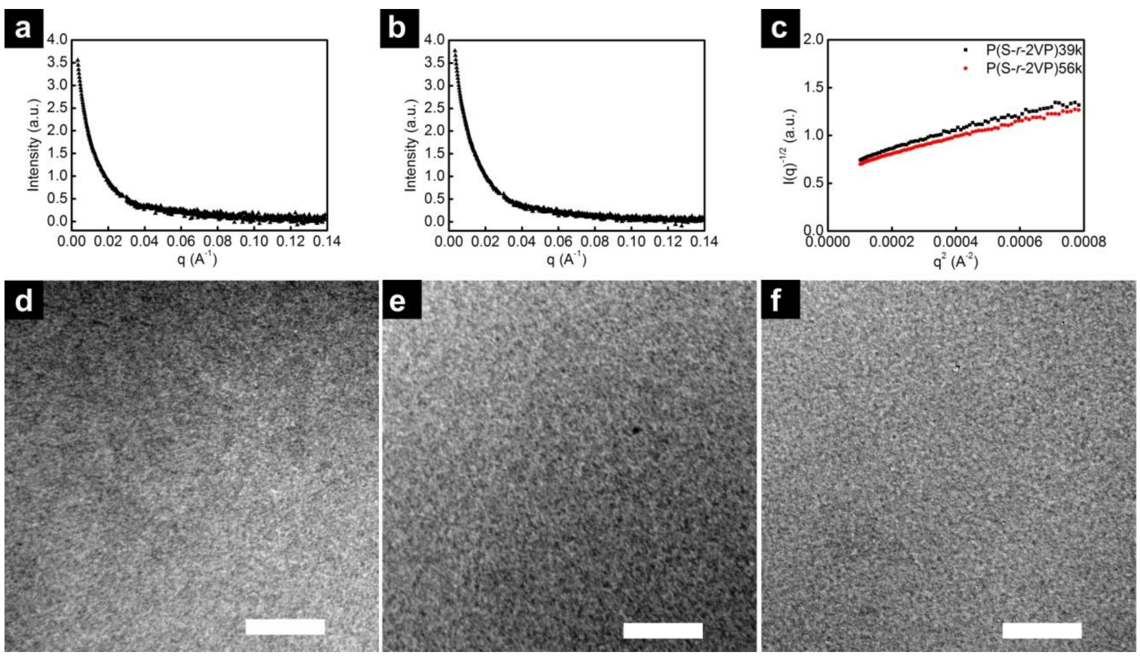

Figure 3.9 SAXS profiles for polymer thin films of (a) P(S-*r*-2VP)39k, (b) P(S-*r*-2VP)56k and (c) the Debye-Buche fittings. TEM micrographs of thin films of (d) P(S-*r*-2VP)39k, (e) P(S-*r*-2VP)56k, and (f) PS26k, that show only features of a few nanometers which are artifacts due to staining by I_2 vapor (scale bars: 100 nm).

3.4 Conclusions

In summary, we have developed a strategy to tune the compatibility of immiscible polymer blends by use of a random copolymer, allowing quenches into the spinodal envelope during solvent casting followed closely by vitrification, leading to co-continuous morphologies with size scales down to tens of nanometers. We find that this simple method is robust to variations in polymer molecular weight and substrate chemistry, not highly sensitive to solvent choice, and provides control over the size of the structures that can be achieved. These co-continuous structured films further provide templates for thin nanoporous membranes and thicker membranes with gradients in structure size, thus offering promise in applications such as filtration membranes.

Reference

1. Hoppe, H. and N.S. Sariciftci, *Morphology of polymer/fullerene bulk heterojunction solar cells.* Journal of Materials Chemistry, 2006. **16**(1): p. 45-61.
2. Ulbricht, M., *Advanced functional polymer membranes.* Polymer, 2006. **47**(7): p. 2217-2262.
3. Bates, F.S. and G.H. Fredrickson, *Block Copolymer Thermodynamics - Theory and Experiment.* Annual Review of Physical Chemistry, 1990. **41**: p. 525-557.
4. Bates, F.S., et al., *Polymeric bicontinuous microemulsions.* Physical Review Letters, 1997. **79**(5): p. 849-852.
5. Pernot, H., et al., *Design and properties of co-continuous nanostructured polymers by reactive blending.* Nature Materials, 2002. **1**(1): p. 54-58.
6. Ishino, S., et al., *Designing a polymer blend with phase separation tunable by visible light for computer-assisted irradiation experiments.* Macromolecular Rapid Communications, 2006. **27**(10): p. 758-762.
7. Kim, B.S., T. Chiba, and T. Inoue, *Morphology development via reaction-induced phase-separation in epoxy poly(ether sulfone) blends - morphology control using poly(ether sulfone) with functional end-groups.* Polymer, 1995. **36**(1): p. 43-47.
8. Cahn, J.W., *On spinodal decomposition.* Acta Metallurgica, 1961. **9**(9): p. 795-801.

9. Van Aartsen, J.J., *Theoretical observations on spinodal decomposition of polymer solutions.* European Polymer Journal, 1970. **6**(7): p. 919.
10. Kwei, T.K., T. Nishi, and R.F. Roberts, *Study of Compatible Polymer Mixtures.* Macromolecules, 1974. **7**(5): p. 667-674.
11. Bank, M., Leffingw.J, and C. Thies, *Influence of solvent upon compatibility of polystyrene and poly(vinyl methyl ether).* Macromolecules, 1971. **4**(1): p. 43.
12. Naito, K., et al., *Compatibility in Blends of Poly(Methyl Methacrylate) and Poly(Styrene-Co-Acrylonitrile) .1. Physical-Properties.* Macromolecules, 1978. **11**(6): p. 1260-1265.
13. Kruse, W.A., et al., *Experimental-Evidence for Molecularly Disperse Character of Mixture of 2 Polymers and Determination of Chemical Potential in These Mixtures.* Makromolekulare Chemie-Macromolecular Chemistry and Physics, 1976. **177**(4): p. 1145-1160.
14. Chung, H., et al., *Self-regulated structures in nanocomposites by directed nanoparticle assembly.* Nano Letters, 2005. **5**(10): p. 1878-1882.
15. Li, L., et al., *Kinetically Trapped Co-continuous Polymer Morphologies through Intraphase Gelation of Nanoparticles.* Nano Letters, 2011. **11**(5): p. 1997-2003.
16. Tanaka, H., A.J. Lovinger, and D.D. Davis, *Pattern evolution caused by dynamic coupling between wetting and phase-separation in binary-liquid mixture containing glass particles.* Physical Review Letters, 1994. **72**(16): p. 2581-2584.
17. Solc, K. and Y.C. Yang, *Phase-Separation in Ternary-Systems Solvent Polymer-1 Polymer-2 .3. Homogeneous Double Critical-Points.* Macromolecules, 1988. **21**(3): p. 829-840.
18. Gutmann, J.S., P. Muller-Buschbaum, and M. Stamm, *Complex pattern formation by phase separation of polymer blends in thin films.* Faraday Discussions, 1999. **112**: p. 285-297.
19. Aubert, J.H. and R.L. Clough, *Low-Density, Microcellular Polystyrene Foams.* Polymer, 1985. **26**(13): p. 2047-2054.
20. Hopkinson, I. and M. Myatt, *Phase separation in ternary polymer solutions induced by solvent loss.* Macromolecules, 2002. **35**(13): p. 5153-5160.
21. Young, A.T., *Microcellular Foams Via Phase-Separation.* Journal of Vacuum Science & Technology a-Vacuum Surfaces and Films, 1986. **4**(3): p. 1128-1133.
22. Hsu, C.C. and Prausnit.Jm, *Thermodynamics of Polymer Compatibility in Ternary-Systems.* Macromolecules, 1974. **7**(3): p. 320-324.
23. Dalnoki-Veress, K., et al., *Phase separation morphology of spin-coated polymer blend thin films.* Physica A, 1997. **239**(1-3): p. 87-94.
24. Krausch, G., et al., *Self-Assembly of a Homopolymer Mixture Via Phase-Separation.* Applied Physics Letters, 1994. **64**(20): p. 2655-2657.
25. Walheim, S., et al., *Structure formation via polymer demixing in spin-cast films.* Macromolecules, 1997. **30**(17): p. 4995-5003.
26. Dalnoki-Veress, K., et al., *Phase separation morphology of thin films of polystyrene/polyisoprene blends.* Journal of Polymer Science Part B-Polymer Physics, 1996. **34**(17): p. 3017-3024.
27. Krausch, G., *Surface-Induced Self-Assembly in Thin Polymer-Films.* Materials Science & Engineering R-Reports, 1995. **14**(1-2): p. 1-94.

28. Boltau, M., et al., *Surface-induced structure formation of polymer blends on patterned substrates.* Nature, 1998. **391**(6670): p. 877-879.
29. Affrossman, S., et al., *Surface topography and composition of deuterated polystyrene-poly(bromostyrene) blends.* Macromolecules, 1996. **29**(14): p. 5010-5016.
30. Shaheen, S.E., et al., *2.5% efficient organic plastic solar cells.* Applied Physics Letters, 2001. **78**(6): p. 841-843.
31. Arias, A.C., et al., *Photovoltaic performance and morphology of polyfluorene blends: A combined microscopic and photovoltaic investigation.* Macromolecules, 2001. **34**(17): p. 6005-6013.
32. Yang, C.Y. and A.J. Heeger, *Morphology of composites of semiconducting polymers mixed with C-60.* Synthetic Metals, 1996. **83**(2): p. 85-88.
33. Chen, D.A., et al., *P3HT/PCBM Bulk Heterojunction Organic Photovoltaics: Correlating Efficiency and Morphology.* Nano Letters, 2010. **11**(2): p. 561-567.
34. Chen, D., et al., *Bulk Heterojunction Photovoltaic Active Layers via Bilayer Interdiffusion.* Nano Letters, 2011. **11**(5): p. 2071-2078.
35. Treat, N.D., et al., *Interdiffusion of PCBM and P3HT Reveals Miscibility in a Photovoltaically Active Blend.* Advanced Energy Materials, 2010. **1**(1): p. 82-89.
36. Campoy-Quiles, M., et al., *Morphology evolution via self-organization and lateral and vertical diffusion in polymer: fullerene solar cell blends 10.1038/nmat2102.* Nature Materials, 2008. **7**(2): p. 158-164.
37. van Ekenstein, G., et al., *Determination of the Flory-Huggins interaction parameter of styrene and 4-vinylpyridine using copolymer blends of poly(styrene-co-4-vinylpyridine) and polystyrene.* Macromolecules, 2000. **33**(10): p. 3752-3756.
38. Schulz, M.F., et al., *Phase behavior of polystyrene-poly(2-vinylpyridine) diblock copolymers.* Macromolecules, 1996. **29**(8): p. 2857-2867.
39. Paul, D.R. and J.W. Barlow, *A Binary Interaction-Model for Miscibility of Copolymers in Blends.* Polymer, 1984. **25**(4): p. 487-494.
40. Kambour, R.P., J.T. Bendler, and R.C. Bopp, *Phase-Behavior of Polystyrene, Poly(2,6-Dimethyl-1,4-Phenylene Oxide), and Their Brominated Derivatives.* Macromolecules, 1983. **16**(5): p. 753-757.
41. ten Brinke, G., F.E. Karasz, and W.J. Macknight, *Phase Behavior in Copolymer Blends: Poly(2 ,6-dimethyl-1,4-phenylenoex ide) and Halogen-Substituted Styrene Copolymers.* Macromolecules, 1983. **16**: p. 1827.
42. Bruder, F. and R. Brenn, *Measuring the Binodal by Interdiffusion in Blends of Deuterated Polystyrene and Poly(Styrene-Co-4-Bromostyrene).* Macromolecules, 1991. **24**(20): p. 5552-5557.
43. Kambour, R.P. and J.T. Bendler, *Miscibilities in Monodisperse Mixtures of Polystyrene, Poly(Para-Bromostyrene), and Their Copolymers.* Macromolecules, 1986. **19**(11): p. 2679-2682.
44. Strobl, G.R., et al., *Miscibilities in monodisperse mixtures of polystyrene, poly(p-bromostyrene) and their copolymers.* Macromolecules, 1986. **19**: p. 2683.

45. Strobl, G.R., et al., *Thermally Reversible Phase-Separation in Polystyrene Poly(Styrene-Co-4-Bromostyrene) Blends.* Macromolecules, 1986. **19**(11): p. 2683-2689.
46. Vukovic, R., et al., *Phase behavior and miscibility in binary blends containing polymers and copolymers of styrene, of 2,6-dimethyl-1,4-phenylene oxide, and of their derivatives.* Journal of Physical and Chemical Reference Data, 1999. **28**(3): p. 851-868.
47. Alexandrovich, P.S., *Studies of polymer compatibility*, in *Polymer Science and Engineering*. 1978, Univerisity of Massachusetts: Amherst. p. 536.
48. Scott, R.L., *Thermodynamics of High Polymer Solutions .6. the Compatibility of Copolymers.* Journal of Polymer Science, 1952. **9**(5): p. 423-432.
49. Scott, R.L., *The Thermodynamics of High Polymer Solutions .5. Phase Equilibria in the Ternary System - Polymer-1 Polymer-2 Solvent.* Journal of Chemical Physics, 1949. **17**(3): p. 279-284.
50. Kudlik, A., et al., *Slow secondary relaxation process in supercooled liquids.* Europhysics Letters, 1997. **40**(6): p. 649-654.
51. Uehara, H., et al., *Nanoporous polyethylene film prepared from bicontinuous crystalline/amorphous structure of block copolymer precursor.* Macromolecules, 2006. **39**(12): p. 3971-3974.
52. Pitet, L.M., M.A. Amendt, and M.A. Hillmyer, *Nanoporous Linear Polyethylene from a Block Polymer Precursor.* Journal of the American Chemical Society, 2010. **132**(24): p. 8230.
53. Jones, B.H. and T.P. Lodge, *High-Temperature Nanoporous Ceramic Monolith Prepared from a Polymeric Bicontinuous Microemulsion Template.* Journal of the American Chemical Society, 2009. **131**(5): p. 1676.
54. Hillmyer, M.A., *Nanoporous materials from block copolymer precursors*, in *Block Copolymers Ii*, V. Abetz, Editor. 2005, Springer-Verlag Berlin: Berlin. p. 137-181.
55. Kesting, R.E., *Synthetic polymeric membranes: a structural perspective*. 1985, New York: Wiley-Interscience. 368.
56. Tanaka, H., H. Hasegawa, and T. Hashimoto, *Ordered Structure in Mixtures of a Block Copolymer and Homopolymers .1. Solubilization of Low-Molecular-Weight Homopolymers.* Macromolecules, 1991. **24**(1): p. 240-251.
57. Matsen, M.W., *Phase-Behavior of Block-Copolymer Homopolymer Blends.* Macromolecules, 1995. **28**(17): p. 5765-5773.

CHAPTER 4

NANOPARTICLE EFFECTS ON THE THERMALLY INDUCED SPINODAL PHASE SEPARATION IN THE QUASI-BINARY BLEND OF POLYSTYRENE/POLY(2-VINYLPYRIDINE)/TETRAHYDROFURAN

4.1 Introduction

Recent efforts have been focused on the assembly of particles at the interface formed during the spinodal demixing of fluids, which subsequently leads to an interfacial jamming of particles and kinetic arrest of co-continuous structures.[1-4] Such a material, termed a "bijel", is characterized by two continuous channels of fluids and a continuous interface made of particles. With the ability to solidify the interfacial particle layer by means of chemical crosslinking[5, 6] and remove the fluid phases, the resultant membrane consisting of a monolayer of densely packed particles has potential applications in micro-fluidic devices and solvent extraction media.[1, 3]

The greatest technical challenge in realizing bijel structures lies in the control of the wettability of the particles, i.e. the particles are neutrally wetted by both phases in order to adsorb to and stabilize the interface.[1-4] It should be emphasized that even particles that irreversibly adsorb to the interface but prefer one of the two phases yield structures that ultimately coarsen and lose their co-continuous nature.[3] Another critical parameter is the particle size, since large particles better stabilize the interfaces given the same interfacial tension between the demixing fluids.[1]

A possible solution to overcome sensitivity to surface chemistry is to manipulate the interfacial energy difference between the demixing fluids, thereby diminishing the preference of particles to partition into either phase, at the price of decreasing the binding energy of particles at the interface. In other words, the particles may not have a preference for the two fluid phases, but they also do not have much preference for the interface either. This may be compensated by increasing the size of the particles, in order to favor interfacial assembly. For polymer blends, the interfacial tension is quite low.[7, 8] Factors like high viscosity have to be taken into consideration, as large particles tend to have slow kinetics for assembly.

Transient co-continuous structures may be generated via SD by quenching the mixture into the spinodal envelope,[9] where a homogeneous mixture should be attained initially. Thermally induced phase separation (TIPS) has been well studied with the thermodynamics and kinetics of phase separation predicted by theories[10-17] and verified by experiments [18-26]. Blends that have an upper critical solution temperature (UCST) demix upon decreasing temperature (e.g. polystyrene/polybutadiene (PS/PBD)[27, 28]), while blends with a lower critical solution temperature (LCST) tend to phase separate with increasing temperature (polystyrene/polyvinyl methyl ether (PS/PVME)[18-21]).However, due to the high molecular weight of polymers and the small combinatorial mixing of entropy, most polymer pairs are completely immiscible, within the experimentally accessible temperature range. Therefore, TIPS is only feasible for a limited set of partially miscible polymer pairs, where the interaction parameter χ is small and temperature dependent.

An alternative to TIPS is the solvent induced phase separation (SIPS), where phase separation is induced by the solvent removal. In a polymer-1/polymer-2/solvent system, the solvent brings the immiscible polymers into a homogenous state and its evaporation drives phase separation. The evaporation of solvent causes a compositional change and may quench the system into the spinodal envelope of the triangle phase diagram (Chapter 1, Figure 1.4).[29-33] However, due to the lack of theoretical studies in quantifying the kinetics of the SIPS, it is not well understood how co-continuous structures are formed, nor how they evolve with time.

Phase diagrams of ternary systems also vary with temperature, giving rise to a three-dimensional prism-shaped phase diagram (Chapter 1, Figure 1.5). A quasi-binary phase diagram is obtained by intercepting a vertical plane from the prism, resulting in a two-dimensional phase diagram at fixed volume ratio of polymers and, temperature and volume fraction of solvent as the two variables.[34, 35] The criteria for TIPS in binary polymer blends,

$$\Delta\mu_1^a = \Delta\mu_1^b \qquad \Delta\mu_2^a = \Delta\mu_2^b, \tag{4.1}$$

$$(\partial^2 \Delta G_m / \partial\phi^2)_{T,p} = 0, \tag{4.2}$$

$$(\partial^3 \Delta G_m / \partial\phi^3)_{T,p} = 0, \tag{4.3}$$

are expected to be applicable to the symmetric quasi-binary polymer-polymer-solvent systems, assuming that the solvent only dilutes the unfavorable interactions between the incompatible pair[36] The simplified solution for the phase separation criteria is to replace the interaction parameter χ by the effective value χ_{eff} = (1-ϕ_s)χ. Co-continuous structures may be obtained by quenching such homogeneous quasi-binary mixture into the spinodal envelop[32] and subsequent coarsening, similar to the case of a binary polymer blend.

Here we present a strategy to utilize solvent to mediate the interaction between immiscible polymers – polystyrene (PS) and poly(2-vinylpyridine) (P2VP), achieving partial miscibility of polymer blends with the use of an almost neutral solvent – tetrahydrofuran (THF). Given the similar favorable polymer/solvent interactions, such ternary blend may be considered as a quasi-binary system, with a two-dimensional phase diagram and experimentally accessible phase mixing temperatures. Analogous to the UCST binary polymer blend, the quasi-binary polymer/polymer/solvent blend undergoes spinodal decomposition induced by appropriate thermal quenching. Consequently, the demixing fluids have a low interfacial energy and low viscosity, which may assist the non-selectivity of the particles to both phases. Our experiments show that the kinetics of spinodal phase separation are slowed down in upon addition of gold nanoparticles, and that the coarsening of the co-continuous structures is slowed and even arrested for a short period of time by the addition of large silica particles, possibly due to the interfacial jamming of particles. The design of the quasi-binary blend system could open ways to control the phase separation for immiscible polymer binary blends in a more controlled manner, and provides fundamental insights into the phase separation behaviors of polymer blends.

4.2 Experimental

4.2.1 Materials and sample preparation

PS (Polymer Source Inc.) with a weight-average molecular weight (M_w) of 26,000 g/mol and a polydispersity index (PDI) of 1.04 and P2VP (Sigma Aldrich) with a M_w of 37,500 g/mol and PDI of 1.07 were employed. Anhydrous tetrahydrofuran (THF) was purchased from Sigma Aldrich. All reagents were used as received.

Colloidal silica particles with diameter ~ 300 nm (Nano Giant LLC) were initially dispersed in water. Repeated centrifugation and redispersing with THF resulted in particle dispersions in THF.

Gold nanoparticles (NP) with diameter ~4 nm and stabilized by the PS-SH were synthesized using a procedure described by Brust et al.[37] The PS-SH with MW 3,600 g/mol and PDI 1.3 was synthesized by atom transfer radical polymerization (ATRP) and subsequent reaction with thiourea in DMF followed by basic hydrolysis to convert bromide into thiol end groups.[38] The feeding ratio of Au to PS-SH is usually 1:2 by weight.

The PS/P2VP/THF solutions were weighed and mixed according to the desired ratio. To prepare the solutions with particles, the particle solution or suspension was first dried, weighed and then the PS/P2VP/THF solution was added. The particle content was recorded with respect to the total polymer volume.

For the light scattering experiments, rectangular glass capillaries were used as the sample cells, with dimensions of 1 mm x 1 mm x 50 mm or 1 mm x 5 mm x 50 mm. One end of the capillary was first sealed by flame. Sample solutions or suspensions were then filled into those glass capillaries. The other end of the glass capillary was either flame-sealed after immersing the sample portion in liquid nitrogen to prevent THF boiling during sealing, or sealed by 5-min-room-temperature epoxy glue. Note that some sample leakage would occur in the case of epoxy sealing. Therefore, all samples were measured within 2 h after preparation and no obvious differences were observed between samples prepared with different sealing methods.

4.2.2 Characterization methods

Time-resolved small angle light scattering (SALS) was performed using a He-Ne laser (623.8 Å) as the light source and a camera equipped with a 2-D CCD detector (Princeton EG&G CCD 512 x 512 array) for image collection. The sample capillary was placed on an INSTEC heating stage (HCS622V) equipped with a liquid nitrogen cooling unit, to control the experimental temperature from -50 ℃ to 300 ℃ with heating/cooling rates from 1 to 100 ℃/min. The scattering signals were projected onto a black board, from which a scattering pattern could be visualized. The scattering images were acquired by the CCD camera and analyzed using a customized LabView application. The obtained images were transformed into the intensity I vs. scattering vector $q = 4\pi/\lambda * \sin(\theta/2)$ plots, by integrating along the azimuthal angle.

The cloud point for a particular composition of the ternary blend was measured using the above light scattering apparatus. The intensity at 0^{o} angle was monitored during heating at a particular rate by a laser sensor on the direct beam pathway after the light had passed through the sample. The nearly linear portion of the intensity curve in the cloudy state was extrapolated to the base line and the intersection was taken as a measured cloud temperature at the particular heating rate. This procedure was performed at several heating rates (1, 2, 3, 4, 5, 7 and 10 ℃/min) and the cloud temperatures as a function of heating rate was extrapolated to an infinitely slow rate to obtain the cloud points.

4.3 Results and discussion

4.3.1 Numerical calculations of the phase diagrams of a quasi-binary blend

We used the modified Flory-Huggins theory to calculate the binodal curves of the quasi-binary blend at different solvent concentrations. A symmetric case of a polymer-A/polymer-B/solvent blend was considered, where $\chi_{AS} = \chi_{BS}$ and $N = N_A = N_B$, that is, polymers of comparable degree of polymerization were dissolved in a solvent having the same interaction parameter with each of the two polymers. We assumed the solvent component contributes to the free energy of mixing with an additional entropic term and two enthalpic terms. The modified Flory-Huggins free energy of mixing can be written as following:

$$\frac{\Delta G_{mix}}{nRT} = \frac{\phi_A}{N_A}\ln\phi_A + \frac{\phi_B}{N_B}\ln\phi_B + \frac{\phi_S}{N_S}\ln\phi_S + \chi_{AB}\phi_A\phi_B + \chi_{AS}\phi_A\phi_S + \chi_{BS}\phi_B\phi_S \qquad (4.4)$$

The phase boundary condition (introduced in Chapter 1) is when the chemical potentials of polymer A and polymer B are equal in the two coexisting phases (Equation 4.1). The values of the binodal curve can be determined from the common tangent to the free energy of mixing curves. Since we assume the blend to be symmetric, we can also use the following equation to get the same numerical solutions:

$$\left(\frac{\partial \Delta G_{mix} / RT}{\partial \phi}\right)_{T,P} = 0 \, . \qquad (4.5)$$

The spinodal condition is defined by Equation 4.2, differentiating the metastable region and the unstable region. The critical point is determined by Equation 4.3.

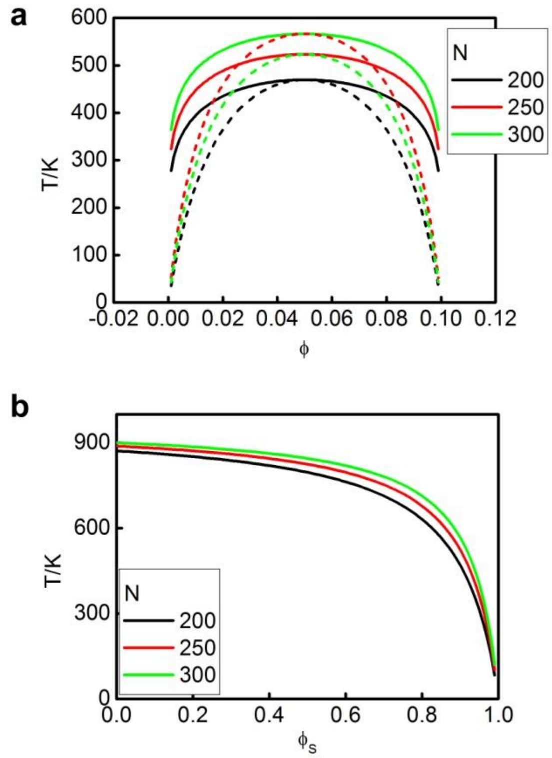

Figure 4.1 The estimated phase diagrams of the quasi-binary blend of PS/P2VP/THF: (a) binodal (solid lines) and spinodal (dotted lines) curves for the case of $\phi_S = 0.9$, $\phi_{PS} = \phi$, $\phi_{P2VP} = 0.1$-ϕ, with various N values; and (b) critical temperatures as a function of ϕ_S

We employed the interaction parameters of the PS/P2VP/THF system, with $\chi_{PS/P2VP}$ = 91.6/T-0.095[39] and $\chi_{PS/THF}$ =$\chi_{P2VP/THF}$ =0.4,[40], and assumed that the polymer-solvent interaction parameters are independent on the solution compositions and temperature for simplification. At a constant ϕ_{THF}, $\phi_{PS} = \phi$, $\phi_{P2VP} = 1$-ϕ_{THF}-ϕ, the temperature dependent phase diagrams with respect to PS volume fraction are shown in Figure 4.1a. The UCST-type phase behavior is predicted, as a result of the temperature-dependent $\chi_{PS/P2VP}$. With the increase of N, the phase diagram is shifted upward.

Figure 4.1b reveals the estimated critical temperature as a function of solvent concentration. As the solvent dilutes the unfavorable interaction between the two polymer components, the phase separation temperatures significantly decrease with the increase of solvent concentration. Specifically, the binary blend shows an estimated critical temperature at slightly below 900K, while the quasi-binary blend with 90 vol % solvent has much lower critical temperature of below 500K. An interesting point is that the addition of solvent decreases the critical temperature of the blend in a non-linear manner. From 0 – 80 vol % solvent content, Equation 4.4 predicts only 200 °C of critical temperature reduction, while a sharp reduction in the critical temperature is anticipated at solvent contents higher than 80 vol %. Based on these estimations, the PS/P2VP/THF blend should exhibit an experimentally accessible phase mixing temperature given enough solvent content and small molecular weights of the polymers.

4.3.2 Phase separation of the quasi-binary blend

The experimentally determined cloud point curve shows the phase mixing temperature is below 20 °C for blends containing 88 vol % solvent (Figure 4.2). The discrepancy between calculation and experiment could arise from the simplified polymer-solvent interactions, which are assumed to be independent with temperature or solution composition. The accessible phase mixing temperature displayed by this ternary system confirms the theoretical prediction[36] qualitatively, that despite the high incompatibility of PS and P2VP, a common solvent can homogenize the blend and significantly decrease the UCST phase boundary.

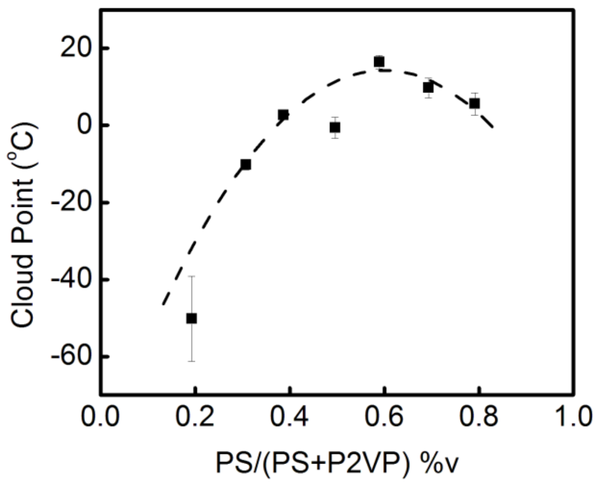

Figure 4.2 Cloud point curve of PS26k/P2VP38k with 88 vol % THF

The kinetics of phase separation were investigated by static SALS and OM experiments for the sample with 4/6 PS/P2VP by volume and 88 vol % solvent. This system shows a cloud point of 2.6 ± 0.7°C. To bypass the metastable region and access the spinodal envelope in the phase diagram, a fast quench was applied with a cooling rate of 100 ℃/min. Upon quenching, a ring pattern appeared and rapidly decreased in diameter, shrinking into the beam stop as shown in Figure 4.3b – 4.3d. With time, a second ring occurred at around 20s after the onset of phase separation (Figure 4.3g – 4.3k). The ring patterns suggest the formation of structures with characteristic sizes during cooling, i.e. due to spinodal decomposition. Optical micrographs confirmed the evolution of co-continuous structures at different stages of phase separation (Figure 4.4), consistent with SALS observations. Initially, the co-continuous structures formed and quickly coarsened from tens-of-microns to hundred-microns over the course of 14s (Figure 4.4b – 4.4e). Then, secondary micron-sized co-continuous structures were observed, which grew more slowly than the first one (Figure 4.4f – 4.4l). The existence of multiple spinodal phase separations is possibly due to the rate and depth of the thermal quench, resulting in the secondary spinodal phase separation in the initially coarsened domains, as temperature drops continuously during the sample heat transfer process (estimated to be ~ 10s for the 1 mm sample cell). However, the mechanism is not fully understood, given the complexity of the quasi-binary solution.

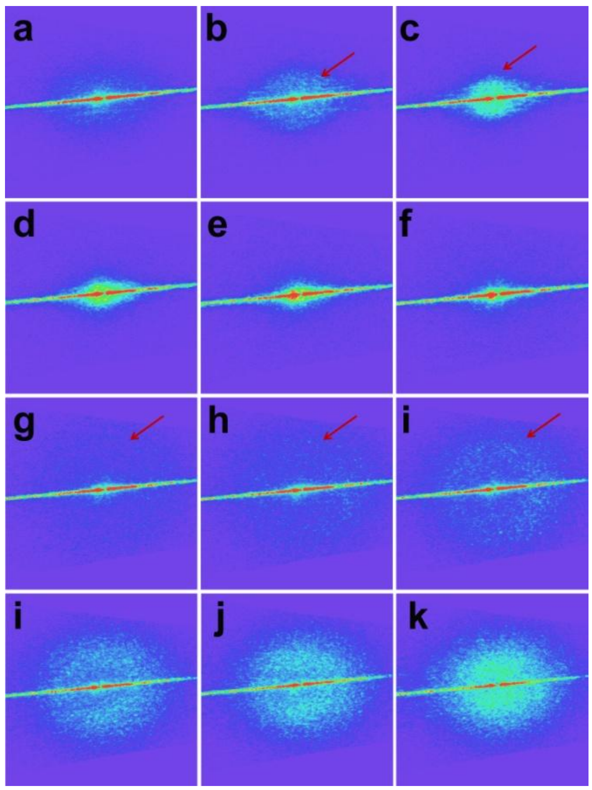

Figure 4.3 Small angle light scattering patterns of the PS/P2VP blend with volume ratio 4/6 containing 88 vol % THF quenched to -30 ℃ at cooling rate of 100 ℃/min, with increasing time: 0s (a), 5s (b), 7s (c), 9s (d), 11s (e), 13s (f), 19s (g), 29s (h), 38s (i), 68s (j), 99s (k) and 162s (l). The onset of phase separation is set as time zero (Red arrow is to guide the eye, indicating ring pattern formation; the bright lines across each image arise from the geometry of the capillary sample cell).

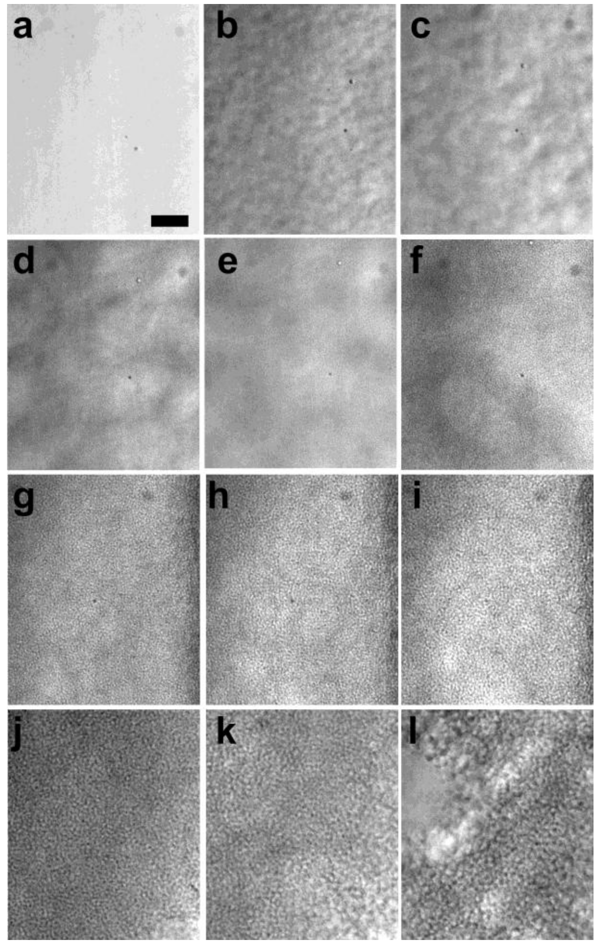

Figure 4.4 Optical micrographs of the PS/P2VP blend with volume ratio 4/6 containing 88 vol % THF quenched to -30 ℃ at cooling rate of 100 ℃, with increasing time: 0s (a), 6s (b), 8s (c), 12s (d), 14s (e), 18s (f), 30s (g), 40s (h), 45s (i), 100s (j), 128s (k) and 170s (l). The onset of phase separation is set as time zero (scale bar: 100 μm).

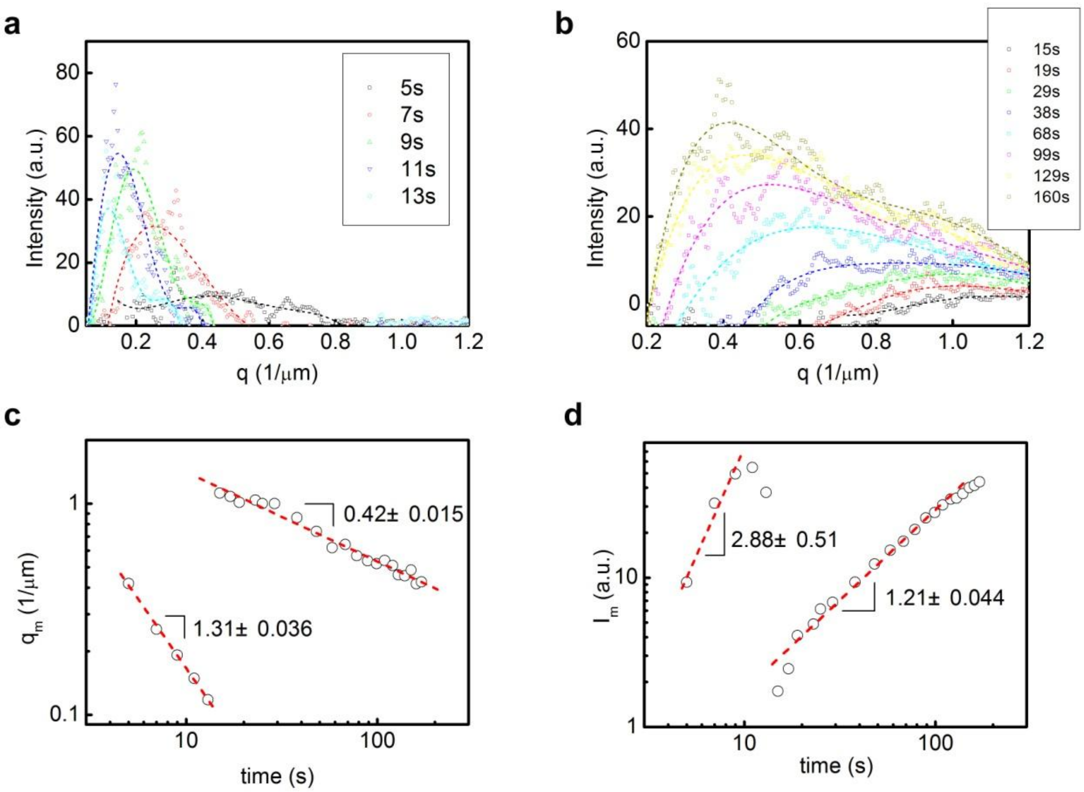

Figure 4.5 Small angle light scattering of the PS/P2VP blend with volume ratio 4/6 containing 86 wt% THF quenched to -30 ℃ at cooling rate of 100 ℃/min: scattering intensity I as a function of wavenumber q (a) and (b) with phase separation time; q_m (c) and I_m (d) as a function of time.

Quantitative information about the structural evolution was extracted from the SALS data. Figure 4.5a and 4.5b, denoting the first and second spinodal decomposition process respectively, show the plots of I vs. q obtained by performing azimuthal integration of the intensity with respect to the center of the scattering ring in the Figure 4.3 time series. The scattering curves were fitted with a fifth-order polynomial equation, from which q_m and I_m, the maximum value of I and the value of q at which it occurs, were extracted and plotted as a function of time (Figure 4.5c and 4.5d). Physically, q_m

represents the wavenumber of fluctuations that can grow at the highest rate, while I_m is related to the number of domains and the contrast between domains at q_m.

It is clear that the early stage of the spinodal decomposition described by Cahn-Hilliard linear theory[10, 11] was not observed in this solvent mediated quasi-binary blend, indicated by the lack of a fixed q_m at which the domain size remains the same and only the intensity grows. The SALS experiments captured the coarsening process. According to scaling theories,[13-16] q_m and I_m should vary with t by power law relationships, with exponents α and β, respectively. Theoretically, the interfacial tension driven Ostwald Ripening mechanism and the diffusion driven coalescence mechanism predict α values of 1/3, while the hydrodynamic flow mechanism leads to an α value of 1. A relationship of $\beta = 3\alpha$ is anticipated.[16] In our experiments, the two SD phase separation processes yielded α and β values of 1.31 and 2.88 for the first instance of coarsening, and 0.42 and 1.21 for the second. These results suggest that the first coarsening process may be more affected by hydrodynamics and the second one could be dominantly driven by interfacial tension as well as diffusion. Roughly we obtained $\beta_1 = 2\alpha_1$ and $\beta_2 = 3\alpha_2$. As there is no agreement with a unified theory quantifying the late stage coarsening process and experimental data vary case by case[15], we simply apply the power law fit on q_m vs. t to characterize the rate at which the phase separation evolves with time in the following discussions.

4.4.3 Effect of the addition of solid particles

Inspired by the work on “bijels”, we studied the SD phase separation of PS/P2VP/THF with the addition Au-PS nanoparticles (~ 4 nm core diameter by TEM) by SALS. Figure 4.6 shows the representative I vs. q profiles with increasing phase separation time. For all the samples studied, only one spinodal pattern appeared and grew with time, suggesting that multiple SD phase separation was suppressed due to the addition of nanoparticles. Similarly to the blend without nanoparticles, the initial linear regime of SD was not observed here, as evidenced by the lack of increasing intensity at a fixed q_m with time. The SD ring continued to shrink into the beam stop, indicating structural coarsening with time.

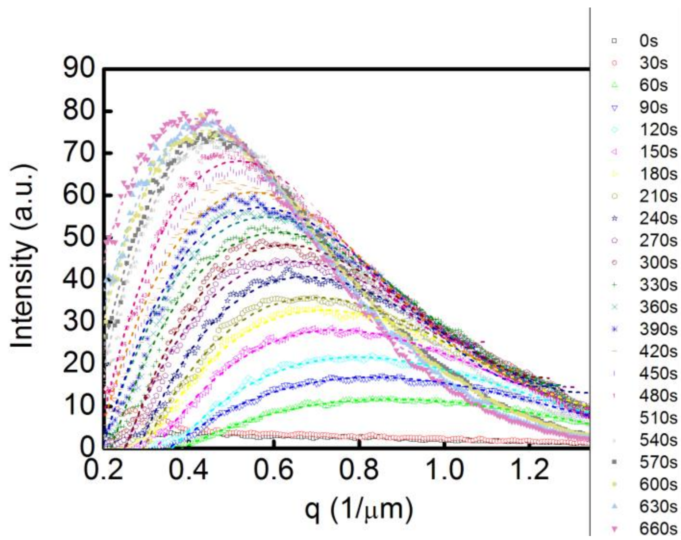

Figure 4.6 Phase separation of PS/P2VP/THF (PS/P2VP 4/6 vol) with 7.6 v% Au-PS NPs quenched to -30 ℃ with cooling rate of 100 ℃/min: I vs. q profiles with increasing phase separation time. The onset of phase separation was set as time zero.

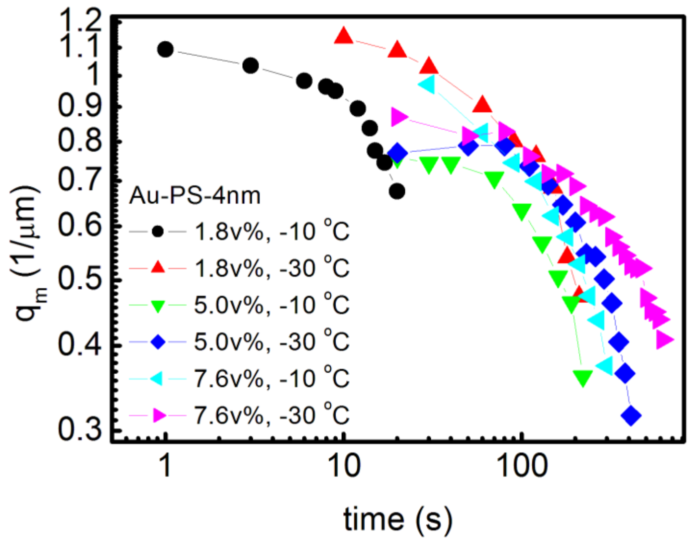

Figure 4.7 Phase-separated PS/P2VP/THF (PS/P2VP 4/6 vol) with Au-PS NPs: q_m vs. t for the blend containing 1.8 v%, 5.0 v% and 7.6 v% nanoparticles quenched to either -10 ℃ or -30 ℃ with cooling rate of 100 ℃/min. The onset of phase separation was set as time zero.

Table 4-1 Estimated α values[a] (as in $q_m \sim t^{-\alpha}$) characterizing the late stage SD of PS/P2VP/THF (PS/P2VP 4/6 vol) with Au-PS NPs

Au-PS NP loading	-10 ℃	-30 ℃
0	-	1.31±0.04 (0.42±0.02[b])
1.8 v%	0.31±0.04	0.23±0.04
5.0 v%	0.27±0.05	0.25±0.04
7.60 v%	0.28±0.02	0.23±0.02

[a] Linear fitting of the intermediate stages of coarsening process.
[b] The α value of the second SD coarsening process for the blend without particle addition.

Figure 4.7 summarizes the plots of q_m *vs.* phase separation time for the blend containing various amounts of nanoparticles subject to different quench depths. The estimated α values according to $q_m \sim t^{-\alpha}$ are listed in Table 4-1. The coarsening dynamics were slowed down by the addition of the nanoparticles. For the same sample composition, deeper quench results in slower dynamics, due to the higher viscosity at the lower temperature.

Previous studies have shown that Au-PS nanoparticles can have controlled preference between PS and P2VP bulk phases through variations in the PS ligand areal density.[41-43] However, in our experiments, the use of a common solvent reduces the difference in wettability of the Au-PS NPs between phases. Indeed, as THF disperses the nanoparticles well, it is most likely that the nanoparticles have little preference for either phase.

Although the neutral wetting condition may be satisfied, the particles can only be adsorbed at and stabilize the interface when the reduction of interfacial energy overcomes thermal energy.[44] In our case, the common solvent THF also reduces the interfacial tension between the phases and increases the difficulty for the particles to be adsorbed at the interface. The interfacial tension between 10 wt% PS/THF and 10 wt% P2VP/THF is less than 10^{-4} N/m, as estimated by a pendent drop measurement. According to theoretical estimates[1], a particle radius larger than 30 nm would be required in order to overcome thermally activated detachment and achieve interfacial adsorption for the neutral wetting case. Considering the large amount of the common solvent in the quasi-binary system, we hypothesize that the size of the particles, rather than their chemical nature, plays the critical role in guiding particle interfacial assembly. Based on this hypothesis, silica particles with 300 nm diameter were added to the PS/P2VP/THF blend.

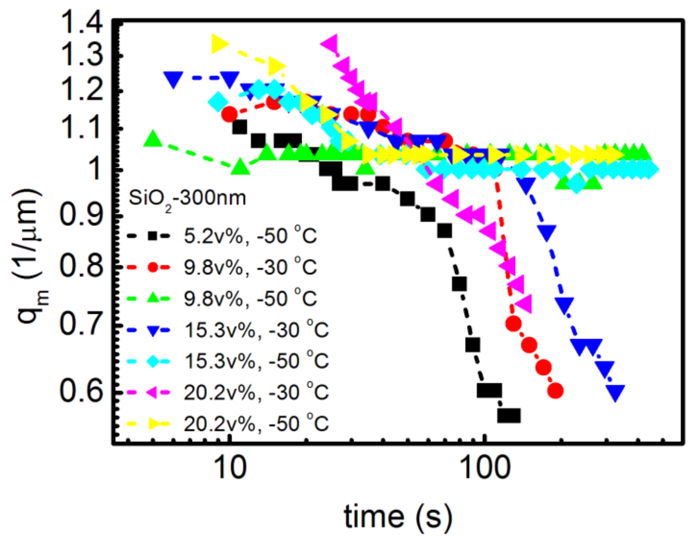

Figure 4.8 Phase-separated PS/P2VP/THF (PS/P2VP 4/6 vol) with silica particles: q_m *vs.* time for the blend containing 5.2 v%, 9.8 v%, 15.3 v% and 20.2 v% SiO_2 particles quenched to either -30 ℃ or -50 ℃ with cooling rate of 100 ℃/min. The onset of phase separation was set as time zero.

Figure 4.8 summarizes the plots of q_m vs. phase separation time for the blend containing various amounts of nanoparticles subject to different quench depths. Similarly to the case of Au-PS NPs, a slowing down of the SD dynamics was observed. More interestingly, for some quench depths and particle concentrations, q_m reached a plateau value at about 1 μm^{-1}. For the samples quenched to -30 ℃ and the sample with the lowest particle loading of 5.2 v% quenched to -50 ℃, an abrupt decrease of q_m was observed, indicating eventual coarsening. For the samples quenched to -50 ℃ (except the one with the lowest particle loading of 5.2 v%), the SD ring pattern stabilized at q_m about 1 μm^{-1} for over 10 min before abrupt coarsening occurred. Figure 4.9 and 4.10 represents the I vs. q curve evolution of the two scenarios, respectively.

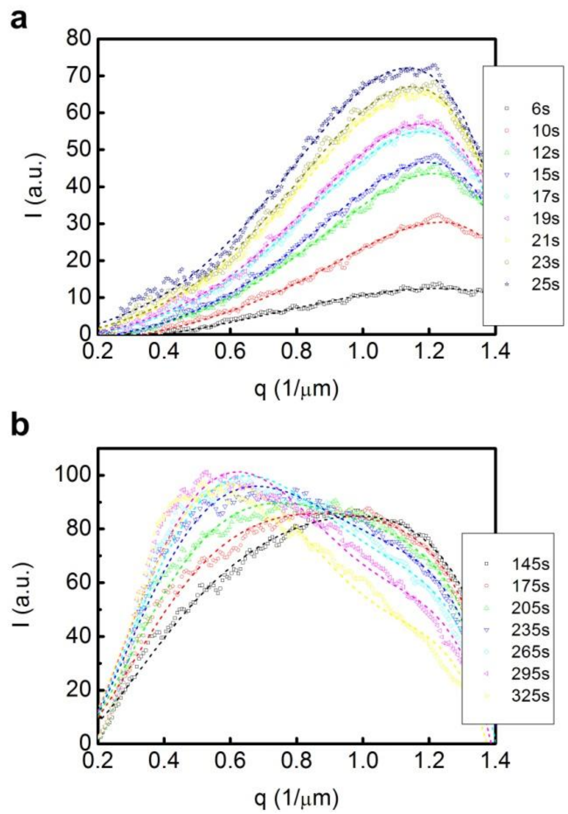

Figure 4.9 Phase separation of PS/P2VP/THF (PS/P2VP 4/6 vol) with 15.3 v% silica particles quenched to -30 ℃ with cooling rate of 100 ℃/min: I vs. q profiles with increasing phase separation time, showing fixed q_m at early times (a) and an abrupt coarsening at late times (b). The onset of phase separation was set as time zero.

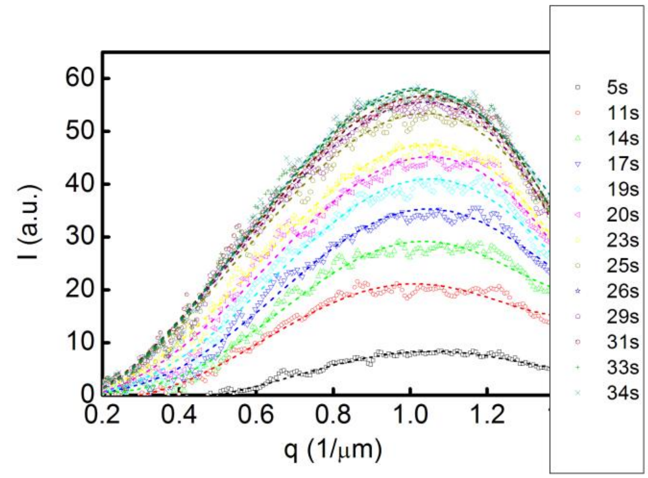

Figure 4.10 Phase separation of PS/P2VP/THF (PS/P2VP 4/6 vol) with 9.8 v% silica particles quenched to -50 ℃ with cooling rate of 100 ℃/min: *I* vs. *q* profiles with increasing phase separation time, showing fixed q_m throughout the experiment. The onset of phase separation was set as time zero.

As the size of the particles is much larger than the critical value for interfacial segregation[1], we speculate that the silica particles stabilize the interface of the co-continuous structure during coarsening. Deeper quench depth favors stabilization, as the probability of thermal desorption decreases with temperature. Although the size scale of the stabilized co-continuous structure should be inversely proportional to the particle loading[45], we did not observe such dependence in our experiments. Possible mechanisms for the eventual coarsening are aggregation and sedimentation of silica particles, adsorption of P2VP chains onto the silica surface,[46] as well as the curvature induced by the particle-interface interaction, which could result in the desorption of particles from the interface and coalescence of the co-continuous structures. The mechanisms of kinetic stabilization with the addition of particles and destabilization process need further investigation.

4.4 Conclusions and future work

In summary, we have designed a quasi-binary blend system based on PS/P2VP compatibilized by the common solvent THF, and achieved experimentally accessible phase mixing temperatures and spinodal decomposition upon thermal quench. The design of the quasi-binary blend system may open ways to guide the phase separation for immiscible polymer binary blends in a more controlled manner, and provides fundamental insights into the phase separation behaviors of polymer blends.

The addition of solid particles significantly slows down the coarsening kinetics of spinodal phase separation and, in some cases, arrests the co-continuous structures at ~6 μm for a short period of time. Future work will be focused on understanding the mechanism of the multiple phase separation and the kinetic arrest of co-continuous structures by particles in such systems.

Reference

1. Stratford, K., et al., *Colloidal jamming at interfaces: A route to fluid-bicontinuous gels.* Science, 2005. **309**(5744): p. 2198-2201.
2. Chung, H., et al., *Self-regulated structures in nanocomposites by directed nanoparticle assembly.* Nano Letters, 2005. **5**(10): p. 1878-1882.
3. Herzig, E.M., et al., *Bicontinuous emulsions stabilized solely by colloidal particles.* Nature Materials, 2007. **6**(12): p. 966-971.
4. Tavacoli, J.W., et al., *Novel, Robust, and Versatile Bijels of Nitromethane, Ethanediol, and Colloidal Silica: Capsules, Sub-Ten-Micrometer Domains, and Mechanical Properties.* Advanced Functional Materials, 2011. **21**(11): p. 2020-2027.
5. Lin, Y., et al., *Ultrathin cross-linked nanoparticle membranes.* Journal of the American Chemical Society, 2003. **125**(42): p. 12690-12691.
6. Russell, J.T., et al., *Self-assembly and cross-linking of bionanoparticles at liquid-liquid interfaces.* Angewandte Chemie-International Edition, 2005. **44**(16): p. 2420-2426.
7. Anastasiadis, S.H., I. Gancarz, and J.T. Koberstein, *Compatibilizing effect of block copolymers added to the polymer polymer interface.* Macromolecules, 1989. **22**(3): p. 1449-1453.

8. Park, D.W. and R.J. Roe, *Effect of added block copolymer on the phase-separation kinetics of a polymer blend .2. optical microscopic observations.* Macromolecules, 1991. **24**(19): p. 5324-5329.
9. Cahn, J.W., *On spinodal decomposition.* Acta Metallurgica, 1961. **9**(9): p. 795-801.
10. Cahn, J.W., *Phase separation by spinodal decomposition in isotropic systems.* Journal of Chemical Physics, 1965. **42**(1): p. 93.
11. Cahn, J.W. and J.E. Hilliard, *Free Energy of a Nonuniform System .1. Interfacial Free Energy.* Journal of Chemical Physics, 1958. **28**(2): p. 258-267.
12. Van Aartsen, J.J., *Theoretical observations on spinodal decomposition of polymer solutions.* European Polymer Journal, 1970. **6**(7): p. 919.
13. Binder, K. and D. Stauffer, *Theory for Slowing Down of Relaxation and Spinodal Decomposition of Binary-Mixtures.* Physical Review Letters, 1974. **33**(17): p. 1006-1009.
14. Lifshitz, I.M. and V.V. Slyozov, *The Kinetics of Precipitation from Supersaturated Solid Solutions.* Journal of Physics and Chemistry of Solids, 1961. **19**(1-2): p. 35-50.
15. Siggia, E.D., *Late Stages of Spinodal Decomposition in Binary-Mixtures.* Physical Review A, 1979. **20**(2): p. 595-605.
16. Furukawa, H., *Dynamics of Phase Separations of a Dissipative System and a Fluid Mixture.* Physical Review A, 1981. **23**(3): p. 1535-1545.
17. McMaster, L.P., *Aspects of polymer-polymer thermodynamics.* Macromolecules, 1973. **6**(5): p. 760-773.
18. Nishi, T., T.T. Wang, and T.K. Kwei, *Thermally induced phase separation behavior of compatible polymer mixtures.* Macromolecules, 1975. **8**(2): p. 227-234.
19. Patterson, D., *Polymer Compatibility with and without a Solvent.* Polymer Engineering and Science, 1982. **22**(2): p. 64-73.
20. Hashimoto, T., J. Kumaki, and H. Kawai, *Time-resolved light-scattering-studies on kinetics of phase-separation and phase dissolution of polymer blends .1. Kinetics of phase-separation of a binary mixture of polystyrene and polyvinyl methyl-ether).* Macromolecules, 1983. **16**(4): p. 641-648.
21. Snyder, H.L., P. Meakin, and S. Reich, *Dynamical Aspects of Phase-Separation in Polymer Blends.* Macromolecules, 1983. **16**(5): p. 757-762.
22. Olabisi, O., *Polymer Compatibility by Gas-Liquid-Chromatography.* Macromolecules, 1975. **8**(3): p. 316-322.
23. Nojima, S., K. Tsutsumi, and T. Nose, *Phase-Separation Process in Polymer Systems .1. Light-Scattering-Studies on a Polystyrene and Poly(Methylphenylsiloxane) Mixture.* Polymer Journal, 1982. **14**(3): p. 225-232.
24. Callaghan, T.A. and D.R. Paul, *Interaction Energies for Blends of Poly(Methyl Methacrylate), Polystyrene, and Poly(Alpha-Methylstyrene) by the Critical Molecular-Weight Method.* Macromolecules, 1993. **26**(10): p. 2439-2450.
25. Shen, S. and J.M. Torkelson, *Miscibility and Phase-Separation in Poly(Methyl Methacrylate) Poly(Vinyl Chloride) Blends - Study of Thermodynamics by Thermal-Analysis.* Macromolecules, 1992. **25**(2): p. 721-728.

26. Rodgers, P.A., D.R. Paul, and J.W. Barlow, *Procedure for Predicting Lower Critical Solution Temperature Behavior in Binary Blends of Polymers.* Macromolecules, 1991. **24**(14): p. 4101-4109.
27. Roe, R.J. and W.C. Zin, *Determination of the Polymer-Polymer Interaction Parameter for the Polystyrene-Polybutadiene Pair.* Macromolecules, 1980. **13**(5): p. 1221-1228.
28. Russell, T.P., G. Hadziioannou, and W.K. Warburton, *Phase-Separation in Low-Molecular Weight Polymer Mixtures.* Macromolecules, 1985. **18**(1): p. 78-83.
29. Aubert, J.H., *Microcellular foams prepared from demixed polymer solutions*. 1990. p. 11.
30. Aubert, J.H., *Microcellular polymer foams prepared by thermally-induced phase separation*. 1989. p. 5.
31. Young, A.T., *Microcellular Foams Via Phase-Separation.* Journal of Vacuum Science & Technology a-Vacuum Surfaces and Films, 1986. **4**(3): p. 1128-1133.
32. Hopkinson, I. and M. Myatt, *Phase separation in ternary polymer solutions induced by solvent loss.* Macromolecules, 2002. **35**(13): p. 5153-5160.
33. Aubert, J.H. and R.L. Clough, *Low-Density, Microcellular Polystyrene Foams.* Polymer, 1985. **26**(13): p. 2047-2054.
34. Koningsveld, R., H.A.G. Chermin, and M. Gordon, *Liquid-Liquid Phase Separation in Multicomponent Polymer Solutions .8. Stability Limits and Consolute States in Quasi-Ternary Mixtures.* Proceedings of the Royal Society of London Series a-Mathematical and Physical Sciences, 1970. **319**(1538): p. 331.
35. Solc, K., *Multiphase Equilibria in Solutions of Polydisperse Homopolymers .1. 3-Phase Equilibria in Ternary and Quasi-Ternary Systems.* Journal of Polymer Science Part B-Polymer Physics, 1982. **20**(10): p. 1947-1961.
36. Scott, R.L., *The Thermodynamics of High Polymer Solutions .5. Phase Equilibria in the Ternary System - Polymer-1 Polymer-2 Solvent.* Journal of Chemical Physics, 1949. **17**(3): p. 279-284.
37. Brust, M., et al., *Synthesis of Thiol-Derivatized Gold Nanoparticles in a 2-Phase Liquid-Liquid System.* Journal of the Chemical Society-Chemical Communications, 1994(7): p. 801-802.
38. Garamszegi, L., et al., *Synthesis of thiol end-functional polystyrene via atom transfer radical polymerization.* Reactive & Functional Polymers, 2003. **55**(2): p. 179-183.
39. Schulz, M.F., et al., *Phase behavior of polystyrene-poly(2-vinylpyridine) diblock copolymers.* Macromolecules, 1996. **29**(8): p. 2857-2867.
40. Brandrup, J., et al., *Polymer Handbook*. 1999, New York: John Wiley & Sons.
41. Chiu, J.J., et al., *Control of nanoparticle location in block copolymers.* Journal of the American Chemical Society, 2005. **127**(14): p. 5036-5037.
42. Kim, B.J., et al., *Effect of areal chain density on the location of polymer-modified gold nanoparticles in a block copolymer template.* Macromolecules, 2006. **39**(12): p. 4108-4114.
43. Kim, B.J., G.H. Fredrickson, and E.J. Kramer, *Effect of polymer ligand molecular weight on polymer-coated nanoparticle location in block copolymers.* Macromolecules, 2008. **41**(2): p. 436-447.

44. Aveyard, R., B.P. Binks, and J.H. Clint, *Emulsions stabilised solely by colloidal particles.* Advances in Colloid and Interface Science, 2003. **100**: p. 503-546.
45. Hore, M.J.A. and M. Laradji, *Microphase separation induced by interfacial segregation of isotropic, spherical nanoparticles.* Journal of Chemical Physics, 2007. **126**(24): p. 244903.
46. Rittigstein, P. and J.M. Torkelson, *Polymer-nanoparticle interfacial interactions in polymer nanocomposites: Confinement effects on glass transition temperature and suppression of physical aging.* Journal of Polymer Science Part B-Polymer Physics, 2006. **44**(20): p. 2935-2943.

CHAPTER 5

CONCLUSIONS AND FUTURE WORK

5.1 Overview

The main focus of the work presented in this thesis has been to generate and kinetically trap co-continuous morphologies at the nano- to micro-scale in phase separated polymer blends. By taking advantage of spinodal phase separation, induced either by thermal quenching or solvent removal, co-continuous morphologies can be fabricated in a controlled manner, for polymer pairs that exhibit partial miscibility or complete immiscibility. Kinetic stabilization of such morphologies is achieved by means of nanoparticle addition or vitrification. Our research has demonstrated ways of kinetically trapping the non-equilibrium interconnected structure at sub-micron to tens-of-nanometer scales, which could afford applications such as active layers of photovoltaic cells and polymer-based membranes.

5.2 Intra-phase gelation of nanoparticles during spinodal decomposition

In Chapter 2, we utilized the partially miscible blend of PS/PVME, which displays LCST-type phase behavior, to generate co-continuous morphologies during spinodal demixing. We showed that CdSe-TOPO nanorods and nanospheres can kinetically arrest the co-continuous morphologies due to gelation of the nanoparticles within the PVME-rich phase. Network formation requires a critical concentration of nanoparticles, which was found to be lower for nanorods than for nanospheres. Once formed, such a network prevents the further structural coarsening and therefore arrests the co-continuous structure with a characteristic length scale of several microns. The effectiveness of the network formation was found to be sensitive to the initial aggregation state of nanoparticles in the blend. For example, network formation was disrupted for the blends containing either severely aggregated CdSe-TOPO nanorods or well dispersed CdSe-PS nanospheres. Only the moderately aggregated CdSe-TOPO nanorods and CdSe-TOPO nanospheres were able to form a percolated network during SD and subsequently lock-in the co-continuous PVME-rich domain that wets the nanoparticle network.

5.2.1 Nanoparticle network formation vs. spinodal decomposition

We propose is that the attractive interaction between particles accounts for the aggregation and even network formation of nanoparticles. To understand the dominant factors that lead to intra-phase gelation, it is important to investigate the interplay between the kinetics of nanoparticle aggregation and those of spinodal decomposition. Preliminary TEM studies indicate that the nanoparticle network may be formed independent of phase separation, as shown in Figure 5.1a and 5.1b for the case of CdSe-TOPO nanospheres. Note that 2 vol% and 4 vol% in homogeneous blend may be similar to 1 vol% and 2 vol% in the demixing blend. Future study may be to understand the relationship between spinodal phase separation and nanoparticle network formation. It is of interest in understanding the structure of colloidal aggregates and the kinetics of the formation. The diffusion of nanoparticles and network solidification, with and without the presence of phase separation, may be studied, i.e. by means of X-ray photon correlation spectroscopy. Mechanisms of aggregation, i.e. diffusion-limited and reaction-limited colloidal aggregation,[1] may therefore be established, which are of fundamental importance in colloidal science.

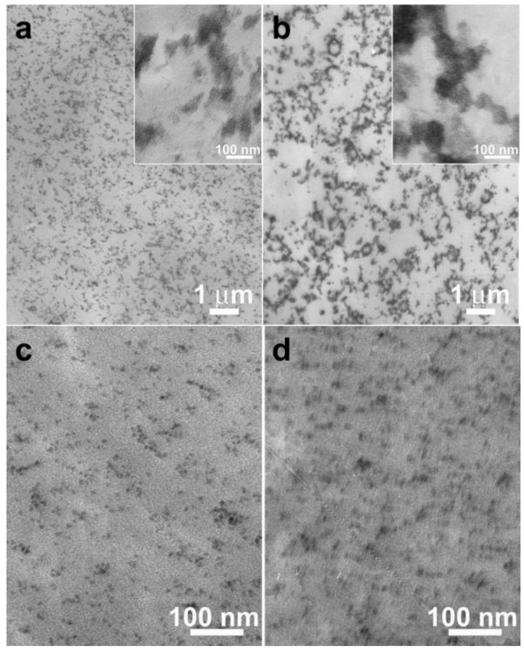

Figure 5.1 The aggregation behaviors of CdSe nanospheres in the PS/PVME (1:1 vol) blends after solution casting. TEM images of the blends containing (a) 2 vol% and (b) 4 vol% CdSe-TOPO nanospheres, reveal a network like structure of the nanoparticles; while the blends containing (c) 2 vol% and (b) 4 vol% CdSe-PS nanospheres, indicate good dispersion with little aggregation (inset: higher magnification TEM images).

5.2.2 Effect of inter-particle interactions on the network formation threshold

Preliminary results showed that micron-sized co-continuous morphologies were stabilized after thermal quenching by the addition of 1 vol % of Fe_3O_4 nanoparticles stabilized with oleic acid and oleic amine (core diameter of 3 – 10 nm), as shown in Figure 5.2. Notably, the phase separated morphologies appeared to be insensitive to the thermal history (with or without pre-annealing) or the quench depth (phase separated at 170 ℃ or 180 ℃), all of which gave rise to co-continuous morphologies of similar size scales. A close look at the particle aggregation behavior reveals that only slight aggregation exists upon casting and after pre-annealing (Figure 5.3), suggesting that a pre-formed, stabilized particle network upon casting is likely the reason for the lack of response to thermal history and the quench depth, as well as the very low percolation threshold regardless of the low aspect ratio of the nanoparticles (below 1 vol% as compared with 1 – 2 vol% for the case of CdSe-TOPO nanorod).

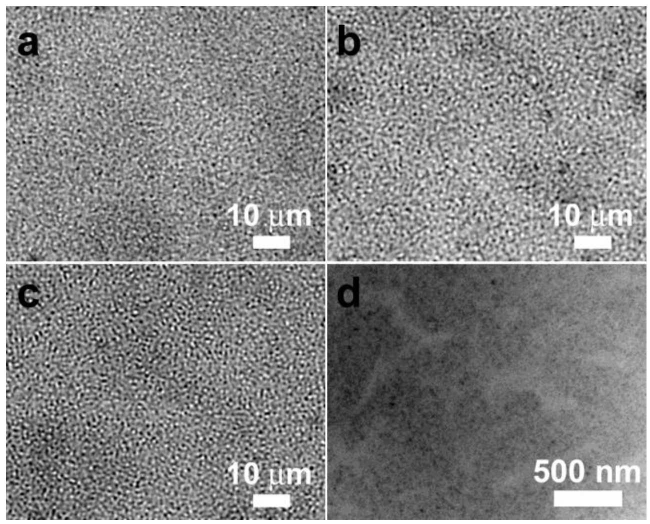

Figure 5.2 Phase separated morphologies of PS/PVME blends (1:1 vol) containing 1 vol % Fe_3O_4 nanoparticles stabilized with oleic acid and oleic amine (core diameter of 3 – 10 nm). Optical micrographs show the morphologies for the blend (a) after annealing at 170 ℃ for 24 h, (b) after pre-annealing at120 ℃ for 12 h and then quenched to 170 ℃ for 24 h and (c) after annealing at 180 ℃ for 24 h; (d) a TEM image taken from the sample in (c) confirms the co-continuous morphology with a percolated network of nanoparticles preferentially located in one phase.

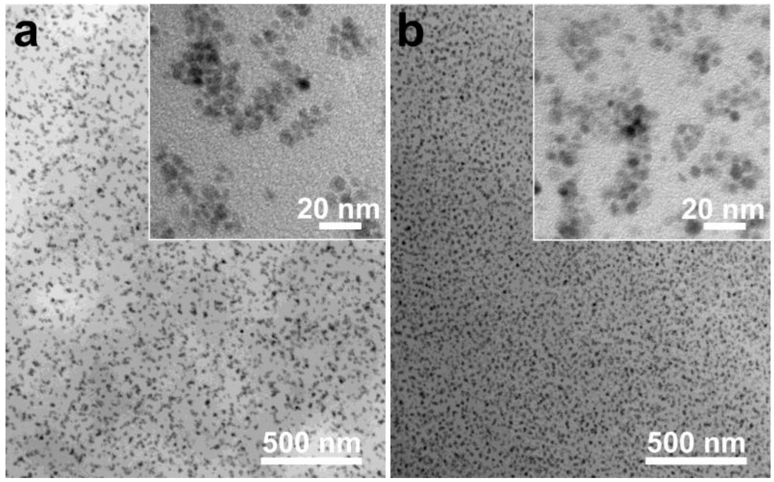

Figure 5.3 The aggregation behaviors of Fe_3O_4 nanoparticles in the PS/PVME (1:1 vol) blends. TEM images of the blend containing 1 vol% Fe_3O_4 nanoparticles (a) following solution casting and (b) annealing at 120 ℃ for 12 h, both reveal slight aggregation.

Future work may also be directed to investigate how the particle/particle interactions and particles/matrix interactions affect the network formation. Based on the understanding of the conditions to form the nanoparticle network, it is intriguingto further tune the nanoparticle interactions by varying the ligand type and ligand coverage, as well as the polymer matrix, to achieve controlled architectures of nanoparticle aggregations. Moreover, it is also very important to elucidate the relationship between the percolation threshold and the particle properties, e.g. aspect ratio, size, inter-particle interactions, etc. These may provide fundamental guidance in generalizing our approach to prepare co-continuous micro-structured blends of polymers and nanoparticles.

5.3 Phase separation of homopolymer/random copolymer blends

In Chapter 3, we designed a strategy to tune the degree of immiscibility between polystyrene (PS) and poly(2-vinylpyridine) (P2VP), by the incorporation of styrene monomers into the backbone of P2VP to form a random copolymer. In such a way, nonfavorable interactions between the two components are mediated and, the chemical mismatch is diminished between the demixing components, allowing the formation of nanoscale co-continuous morphologies via solvent induced phase separation. The size scale of the co-continuous morphology was controlled by varying the molecular weights of the components and the film thickness. This approach involves a simple solution-casting process, and only requires that the solvent dissolves both components. Moreover the co-continuous morphology formation is insensitive to the substrate surface chemistry. Porous membranes with continuous channels and gradient co-continuous structures can also be generated from the phase separated blend films.

5.3.1 Functional membranes based on homopolymer/random copolymer phase separated templates

Functional materials may be generated from the co-continuous structured templates. For example, the nanoporous films may be backfilled with inorganic materials, by means of electrochemical deposition, since the co-continuous morphology may be generated on conducting substrates and the continuous pathway of the pores allows precursor electrolyte to reach the substrate.[2] In addition, the capability of generating gradient co-continuous morphologies may initiate new applications including filtration and coating.[3] Efforts may be made towards the control of the porosity and size gradient by varying the process conditions and additional solvent or thermal annealing.

5.3.2 UCST behavior of homopolymer/random copolymer blends

The tunable interaction between the PS and P(S-*r*-2VP) could also lead to a UCST phase behavior with measurable phase mixing temperatures. With $\chi_{PS/P2VP}$ = 91.6/*T*-0.095,[4] $\chi_{eff} = (1 - x)^2\chi_{PS/P2VP}$ and $\chi_c = (1/\sqrt{N_1} + 1/\sqrt{N_2})^2/2$, we estimated the critical temperatures for the PS/P(S-*r*-2VP) blend with different molecular weights summarized in Figure 5.4. With decreasing MWs, the critical temperature approaches room temperature for the case of PS10k/P(S-*r*-2VP)39k. The experimentally accessible phase mixing temperature opens the possibility for the thermally induced phase separation (TIPS) of the blend, which can give rise to co-continuous morphologies at appropriate conditions. Future studies can focus on the TIPS of the UCST blend. With the measurable phase diagram and tunable spinodal temperature by the use of random copolymer, the size of co-continuous morphology may be controlled depending on the quenching conditions and the MWs.[5]

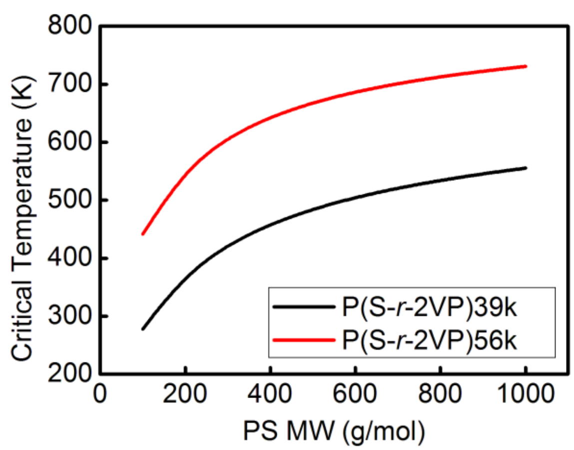

Figure 5.4 The estimated critical temperatures for the PS/P(S-*r*-2VP) blends

5.4 Spinodal phase separation of a quasi-binary blend

In Chapter 4, we studied a quasi-binary blend system based on the PS/P2VP pair with the addition of a common solvent, and achieved co-continuous morphologies by temperature induced phase separation via spinodal decomposition. The addition of solid particles significantly decreased the rate of coarsening and, in some cases, the co-continuous structures were stabilized at ~6 μm for a short period of time until an abrupt coarsening.

We have made many unexplained, although interesting, observations in this system. The multiple spinodal phase separations for the blend without particle addition are not well understood. Although we anticipated a quasi-binary phase behavior, the evolution of co-continuous morphology, i.e. the multiple spinodal, is inconsistent with classical binary blend phase separation theories. The incomprehensible kinetics of the blend indeed complicates the understanding of kinetic stabilization during spinodal phase separation induced by the addition of particles. Future study may employ fluorescent-labeled polymers and particles to allow the observation of the diffusion of polymers and particles using confocal microscopy techniques, in order to understand the morphology evolution and particle segregation during the quasi-binary blend phase separation. Furthermore, colloidal silica may be functionalized by a “wax-emulsion” method[6] and produce Janus type particles in a controlled manner, which is desirable to guide the interfacial assembly in future work.

5.5 Summary

Overall, we have designed various strategies to compatibilize polymer blends, based on phase separation physics, colloidal science, chemical modification and balance of kinetics. Using our methodologies, every polymer pair could be compatibilized, generating co-continuous morphologies in a controlled manner, regardless of the primitive immisciblility. The ability to kinetically stabilize the co-continuous structures at nano- to micro- size scales is of practical importance for the enhanced mechanical properties, selective transport, and controlled optical, electrical properties. Furthermore, various fields of research such as colloidal science and membrane technology can also benefit from the methodologies described in this thesis.

Reference

1. Lin, M.Y., et al., *Universality in colloid aggregation.* Nature, 1989. **339**(6223): p. 360-362.
2. Crossland, E.J.W., et al., *Control of gyroid forming block copolymer templates: effects of an electric field and surface topography*. Soft Matter, 2010. **6**(3): p. 670-676.
3. Ulbricht, M., *Advanced functional polymer membranes.* Polymer, 2006. **47**(7): p. 2217-2262.
4. Schulz, M.F., et al., *Phase behavior of polystyrene-poly(2-vinylpyridine) diblock copolymers.* Macromolecules, 1996. **29**(8): p. 2857-2867.
5. Van Aartsen, J.J., *Theoretical observations on spinodal decomposition of polymer solutions.* European Polymer Journal, 1970. **6**(7): p. 919.
6. Hong, L., S. Jiang, and S. Granick, *Simple method to produce Janus colloidal particles in large quantity.* Langmuir, 2006. **22**(23): p. 9495-9499.

BIBLIOGRAPHY

Affrossman, S., G. Henn, et al. (1996). "Surface topography and composition of deuterated polystyrene-poly(bromostyrene) blends." Macromolecules **29**(14): 5010-5016.

Alexandrovich, P. S. (1978). Studies of polymer compatibility. Polymer Science and Engineering. Amherst, Univerisity of Massachusetts. **PhD:** 536.

Anastasiadis, S. H., I. Gancarz, et al. (1989). "Compatibilizing effect of block copolymers added to the polymer polymer interface." Macromolecules **22**(3): 1449-1453.

Araki, T. and H. Tanaka (2006). "Wetting-induced depletion interaction between particles in a phase-separating liquid mixture." Physical Review E **73**(6): 061506.

Arias, A. C., J. D. MacKenzie, et al. (2001). "Photovoltaic performance and morphology of polyfluorene blends: A combined microscopic and photovoltaic investigation." Macromolecules **34**(17): 6005-6013.

Aubert, J. H. (1989). Microcellular polymer foams prepared by thermally-induced phase separation**:** 5.

Aubert, J. H. (1990). Microcellular foams prepared from demixed polymer solutions**:** 11.

Aubert, J. H. and R. L. Clough (1985). "Low-Density, Microcellular Polystyrene Foams." Polymer **26**(13): 2047-2054.

Aveyard, R., B. P. Binks, et al. (2003). "Emulsions stabilised solely by colloidal particles." Advances in Colloid and Interface Science **100**: 503-546.

Balsara, N. P., S. V. Jonnalagadda, et al. (1993). "Thermodynamic interactions and correlations in mixtures of 2 homopolymers and a block-copolymer by small-angle neutron-scattering." Journal of Chemical Physics **99**(12): 10011-10020.

Bank, M., Leffingw.J, et al. (1971). "Influence of solvent upon compatibility of polystyrene and poly(vinyl methyl ether)." Macromolecules **4**(1): 43.

Bates, F. S. and G. H. Fredrickson (1990). "Block Copolymer Thermodynamics - Theory and Experiment." Annual Review of Physical Chemistry **41**: 525-557.

Bates, F. S., W. W. Maurer, et al. (1997). "Polymeric bicontinuous microemulsions." Physical Review Letters **79**(5): 849-852.

Bell, J. R., K. Chang, et al. (2010). "Annealing of cocontinuous polymer blends: effect of block copolymer molecular weight and architecture." Macromolecules **43**(11): 5024-5032.

Berek, D., D. Lath, et al. (1967). "Phase Relations in Ternary System Atactic Polystyrene-Atactic Polypropylene-Toluene." Journal of Polymer Science Part C-Polymer Symposium(16PC): 659.

Binder, K. and D. Stauffer (1974). "Theory for Slowing Down of Relaxation and Spinodal Decomposition of Binary-Mixtures." Physical Review Letters **33**(17): 1006-1009.

Boltau, M., S. Walheim, et al. (1998). "Surface-induced structure formation of polymer blends on patterned substrates." Nature **391**(6670): 877-879.

Brandrup, J., E. H. Immergut, et al. (1999). Polymer Handbook. New York, John Wiley & Sons.

Bruder, F. and R. Brenn (1991). "Measuring the Binodal by Interdiffusion in Blends of Deuterated Polystyrene and Poly(Styrene-Co-4-Bromostyrene)." Macromolecules **24**(20): 5552-5557.

Brust, M., M. Walker, et al. (1994). "Synthesis of Thiol-Derivatized Gold Nanoparticles in a 2-Phase Liquid-Liquid System." Journal of the Chemical Society-Chemical Communications(7): 801-802.

Cahn, J. W. (1961). "On spinodal decomposition." Acta Metallurgica **9**(9): 795-801.

Cahn, J. W. (1965). "Phase separation by spinodal decomposition in isotropic systems." Journal of Chemical Physics **42**(1): 93.

Cahn, J. W. and J. E. Hilliard (1958). "Free Energy of a Nonuniform System .1. Interfacial Free Energy." Journal of Chemical Physics **28**(2): 258-267.

Callaghan, T. A. and D. R. Paul (1993). "Interaction Energies for Blends of Poly(Methyl Methacrylate), Polystyrene, and Poly(Alpha-Methylstyrene) by the Critical Molecular-Weight Method." Macromolecules **26**(10): 2439-2450.

Campoy-Quiles, M., T. Ferenczi, et al. (2008). "Morphology evolution via self-organization and lateral and vertical diffusion in polymer: fullerene solar cell blends 10.1038/nmat2102." Nature Materials **7**(2): 158-164.

Chen, D., F. Liu, et al. (2011). "Bulk Heterojunction Photovoltaic Active Layers via Bilayer Interdiffusion." Nano Letters **11**(5): 2071-2078.

Chen, D. A., A. Nakahara, et al. (2010). "P3HT/PCBM Bulk Heterojunction Organic Photovoltaics: Correlating Efficiency and Morphology." Nano Letters **11**(2): 561-567.

Chiu, J. J., B. J. Kim, et al. (2005). "Control of nanoparticle location in block copolymers." Journal of the American Chemical Society **127**(14): 5036-5037.

Chung, H., K. Ohno, et al. (2005). "Self-regulated structures in nanocomposites by directed nanoparticle assembly." Nano Letters **5**(10): 1878-1882.

Chung, H. J., A. Taubert, et al. (2004). "Mobile nanoparticles and their effect on phase separation dynamics in thin-film polymer blends." Europhysics Letters **68**(2): 219-225.

Crossland, E. J. W., S. Ludwigs, et al. (2010). "Control of gyroid forming block copolymer templates: effects of an electric field and surface topography." Soft Matter **6**(3): 670-676.

Dalnoki-Veress, K., J. A. Forrest, et al. (1996). "Phase separation morphology of thin films of polystyrene/polyisoprene blends." Journal of Polymer Science Part B-Polymer Physics **34**(17): 3017-3024.

Dalnoki-Veress, K., J. A. Forrest, et al. (1997). "Phase separation morphology of spin-coated polymer blend thin films." Physica A **239**(1-3): 87-94.

Filippone, G., N. T. Dintcheva, et al. (2008). "The role of organoclay in promoting co-continuous morphology in high-density poly(ethylene)/poly(amide) 6 blends." Polymer **49**(5): 1312-1322.

Frischknecht, A. L. (2008). "Forces between nanorods with end-adsorbed chains in a homopolymer melt." Journal of Chemical Physics **128**(22): 224902.

Furukawa, H. (1981). "Dynamics of Phase Separations of a Dissipative System and a Fluid Mixture." Physical Review A **23**(3): 1535-1545.

Galloway, J. A., H. K. Jeon, et al. (2005). "Block copolymer compatibilization of cocontinuous polymer blends." Polymer **46**(1): 183-191.

Garamszegi, L., C. Donzel, et al. (2003). "Synthesis of thiol end-functional polystyrene via atom transfer radical polymerization." Reactive & Functional Polymers **55**(2): 179-183.
Gharachorlou, A. and F. Goharpey (2008). "Rheologically determined phase behavior of LCST blends in the presence of spherical nanoparticles." Macromolecules **41**(9): 3276-3283.
Ginzburg, V. V. (2005). "Influence of nanoparticles on miscibility of polymer blends. A simple theory." Macromolecules **38**(6): 2362-2367.
Gubbels, F., S. Blacher, et al. (1995). "Design of electrical conductive composites - key role of the morphology on the electrical-properties of carbon-black filled polymer blends." Macromolecules **28**(5): 1559-1566.
Gubbels, F., R. Jerome, et al. (1994). "Selective Localization of Carbon-Black in Immiscible Polymer Blends - a Useful Tool to Design Electrical Conductive Composites." Macromolecules **27**(7): 1972-1974.
Gutmann, J. S., P. Muller-Buschbaum, et al. (1999). "Complex pattern formation by phase separation of polymer blends in thin films." Faraday Discussions **112**: 285-297.
Hashimoto, T., J. Kumaki, et al. (1983). "Time-resolved light-scattering-studies on kinetics of phase-separation and phase dissolution of polymer blends .1. Kinetics of phase-separation of a binary mixture of polystyrene and polyvinyl methyl-ether)." Macromolecules **16**(4): 641-648.
Herzig, E. M., K. A. White, et al. (2007). "Bicontinuous emulsions stabilized solely by colloidal particles." Nature Materials **6**(12): 966-971.
Hillmyer, M. A. (2005). Nanoporous materials from block copolymer precursors. Block Copolymers Ii. V. Abetz. Berlin, Springer-Verlag Berlin. **190:** 137-181.
Hong, L., S. Jiang, et al. (2006). "Simple method to produce Janus colloidal particles in large quantity." Langmuir **22**(23): 9495-9499.
Hopkinson, I. and M. Myatt (2002). "Phase separation in ternary polymer solutions induced by solvent loss." Macromolecules **35**(13): 5153-5160.
Hoppe, H. and N. S. Sariciftci (2006). "Morphology of polymer/fullerene bulk heterojunction solar cells." Journal of Materials Chemistry **16**(1): 45-61.
Hore, M. J. A. and R. J. Composto (2010). "Nanorod Self-Assembly for Tuning Optical Absorption." ACS Nano **4**(11): 6941-6949.
Hore, M. J. A. and M. Laradji (2007). "Microphase separation induced by interfacial segregation of isotropic, spherical nanoparticles." Journal of Chemical Physics **126**(24): 244903.
Hore, M. J. A. and M. Laradji (2008). "Prospects of nanorods as an emulsifying agent of immiscible blends." Journal of Chemical Physics **128**(5): 054901.
Hsu, C. C. and Prausnit.Jm (1974). "Thermodynamics of Polymer Compatibility in Ternary-Systems." Macromolecules **7**(3): 320-324.
Hudson, S. D. and A. M. Jamieson (2000). Morphology and Properties of Blends Containing Block Copolymers. New York, John Wiley & Sons, Inc.
Ishino, S., H. Nakanishi, et al. (2006). "Designing a polymer blend with phase separation tunable by visible light for computer-assisted irradiation experiments." Macromolecular Rapid Communications **27**(10): 758-762.

Jones, B. H. and T. P. Lodge (2009). "High-Temperature Nanoporous Ceramic Monolith Prepared from a Polymeric Bicontinuous Microemulsion Template." Journal of the American Chemical Society **131**(5): 1676.

Kambour, R. P. and J. T. Bendler (1986). "Miscibilities in Monodisperse Mixtures of Polystyrene, Poly(Para-Bromostyrene), and Their Copolymers." Macromolecules **19**(11): 2679-2682.

Kambour, R. P., J. T. Bendler, et al. (1983). "Phase-Behavior of Polystyrene, Poly(2,6-Dimethyl-1,4-Phenylene Oxide), and Their Brominated Derivatives." Macromolecules **16**(5): 753-757.

Karim, A., D. W. Liu, et al. (2000). "Modification of the phase stability of polymer blends by fillers." Polymer **41**(23): 8455-8458.

Kesting, R. E. (1985). Synthetic polymeric membranes: a structural perspective. New York, Wiley-Interscience.

Kim, B. J., J. Bang, et al. (2006). "Effect of areal chain density on the location of polymer-modified gold nanoparticles in a block copolymer template." Macromolecules **39**(12): 4108-4114.

Kim, B. J., G. H. Fredrickson, et al. (2008). "Effect of polymer ligand molecular weight on polymer-coated nanoparticle location in block copolymers." Macromolecules **41**(2): 436-447.

Kim, B. S., T. Chiba, et al. (1995). "Morphology development via reaction-induced phase-separation in epoxy poly(ether sulfone) blends - morphology control using poly(ether sulfone) with functional end-groups." Polymer **36**(1): 43-47.

Kim, J. K., J. Jang, et al. (2004). "Phase behavior of polystyrene and poly(n-pentyl methacrylate) blend with small amounts of symmetric polystyrene-block-poly(n-pentyl methacrylate) copolymers." Macromolecules **37**(23): 8599-8605.

Kim, J. K. and H. Lee (1996). "The effect of PS-GMA as an in situ compatibilizer on the morphology and rheological properties of the immiscible PBT/PS blend." Polymer **37**(2): 305-311.

Koningsveld, R., H. A. G. Chermin, et al. (1970). "Liquid-Liquid Phase Separation in Multicomponent Polymer Solutions .8. Stability Limits and Consolute States in Quasi-Ternary Mixtures." Proceedings of the Royal Society of London Series a-Mathematical and Physical Sciences **319**(1538): 331.

Koningsveld, R., L. A. Kleintjens, et al. (1974). "Thermodynamic Aspects of Polymer Compatibility." Pure and Applied Chemistry **39**(1-2): 1-32.

Krausch, G. (1995). "Surface-Induced Self-Assembly in Thin Polymer-Films." Materials Science & Engineering R-Reports **14**(1-2): 1-94.

Krausch, G., E. J. Kramer, et al. (1994). "Self-Assembly of a Homopolymer Mixture Via Phase-Separation." Applied Physics Letters **64**(20): 2655-2657.

Kruse, W. A., R. G. Kirste, et al. (1976). "Experimental-Evidence for Molecularly Disperse Character of Mixture of 2 Polymers and Determination of Chemical Potential in These Mixtures." Makromolekulare Chemie-Macromolecular Chemistry and Physics **177**(4): 1145-1160.

Kudlik, A., C. Tschirwitz, et al. (1997). "Slow secondary relaxation process in supercooled liquids." Europhysics Letters **40**(6): 649-654.

Kwei, T. K., T. Nishi, et al. (1974). "Study of Compatible Polymer Mixtures." Macromolecules **7**(5): 667-674.

Leibler, L. (1982). "Theory of phase-equilibria in mixtures of copolymers and homopolymers. 2. Interfaces near the consolute point." Macromolecules **15**(5): 1283-1290.
Leibler, L. (1988). "Emulsifying effects of block copolymers in incompatible polymer blends." Makromolekulare Chemie-Macromolecular Symposia **16**: 1-17.
Li, L., C. Miesch, et al. (2011). "Kinetically Trapped Co-continuous Polymer Morphologies through Intraphase Gelation of Nanoparticles." Nano Letters **11**(5): 1997-2003.
Li, Y. J. and H. Shimizu (2004). "Novel morphologies of poly(phenylene oxide) (PPO)/polyamide 6 (PA6) blend nanocomposites." Polymer **45**(22): 7381-7388.
Lifshitz, I. M. and V. V. Slyozov (1961). "The Kinetics of Precipitation from Supersaturated Solid Solutions." Journal of Physics and Chemistry of Solids **19**(1-2): 35-50.
Lin, M. Y., H. M. Lindsay, et al. (1989). "Universality in colloid aggregation." Nature **339**(6223): 360-362.
Lin, Y., H. Skaff, et al. (2003). "Ultrathin cross-linked nanoparticle membranes." Journal of the American Chemical Society **125**(42): 12690-12691.
Lipatov, Y. S. (2002). "Polymer blends and interpenetrating polymer networks at the interface with solids." Progress in Polymer Science **27**(9): 1721-1801.
Lu, P. J., E. Zaccarelli, et al. (2008). "Gelation of particles with short-range attraction." Nature **453**(7194): 499-U4.
Lyu, S., T. D. Jones, et al. (2002). "Role of block copolymers on suppression of droplet coalescence." Macromolecules **35**(20): 7845-7855.
Macosko, C. W., P. Guegan, et al. (1996). "Compatibilizers for melt blending: Premade block copolymers." Macromolecules **29**(17): 5590-5598.
Mathiowitz, E., J. S. Jacob, et al. (2001). "Novel desiccants based on designed polymeric blends." Journal of Applied Polymer Science **80**(3): 317-327.
Matsen, M. W. (1995). "Phase-Behavior of Block-Copolymer Homopolymer Blends." Macromolecules **28**(17): 5765-5773.
McMaster, L. P. (1973). "Aspects of polymer-polymer thermodynamics." Macromolecules **6**(5): 760-773.
Mekhilef, N., B. D. Favis, et al. (1997). "Morphological stability, interfacial tension, and dual-phase continuity in polystyrene-polyethylene blends." Journal of Polymer Science Part B-Polymer Physics **35**(2): 293-308.
Naito, K., G. E. Johnson, et al. (1978). "Compatibility in Blends of Poly(Methyl Methacrylate) and Poly(Styrene-Co-Acrylonitrile) .1. Physical-Properties." Macromolecules **11**(6): 1260-1265.
Nishi, T., T. T. Wang, et al. (1975). "Thermally induced phase separation behavior of compatible polymer mixtures." Macromolecules **8**(2): 227-234.
Nojima, S., K. Tsutsumi, et al. (1982). "Phase-Separation Process in Polymer Systems .1. Light-Scattering-Studies on a Polystyrene and Poly(Methylphenylsiloxane) Mixture." Polymer Journal **14**(3): 225-232.
Noolandi, J. and K. M. Hong (1984). "Effect of block copolymers at a demixed homopolymer interface." Macromolecules **17**(8): 1531-1537.
Olabisi, O. (1975). "Polymer Compatibility by Gas-Liquid-Chromatography." Macromolecules **8**(3): 316-322.

Park, D. W. and R. J. Roe (1991). "Effect of added block copolymer on the phase-separation kinetics of a polymer blend .2. optical microscopic observations." Macromolecules **24**(19): 5324-5329.
Patterson, D. (1982). "Polymer Compatibility with and without a Solvent." Polymer Engineering and Science **22**(2): 64-73.
Paul, D. R. (1978). Polymer blends. New York, Academic Press, Inc.
Paul, D. R. and J. W. Barlow (1984). "A Binary Interaction-Model for Miscibility of Copolymers in Blends." Polymer **25**(4): 487-494.
Peng, G. W., F. Qiu, et al. (2000). "Forming supramolecular networks from nanoscale rods in binary, phase-separating mixtures." Science **288**(5472): 1802-1804.
Peng, Z. A. and X. G. Peng (2001). "Formation of high-quality CdTe, CdSe, and CdS nanocrystals using CdO as precursor." Journal of the American Chemical Society **123**(1): 183-184.
Peng, Z. A. and X. G. Peng (2002). "Nearly monodisperse and shape-controlled CdSe nanocrystals via alternative routes: Nucleation and growth." Journal of the American Chemical Society **124**(13): 3343-3353.
Pernot, H., M. Baumert, et al. (2002). "Design and properties of co-continuous nanostructured polymers by reactive blending." Nature Materials **1**(1): 54-58.
Pitet, L. M., M. A. Amendt, et al. (2010). "Nanoporous Linear Polyethylene from a Block Polymer Precursor." Journal of the American Chemical Society **132**(24): 8230.
Polios, I. S., M. Soliman, et al. (1997). "Late stages of phase separation in a binary polymer blend studied by rheology, optical and electron microscopy, and solid state NMR." Macromolecules **30**(15): 4470-4480.
Poon, W. C. K. and M. D. Haw (1997). "Mesoscopic structure formation in colloidal aggregation and gelation." Advances in Colloid and Interface Science **73**: 71-126.
Potschke, P. and D. R. Paul (2003). "Formation of Co-continuous structures in melt-mixed immiscible polymer blends." Journal of Macromolecular Science-Polymer Reviews **C43**(1): 87-141.
Ramos, A. R. and R. E. Cohen (1977). "Influence of diblock copolymers on structure and properties of polybutadiene-polyisoprene blends." Polymer Engineering and Science **17**(8): 639-646.
Rittigstein, P. and J. M. Torkelson (2006). "Polymer-nanoparticle interfacial interactions in polymer nanocomposites: Confinement effects on glass transition temperature and suppression of physical aging." Journal of Polymer Science Part B-Polymer Physics **44**(20): 2935-2943.
Robeson, L. M. (2007). Polymer Blends: A Comprehensive Review. Cicinnati, OH, Hanser Gardner Publications, Inc.
Rodgers, P. A., D. R. Paul, et al. (1991). "Procedure for Predicting Lower Critical Solution Temperature Behavior in Binary Blends of Polymers." Macromolecules **24**(14): 4101-4109.
Roe, R. J. and C. M. Kuo (1990). "Effect of added block copolymer on phase-separation kinetics of a polymer blend .1. A light-scattering study." Macromolecules **23**(21): 4635-4640.
Roe, R. J. and W. C. Zin (1980). "Determination of the Polymer-Polymer Interaction Parameter for the Polystyrene-Polybutadiene Pair." Macromolecules **13**(5): 1221-1228.

Russell, J. T., Y. Lin, et al. (2005). "Self-assembly and cross-linking of bionanoparticles at liquid-liquid interfaces." Angewandte Chemie-International Edition **44**(16): 2420-2426.

Russell, T. P., G. Hadziioannou, et al. (1985). "Phase-Separation in Low-Molecular Weight Polymer Mixtures." Macromolecules **18**(1): 78-83.

Schulz, M. F., A. K. Khandpur, et al. (1996). "Phase behavior of polystyrene-poly(2-vinylpyridine) diblock copolymers." Macromolecules **29**(8): 2857-2867.

Scott, R. L. (1949). "The Thermodynamics of High Polymer Solutions .5. Phase Equilibria in the Ternary System - Polymer-1 Polymer-2 Solvent." Journal of Chemical Physics **17**(3): 279-284.

Scott, R. L. (1952). "Thermodynamics of High Polymer Solutions .6. the Compatibility of Copolymers." Journal of Polymer Science **9**(5): 423-432.

Semenov, A. N. (1992). "Theory of diblock-copolymer segregation to the interface and free-surface of a homopolymer layer." Macromolecules **25**(19): 4967-4977.

Shaheen, S. E., C. J. Brabec, et al. (2001). "2.5% efficient organic plastic solar cells." Applied Physics Letters **78**(6): 841-843.

Shen, S. and J. M. Torkelson (1992). "Miscibility and Phase-Separation in Poly(Methyl Methacrylate) Poly(Vinyl Chloride) Blends - Study of Thermodynamics by Thermal-Analysis." Macromolecules **25**(2): 721-728.

Shull, K. R., A. J. Kellock, et al. (1992). "Vanishing interfacial-tension in an immiscible polymer blend." Journal of Chemical Physics **97**(3): 2095-2104.

Shull, K. R., E. J. Kramer, et al. (1990). "Segregation of Block Copolymers to Interfaces between Immiscible Homopolymers." Macromolecules **23**(22): 4780-4787.

Siggia, E. D. (1979). "Late Stages of Spinodal Decomposition in Binary-Mixtures." Physical Review A **20**(2): 595-605.

Snyder, H. L., P. Meakin, et al. (1983). "Dynamical Aspects of Phase-Separation in Polymer Blends." Macromolecules **16**(5): 757-762.

Solc, K. (1982). "Multiphase Equilibria in Solutions of Polydisperse Homopolymers .1. 3-Phase Equilibria in Ternary and Quasi-Ternary Systems." Journal of Polymer Science Part B-Polymer Physics **20**(10): 1947-1961.

Solc, K. and Y. C. Yang (1988). "Phase-Separation in Ternary-Systems Solvent Polymer-1 Polymer-2 .3. Homogeneous Double Critical-Points." Macromolecules **21**(3): 829-840.

Stratford, K., R. Adhikari, et al. (2005). "Colloidal jamming at interfaces: A route to fluid-bicontinuous gels." Science **309**(5744): 2198-2201.

Strobl, G. R., J. T. Bendler, et al. (1986). "Miscibilities in monodisperse mixtures of polystyrene, poly(p-bromostyrene) and their copolymers." Macromolecules **19**: 2683.

Strobl, G. R., J. T. Bendler, et al. (1986). "Thermally Reversible Phase-Separation in Polystyrene Poly(Styrene-Co-4-Bromostyrene) Blends." Macromolecules **19**(11): 2683-2689.

Tanaka, H., H. Hasegawa, et al. (1991). "Ordered Structure in Mixtures of a Block Copolymer and Homopolymers .1. Solubilization of Low-Molecular-Weight Homopolymers." Macromolecules **24**(1): 240-251.

Tanaka, H., A. J. Lovinger, et al. (1994). "Pattern evolution caused by dynamic coupling between wetting and phase-separation in binary-liquid mixture containing glass particles." Physical Review Letters **72**(16): 2581-2584.

Tavacoli, J. W., J. H. J. Thijssen, et al. (2011). "Novel, Robust, and Versatile Bijels of Nitromethane, Ethanediol, and Colloidal Silica: Capsules, Sub-Ten-Micrometer Domains, and Mechanical Properties." Advanced Functional Materials **21**(11): 2020-2027.

ten Brinke, G., F. E. Karasz, et al. (1983). "Phase Behavior in Copolymer Blends: Poly(2 ,6-dimethyl-1,4-phenylenoex ide) and Halogen-Substituted Styrene Copolymers." Macromolecules **16**: 1827.

Trappe, V., V. Prasad, et al. (2001). "Jamming phase diagram for attractive particles." Nature **411**(6839): 772-775.

Treat, N. D., M. A. Brady, et al. (2010). "Interdiffusion of PCBM and P3HT Reveals Miscibility in a Photovoltaically Active Blend." Advanced Energy Materials **1**(1): 82-89.

Uehara, H., T. Yoshida, et al. (2006). "Nanoporous polyethylene film prepared from bicontinuous crystalline/amorphous structure of block copolymer precursor." Macromolecules **39**(12): 3971-3974.

Ulbricht, M. (2006). "Advanced functional polymer membranes." Polymer **47**(7): 2217-2262.

Van Aartsen, J. J. (1970). "Theoretical observations on spinodal decomposition of polymer solutions." European Polymer Journal **6**(7): 919.

van Ekenstein, G., R. Meyboom, et al. (2000). "Determination of the Flory-Huggins interaction parameter of styrene and 4-vinylpyridine using copolymer blends of poly(styrene-co-4-vinylpyridine) and polystyrene." Macromolecules **33**(10): 3752-3756.

Veenstra, H., J. Van Dam, et al. (2000). "On the coarsening of co-continuous morphologies in polymer blends: effect of interfacial tension, viscosity and physical cross-links." Polymer **41**(8): 3037-3045.

Vukovic, R., G. Bogdanic, et al. (1999). "Phase behavior and miscibility in binary blends containing polymers and copolymers of styrene, of 2,6-dimethyl-1,4-phenylene oxide, and of their derivatives." Journal of Physical and Chemical Reference Data **28**(3): 851-868.

Walheim, S., M. Boltau, et al. (1997). "Structure formation via polymer demixing in spin-cast films." Macromolecules **30**(17): 4995-5003.

Wu, G. Z., B. P. Li, et al. (2010). "Carbon black self-networking induced co-continuity of immiscible polymer blends." Polymer **51**(9): 2077-2083.

Wu, K. H. and S. Y. Lu (2006). "Preferential partition of nanowires in thin films of immiscible polymer blends." Macromolecular Rapid Communications **27**(6): 424-429.

Yang, C. Y. and A. J. Heeger (1996). "Morphology of composites of semiconducting polymers mixed with C-60." Synthetic Metals **83**(2): 85-88.

Yi, J. Y. and G. M. Choi (1999). "Percolation behavior of conductor-insulator composites with varying aspect ratio of conductive fiber." Journal of Electroceramics **3**(4): 361-369.

Young, A. T. (1986). "Microcellular Foams Via Phase-Separation." Journal of Vacuum Science & Technology a-Vacuum Surfaces and Films **4**(3): 1128-1133.

Yuan, Z. H. and B. D. Favis (2006). "Influence of the efficacy of interfacial modification on the coarsening of cocontinuous PS/HDPE blends during quiescent annealing." Journal of Polymer Science Part B-Polymer Physics **44**(4): 711-721.

Yurekli, K., A. Karim, et al. (2003). "Influence of layered silicates on the phase-separated morphology of PS-PVME blends." Macromolecules **36**(19): 7256-7267.

Zaccarelli, E. (2007). "Colloidal gels: equilibrium and non-equilibrium routes." Journal of Physics-Condensed Matter **19**(32): 323101.

Zeman, L. and Patterso.D (1972). "Effect of Solvent on Polymer Incompatibility in Solution." Macromolecules **5**(4): 513.

Zhang, Q., H. Yang, et al. (2004). "Kinetics-controlled compatibilization of immiscible polypropylene/polystyrene blends using nano-SiO2 particles." Polymer **45**(6): 1913-1922.

Zou, H., N. Ning, et al. (2007). "Manipulating the phase morphology in PPS/PA66 blends using clay." Journal of Applied Polymer Science **106**(4): 2238-2250.